Title
The Role of NOTCH1 Signaling in Aortic Valve Calcification

Author
White, Mark Philip

Publication Date
2012

Peer reviewed|Thesis/dissertation

The Role of NOTCH1 Signaling in Aortic Valve Disease

by

Mark P. White

DISSERTATION

Submitted in partial satisfaction of the requirements for the degree of

DOCTOR OF PHILOSOPHY

in

Biomedical Sciences

in the

GRADUATE DIVISION

of the

UNIVERSITY OF CALIFORNIA, SAN FRANCISCO

Acknowledgements

Publications and Contributions

The data presented in Chapter 2 is the result of many successful collaborations. Alexander Williams and Sean Thomas performed the bioinformatic data analysis used to generate Figures 2.2-2.5. Christina Theodoris contributed significantly to Figure 2.7.

The work presented in Chapter 3 is published in the journal, Stem Cells. 2012. Oct 18 (epub ahead of print) and is titled “Limited Gene Expression Variation in Human Embryonic Stem Cell and Induced Pluripotent Stem Cell Derived Endothelial Cells” by Mark P. White, Abdul J. Rufaihah, Lei Liu, Yohannes T. Ghebremariam, Kathryn N. Ivey, John P. Cooke, and Deepak Srivastava.

Personal Acknowledgements

Completing a PhD program is the most challenging process I have experienced and would not be possible without help from many people. I am truly grateful for all of the mentorship, advice and support I have received.

I came to UCSF with the goal of trying to uncover a deeper understanding of the aortic valve disease process and I am lucky that my mentor, Dr. Deepak Srivastava, gave me a chance to pursue this research. Deepak has provided one of the best training environments in the world and the people who fill his lab reflect this. He has given me the freedom to ask many questions and explore as I was learning

to be a scientist. He taught me about the power of collaboration. Deepak's guidance has molded my scientific thought process and he has always pushed me to make a significant impact. I have grown personally and scientifically during the last 6 years and owe much of this to Deepak.

When I started graduate school I was an average scientist at best. Dr. Kathy Ivey has been instrumental in my scientific training and truly complements Deepak. I always strive to plan and execute all experiments to the level of thoroughness and precision that Kathy uses to complete her work. She has also helped to train my scientific writing process and she is definitely responsible for turning me into the scientist I am today.

To answer the most important questions in our field, we must seek advice and collaborate with experts. The leadership at the Gladstone Institutes provides a research environment that fosters collaboration not only within labs, but also between labs. I am fortunate to work with some truly exceptional people who are too many to name. They have given advice, helped both scientifically and personally and allowed me to finally successfully complete my PhD program. I am grateful for all they have done and hope to one day repay everything I have received.

I could not have completed my PhD with out the love and support of my amazing family. As teachers, my parents, Janet and Philip White, instilled in me the power of education and inspired me to "follow my passion". My siblings, Lauren and Dave, their spouses Steve and Leah, and my second family, Beth, Bud, Alex, and Allie have cheered me on from the sidelines, urging me to continue despite setbacks

and uncertainty. My daughter, Penny, helped me step back from the stress and pressure and take my time enjoying the end of my tenure at UCSF. And finally, to my beautiful wife, Emily, we finally did it! Your support during this journey has been unwavering. You helped me through the tough times, urged me to be patient, and inspired me to complete my goal. I would not be where I am today without you.

Abstract

Calcification of the aortic valve is a common disease affecting many people, and requires invasive valve replacement surgery to prevent irreparable damage to the heart. Understanding the molecular mechanisms that contribute to this disease will allow us to hopefully development non-invasive treatments that can slow or reverse this disease process and could potentially help treat the similar and related process of atherosclerosis. Shear stress and NOTCH1 have both been linked to aortic valve calcification and are important regulators of endothelial cell biology. We showed using RNA-seq in primary endothelial cells from human aortic valve, that shear stress controled a genetic program normally responsible for maintaining epiphyseal plates in a proliferative, non-calcified state. In addition, using siRNA knockdown of the NOTCH1 receptor and ChIP-seq, we showed activation of many of these genes including the potent inhibitor of soft tissue calcification, MGP, are directly regulated by NOTCH1 in the endothelium. Furthermore, we developed an efficient method to direct the differentiation of embryonic stem (ES) or induced pluripotent stem (iPS) cells into endothelial cells and determined that this highly pure somatic cell population has limited gene expression variation between cell lines. This method will be used to test human iPS cells derived from patients with valve calcification and NOTCH1 mutations in order to more fully define the mechanism of their disease, and hopefully allow us to directly target important signaling cascades responsible for this ectopic calcification.

Table of Contents

List of Tables

List of Figures

Chapter 1

Introduction: Aortic Valve Calcification

Disease Overview, Causes and Modeling

1.1 Aortic Valve Disease Overview and Significance

The aortic valve is a thin, pliable, extracellular matrix rich structure that prevents blood regurgitation from the aorta into the left ventricle during diastole. Aortic valve calcification is a progressive disease that usually occurs in the 7^{th} or 8^{th} generation of life whereby the valve stiffens and eventually leads to pressure overload and heart failure if left untreated (Akat et al., 2008). Each year there are over 100,000 valve replacement surgeries in the United States alone, at a cost of billions of dollars (Bossé et al., 2008). In addition, valve replacement is very invasive, requiring open-heart surgery with cardiopulmonary bypass. Some high-risk patients receive new aortic valves through catheter-based approaches, but this method is associated with an increased stroke risk (Rodés-Cabau et al., 2011). Slowing the progression or reversing this disease process would therefore have a large impact on patient health and decrease medical costs.

1.2 Normal Aortic Valve Anatomy

The human aortic valve is composed of three layers, the ventricularis, spongiosa, and fibrosa (Schoen, 2008). The ventricularis is the valvular layer closest to the left ventrical of the heart and is composed primarily of elastin fibers. The spongiosa is the medial layer of the valve and named for the spongy appearance of the glycosoaminoglycans that make up its structure. Finally, the aortic side of the valve is called the fibrosa and is composed mainly of collagens that provide strength to the valve during the high pressure of diastole. The fibrosa is also the first layer of the valve where calcific lesions form during aortic valve disease (Weinberg et al., 2010). A normal healthy valve is comprised of two main types of cells. Endothelial cells line both sides of the valve and serve to mediate inflammation and provide an anti-thrombotic cell layer. In addition, increasing evidence indicates the endothelium maintains a quiescent, inactive pool of valve interstitial cells (Butcher and Nerem, 2006). Interstitial cells are scattered throughout all three valve layers and serve to secrete and remodel matrix over time to maintain the mechanical properties of the valves. Both cell types also play important roles in the valve disease process.

1.3 Aortic Valve Disease Process

Aortic valve disease is generally thought to begin via an inflammatory activation of the endothelium on the aortic side of the valve. Cardiovascular risk factors such as age, smoking and circulating LDL levels, in addition to the high mechanical strain present on the cells of the valve over many years, are thought to result in endothelial

cell leakage and activation (Stewart et al., 1997). This process allows low-density lipoproteins (LDL) to accumulate under the valve endothelium. In addition, the activated endothelium triggers recruitment of monocytes, leukocytes and T-cells that secrete cytokines, generating an inflammatory microenvironment that subsequently activates the valve interstitial cells (Ghaisas et al., 2000). These activated interstitial cells, or smooth muscle actin positive myofibroblasts, then undergo a trans-differentiation into osteoblast like cells (Liu et al., 2007). New evidence suggests that circulating osteogenic progenitor cells may also play a role in valve calcification (Egan et al., 2011). The activation of the RUNX2 osteoblast master regulator by BMP/ SMAD signaling is thought to be the first step in establishing the ectopic expression of the bone gene program (Akat et al., 2008). In addition, extracellular matrix in the valve is actively remodeled and replaced with bone matrix proteins via matrix metalloproteinases (MMPs). This matrix will eventually calcify, leading to valve stiffening and stenosis. Another hallmark of valve disease is neoangiogenesis in the valve itself, which is normally a-vascular (Johnson et al., 2006). New blood vessels are found near calcific lesions in the valve and are thought to play two roles. The first role is to provide a route for circulating immune cells and mesenchymal stem cells to access the growing lesion where they secrete inflammatory cytokines and/or differentiate into bone forming cells (Johnson et al., 2006). The other suspected role of the newly formed vessels is the secretion of cytokines that promote differentiation (BMP 2/4) and migration (VEGF) of osteoblasts (Johnson et al., 2006). These factors combined lead to stiffening of the valve, impedance of

blood flow, and eventually left ventricular enlargement and subsequent heart failure. Many of the molecular mechanisms driving this disease process have been discovered though few treatments other than valve replacement are used clinically.

1.4 Aortic Valve Disease Molecular Mechanisms

1.4.1 Molecular Mechanisms from Human Disease

Studies of human disease provide mechanistic insights to the cause of aortic valve disease. Bicuspid aortic valves are strongly associated with an increased risk of calcification (Roberts, 2005). A bicuspid aortic valve is the most common congenital heart defect with an incidence of 1-2% of all live births, though this may be higher as many patients remain undiagnosed until the onset of disease symptoms (Lewin, 2005). The normal aortic valve is composed of three leaflets and in bicuspid aortic valves result from fusion of two of the three leaflets. Roughly 50% of people who require surgical correction for a calcified valve also have a bicuspid morphology (Fedak, 2002). Two theories have been proposed to explain this morphological defect's association with calcification. Bicuspid valves do not usually open as fully as a tricuspid valve, resulting in altered hemodynamics and an increase in turbulent blood flow on the aortic side of the valve (Chandra et al., 2012). It is thought that this decreased or turbulent shear stress then leads to the activation inflammation and a pro-osteogenic microenvironment (Davies et al., 2010). On the other hand, the presence of a bicuspid valve could simply mark a genetic event that also

predisposes a person to valve calcification. A study detailing the calcification of a set of 62-year-old identical twins may help discriminate between these two theories (Lewis and Henderson, 1990). Both men had an aortic valve replacement, within one year of each other, due to severe stenosis and calcification. Interestingly, one patient had a bicuspid valve while the other had a tricuspid valve. This suggests that in these patients, the bicuspid valve in one identical twin was the result of a stochastic developmental event that occurred in the context of a genetic predisposition for calcification. The bicuspid valve related hemodynamic alterations may have played a more minor role in this patients disease process as his twin brother's tricuspid valve also calcified. This study in twins also points to the power of genetics to help explain this disease.

NOTCH1 was the first genetic mutation linked to bicuspid valves and subsequent calcification (Garg et al., 2005). Two separate families were identified with NOTCH1 mutations and bicuspid valves with early onset calcification in the 20-30th year of life. Both families had different mutations in the extracellular domain of NOTCH1, resulting in haploinsufficiency of the receptor via non-sense mediated decay. NOTCH1 is a transmembrane protein that is cleaved upon binding to its ligands, Delta-like 1, 3, and 4 and Jagged 1, and 2, which are expressed on neighboring cells (Bray, 2006). Upon cleavage, the intracellular domain translocates to the nucleus and usually binds to the DNA binding adaptor protein CSL, though interaction with other adaptor proteins is possible (Bray, 2006). Then, co-activators including MAML and histone acetyl transferases are recruited to the CSL complex,

resulting in chromatin modification and target gene activation (Bray, 2006). Presumably, a 50% reduction in the number of receptor molecules would more adverse affect target gene activation in cells with maximal NOTCH signaling activation than cells in which the NOTCH receptor pool is underutilized. In the NOTCH1 haploinsufficient families, HRT1 and HRT2, two canonical NOTCH activated proteins, were shown to inhibit the activity of RUNX2 on the osteocalcin promoter. The authors went on to speculate that decreases in NOTCH1 signaling in the valve interstitial cells resulted in the de-repression of RUNX2 activity. While this data is intriguing and may impact osteoblast like cells already expressing RUNX2, quiescent valve interstitial cells do not express RUNX2. Therefore, the impact of NOTCH1 signaling on the initial molecular events triggering trans-differentiation remains unknown.

Chronic kidney disease (CKD) also results in increased vascular calcification including the aortic valve, compared to age matched controls (Savage et al., 1998). CKD patients have decreased liver function and hyperparathyroidism, resulting in elevated levels of serum phosphates (Johnson et al., 2006). This was originally thought to lead to serum saturation and eventual precipitation of phosphates, triggering hydroxyapatite formation. Hydoxyapatite is the naturally occurring crystal form of calcium and phosphate that mineralizes the extracellular matrix of bones to give them their strength and rigidity (Schoen and Levy, 2005). More recent studies suggest phosphates can directly activate bone related gene expression and subsequent mineralization of valve interstitial cells (Rattazzi et al., 2008). In addition,

CKD patients have elevated levels of parathyroid hormone (PTH) and are treated with phosphate binders and vitamin D, both of which have been shown to exacerbate vascular calcification (Johnson et al., 2006). These observations provide additional clues to the potential molecular underpinnings of valve calcification, though they are more correlations than causations.

Recent clinical studies have identified an association between long–term warfarin therapy and an increased risk of aortic valve calcification (Holden et al., 2007) (Danziger, 2008) (Shea and Holden, 2012). Warfarin therapy is used to prevent blood clotting in at-risk patients by inhibiting vitamin K epoxide reductase. This enzyme recycles inactive vitamin K into its active form and thus blocking it with warfarin decreases the pool of active vitamin K in a patient's body (Schurgers et al., 2007a). Active vitamin K is required by γ-glutamyl carboxylase (GGC) to carboxylate glutamic acid residues of many calcium dependent clotting factors, converting them from an inactive to active form (Danziger, 2008). Also activated via carboxylation in a vitamin K dependent manner are two genes involved in bone formation, bone gla protein (BGP or Osteocalcin) and matrix gla protein (MGP). Considering these bone related genes becomes importanat because patients taking oral anticoagulants have increased amounts of calcium deposition in their coronary arteries and aortic valves (Koos et al., 2005). In addition, rats fed warfarin develop artery and valve calcification in as little as four weeks (Price et al., 1998) (Schurgers et al., 2007b). The warfarin induced clotting defect in these animals was rescued by feeding vitamin K1 (phyloquinone). Vitamin K1 is efficiently shuttled to the liver and thus

preferentially activates clotting factors and not the systemic gla proteins MGP and Osteocalcin. Instead, these proteins are preferentially activated by Vitamin K2 (menaquinone) in the periphery. Thus, the warfarin induced valve calcification is most likely due to peripheral gla protein inactivation, mainly MGP. The mouse knockout of the *Mgp* gene provides additional evidence supporting this conclusion and points to the important role mouse models of calcification have played in understanding the mechanisms of this disease.

1.4.2 Mouse Models of Calcific Aortic Valve Disease

The molecular mechanisms of aortic valve calcification have mostly been studied using mouse models and primary cell culture of valve interstitial cells. Most inbred mouse strains seem highly resistant to spontaneous calcification, unlike humans. Whether this is due to a more active anti-calcific gene program or the result of a much shorter lifespan remains to be determined. Therefore, mouse models usually rely on a diet of high fat or a combination of high cholesterol and cholic acid, in addition to genetic mutations to produce valve calcification (Sider et al., 2011). Numerous studies identify low-density lipoprotein (LDLs) cholesterol as an inducer of vascular and valvular calcification (Sider et al., 2011). Genetic mouse knockouts of the *Ldl receptor* (*Ldlr*) or *Apoe* in addition to a high fat diet also increase the speed of calcification (Ishibashi et al., 1994) (Tanaka et al., 2005). The mouse model with the most severe form of vascular calcification is the *Mgp* -/- mouse (Luo et al., 1997). These mice experience rapid calcification of the whole arterial system including the

valve as well as the epiphyseal plates of the long bones within a few weeks of birth. They die within a month of birth due to aortic rupture after severe calcification, suggesting that MGP is a potent inhibitor of soft tissue calcification. Double knockouts of *Mgp* with Osteopontin show an even greater rate of ectopic bone formation, indicating an active repression of bone gene programs (Speer et al., 2002). Other mouse models of calcific aortic valve disease include knockouts of *Fibulin4, Postn* (increased bicuspid valve incidence)*, Chml, Madh6, Il1rn, and Nos3* (50% bicuspid valves) (Sider et al., 2011). Heterozygotes of *Eln,* persistant Twist1 expression and mice with hypomorphic *Egfr* also have valve calcification phenotypes (Sider et al., 2011).

Because haploinsufficiency of NOTCH1 leads to aortic valve disease in humans, labs have attempted to phenocopy this genetic alteration in mice. *Notch1* (+/-) mice on a high fat diet have a very mild calcification phenotype in their valves (Nigam and Srivastava, 2009). In contrast, *Csl* (+/-) mice on a diet with high cholesterol, sodium cholate and vitamin D3 had increased trans–valvular blood velocity, and increased valve thickness and calcification (Nus et al., 2011). In addition, an endothelial cell specific knockout of the NOTCH ligand, Jagged 1 (*Jag1*), led to development of thickened valves that also calcified during adulthood (Hofmann et al., 2012). It is important to note that this deletion resulted in JAG1 loss in both the endothelium and interstitial cells because the valve interstitial cells arise from the endothelium during development. However, this does indicate that altered NOTCH signaling in immune cells is most likely not playing a role in this disease.

The discrepancy between the *Notch1* and *Csl/Jag1* phenotypes indicates other Notch receptors can compensate for loss of a single copy of the NOTCH1 receptor in mice, unlike in the human case.

1.5 Cellular Origins of Calcifying Osteoblast-like Valve Cells

Many studies have uncovered the signaling mechanisms important for valve interstitial cell (VIC) activation and subsequent calcification using *in vitro* models. Most of these studies rely on more easily obtainable VICs from pig or sheep valves and a more limited number use human derived cells. Human VICs are usually sourced from cadavers or discarded hearts from heart transplants. VICs from calcified human aortic valves are routinely obtained after valve replacement surgery.

Valve interstitial cells are derived from the cardiac cushion endothelium through an epithelial to mesenchymal transition EMT (Combs and Yutzey, 2009). Quiecent VICs (qVICs) serve to maintain the structure and function of the valve matrix and prevent angiogenesis (Liu et al., 2007). Progenitor VICs (pVICs) are a heterogeneous pool of cells either resident within the valve or potentially from a separate progenitor pool such as hematopoietic stem cells or circulating progenitor cells (Liu et al., 2007). pVICs give rise to qVICs and may directly contribute to the pool of osteoblastic VICs (obVICs), cells expressing the bone gene program and contributing to matrix mineralization. During valve injury or disease, qVICs become activated (aVICs) and start expressing smooth muscle actin (Tao et al., 2012). These aVICs are proliferative, migratory and can remodel extracellular matrix,

contributing to cellular repair. Unfortunately, prolonged inflammation and/or presence of bone inducing morphogens can also stimulate aVICs to transdifferentiate into obVICs (Meng et al., 2008) (Yang et al., 2009).

The idea that valve interstitial cells can trans-differentiate into obVICs comes from many years of *in vitro* studies, but these experiments usually push the cells towards this fate with multiple factors including dexamethasone, ascorbic acid, β glycerophosphate, vitamin D3 and/or high levels of BMP proteins (Osman et al., 2006) (Wallin et al., 2001) (Yang et al., 2009). In addition, few markers distinguish subpopulations of interstitial cells and thus these cells are treated as homogeneous. Similar conclusions about the ability of smooth muscle cells to trans– or de–differentiate in atherosclerosis were made based on *in vitro* experiments. Recently, an important *in vivo* study suggests calcifying cells in atheromas may not originate from the resident smooth muscle cell population, instead arising from a multipotent vascular stem cell (MVSC) (Tang et al., 1AD). MVSCs are highly proliferative and differentiate into neurons, Schwann cells and mesenchymal stem cells that subsequently differentiate into chondrocytes, adipoctes, osteblasts, and differentiated smooth muscle cells. Recent evidence suggests the existence of multipotent progenitor cells with similar properties in the human aortic valve. Even in adulthood, the valve endothelium gives rise to interstitial cells through an EMT process similar to valve development (Bischoff and Aikawa, 2011). These newly formed interstitial cells are capable of forming chondrocyte and osteoblast–like cells but not adipocytes. In addition, a very detailed study of the mesenchymal progenitor

cell population of the aortic valve found at least 4 distinct cell phenotypes, some with a higher propensity to differentiate into osteoblasts than others (Chen et al., 2009). It is unclear if these cells are resident populations or circulating progenitors, potentially of a hematopoietic origin. Fate mapping in the adult during the onset of aortic valve disease may help uncover the origin of the calcifying cells, with multiple pools of cell potentially contributing to different types of calcification (ie. LDL/inflammation induced or loss of calcification inhibitors).

1.6 Shear Stress and Vascular Calcification

The ability of endothelial cells to sense and respond to different types of shear forces has been appreciated for over 150 years (Resnick et al., 2003). Different regions of the arterial system experience various forms of shear stress, which is calculated as force over area or dynes/cm^2, with large arteries experiencing 10-40 dynes/cm^2 (Resnick et al., 2003). Most regions of the arterial system are exposed to laminar pulsatile shear stress, which seems atheroprotective as evidenced by a lack of lesion formation (Traub and Berk, 1998). Laminar shear stress activates an initial response and then down-regulates and dampens this response over time (Tzima et al., 2005). On the other hand, the inner curvatures of the aorta, and arterial branch points/bifurcations result in more turbulent fluid flow, and result in alterations in the periodicity and cycle of the shear forces on the endothelium (Davies et al., 2010). These constant changes in shear stress levels result in sustained activation of shear stress related genes including NF–κB regulated inflammatory genes (Tzima et al.,

2005). The backside of the aortic valve experiences very little if any shear stress (Weinberg et al., 2010).

Many studies have attempted to determine the effect of shear stress on endothelial cell gene expression, alterations in endothelial identity, and susceptibility to calcification. One particular study focused on the differential gene expression responses to laminar or oscillatory shear stress by either the aortic or ventricular valve endothelium in vitro (Holliday et al., 2011). While over 1000 genes were activated or repressed when comparing oscillatory to laminar shear stress conditions, very few differences were observed in gene expression between endothelial cells from opposite sides of the valve. This indicates that cells taken out of their normal context and placed *in vitro,* lose the gene expression differences present *in vivo* between each side. Thus, the endothelium from each side of the valve may gain different patterns of gene expression from the physical forces applied *in vivo. KLF2*, *BMP4* and *eNOS*, three canonical shear stress-activated genes, were present in these data. In addition, genes involved in LPS inhibition of retinoid X receptor function, keratin sulfate biosysthesis, and neuregulin signaling were also involved. New fluid mechanics models of the backside of the valve predict little if any shear forces on this endothelium and thus, a more accurate comparison would be no flow versus periodic, laminar flow conditions (Weinberg et al., 2010).

One of the outstanding questions in the field of shear stress and endothelial cell biology is how the cells physically sense these forces. In other words, what is the mechano-sensor for shear stress? Three main possibilities have been proposed

and are not mutually exclusive. The first possibility is through cell-cell adhesions that are stretched during shear stress. A recent study proposes a mechanosensory complex that includes PECAM–1, VE–Cadherin, and VEGFR2. PECAM1 directly transmits mechanical force and with the adaptor protein VE–Cadherin, VEGFR2 activates PI3 Kinase, triggering integrin activation (Tzima et al., 2005). The second possibility is through cell-matrix junctions via integrins. Blocking antibodies to specific integrin subunits have effectively blocked flow-induced vasodialations *in vivo,* though this seems downstream of the mechanosensory complex (Resnick et al., 2003). The third possibility is activation of ion channels, signaling molecules like GPCRs and even changes in membrane fluidity (Li et al., 2005). These three possibilities occur within seconds or minutes of the onset of shear stress and culminate in alterations in transcription factors and ultimately gene expression, culminating in the physiologic response of the cells to this force.

1.7 Stem Cell Models of Valve Disease

The only known genetic mutation associated with bicuspid valves and calcification is in the NOTCH1 receptor (Garg et al., 2005). To gain insight into the molecular mechanisms involved in these patients, induced pluripotent stem cells (iPSCs) were generate from affected and unaffected members of both families identified by Garg et al. (Garg et al., 2005). iPSCs uniquely provide pluripotent stem cell lines with the same genetic mutations as the starting patient derived somatic cells (Takahashi et al., 2007). Successful models of human diseases using this method include Long-QT

syndrome, Marfan syndrome, and Pompe disease (Moretti et al., 2010), (Quarto et al., 2012), (Huang et al., 2011). Differentiating iPS cells into the cell type affected by the disease provides a way to test otherwise unobtainable patient specific cells.

Three main cell types must be considered in order to understand NOTCH signaling related valve calcification. The first are valve interstitial cells, shown to trans-differentiate into osteoblast-like cells. Generating these cells would be very difficult in an *in vitro* setting. The second type are endothelial cells (ECs), which can be generated *in vitro*, though previous protocols are not efficient or reproducible. The third cell type to consider are immune cells as they potentially initiate and exacerbates the disease via inflammatory processes. The endothelial specific knockout of the NOTCH ligand JAG1 in mice resulted in decreased NOTCH signaling in the valve endothelium and interstitial cells, but not cells of the immune system (Hofmann et al., 2012). The valves of these mice calcify over time, potentially ruling out the importance of altered NOTCH signaling in the immune system as the source of the valve disease phenotype in this context. Because the endothelium senses shear stress and NOTCH1 is required for the arterialization of the endothelium during development, we decided to focus on generating endothelial cells from our disease specific iPSCs.

Protocols to differentiate endothelial cells from human pluripotent stem cells have been published, but result in small cell numbers or are hard to reproduce (James et al., 2010) (Kane et al., 2010) (Nourse et al., 2010) (Tatsumi et al., 2011). In addition, these protocols have not adequately compared either A) endothelial cells

derived via these methods to primary cell cultures, or B) endothelial cells derived from embryonic stem cells to induced pluripotent stem cells. This deficiency must be addressed in order to accurately model human disease in a dish.

1.8 Summary of Our Investigation of the Role of NOTCH1 Signaling in Valve Disease

We previously identified two families with aortic valve disease caused by *NOTCH1* mutations, but the mechanism by which premature valve calcification occurs remains unknown. In addition, NOTCH1 is activated by laminar shear stress, a force on the vascular endothelium that alters the rate of vascular calcification. We wondered how alterations in NOTCH1 receptor expression in the context of different levels of shear stress might impact the rate of valve and potentially vascular calcification. In order to interrogate this question, we carried out mRNA-seq using normal Human Aortic Valve Endothelial Cells (HAVECs) with siRNA knockdown of *NOTCH1* in static or laminar shear stress conditions. We believed this would mimick the diseased state and flow patterns of sides of the valve. We found a decrease in many genes involved in epiphyseal plate maintenance including *ITGA1, PLAT, SOX6* in addition to genes like *MGP, CALU, GJA5 and SAT1* that play important roles in atherosclerosis, vascular calcification, and angiogenesis. Other identified genes play a role in aortic valve development and the remodeling of the extracellular matrix. Further analysis of the genome wide occupancy of the NOTCH1 intracellular domain indicates that

many of these genes could be directly targeted for activation by NOTCH1. In some cases, NOTCH1 may interact with an unknown transcription factor other than the canonical CSL. Included in this list of potentially directly targeted genes is *Matrix GLA Protein* (*MGP*), a gene when knocked out in mice leads to the most rapid and severe calcification of the arterial vascular system identified.

MGP inhibits calcification of soft tissue by sequestering bone morphogenetic proteins (BMPs) and is highly expressed in human aortic valves. Altering NOTCH1 levels specifically affected MGP mRNA and protein levels in HAVECs but not in valve interstitial cells. Furthermore, laminar flow activated NOTCH signaling and MGP expression in a NOTCH1-dependent manner in HAVECs. In addition, we have identified a novel endothelial enhancer 20kb upstream of the MGP gene that is bound by NOTCH1 and its canonical DNA binding partner CSL. These studies reveal a novel regulatory pathway in endothelial cells that may function to repress aortic valve calcification.

Next, we set out to test if these potential calcification related regulatory pathways play a role in our NOTCH1 patients. We generated iPS cell lines from multiple affected and unaffected patients from the two separate families with NOTCH1 mutations. We also developed a novel method to generate endothelial cells (ECs) based on normal embryonic development that consistently yielded large numbers of ECs derived from multiple human ES or iPS cells. Mesoderm differentiation of embryoid bodies was maximized and defined growth factors were used to generate KDR^{+} EC progenitors. Magnetic purification of a KDR^{+} progenitor

subpopulation resulted in an expanding, homogeneous pool of ECs that expressed EC markers and had functional properties of ECs. Unfortunately, while this protocol yields cells that are arterial-like, they do not express detectable levels of *MGP,* and thus we were unable to test our hypothesis in patient ECs with NOTCH1 mutations.

Recent evidence suggests human embryonic stem (ES) and induced pluripotent stem (iPS) cell lines have differences in their epigenetic marks and transcriptomes, yet the impact of these differences on subsequent terminally differentiated cells is less well understood. We compared our purified, homogeneous populations of ECs derived from multiple independent human iPS and ES lines to help address this question. Comparison of the transcriptomes from different types of ECs revealed limited gene expression variability between multiple lines of human iPS–derived ECs, or between lines of ES– and iPS–derived ECs. These results demonstrated a method to generate large numbers of pure human EC progenitors and differentiated ECs from pluripotent stem cells, and suggest individual lineages derived from human iPS cells may have significantly less variance than their pluripotent founders.

Chapter 2

Shear Stress Activates an Epiphyseal Plate Gene Program Including Matrix Gla Protein in a NOTCH1 Dependent Manner in Aortic Valve Endothelium

2.1 Contributions

The author has contributed significantly to the work described in this chapter. The author is responsible for the conception and design, provision of study material or patients, collection and/or assembly of data, data analysis and interpretation, writing and critical revision of the manuscript. Christina Theodoris helped with collection and/or assembly of data, data analysis and interpretation. Lei Liu, William Collins and Kathleen W Blue helped with collection and/or assembly of data. Sean Thomas and Alexander Williams provided bioinformatic analysis of genome wide data sets. Joon Lee, Xianzhong Meng, and Robert C. Robbins provided cell lines and human tissues. Kathryn N. Ivey helped with conception and design, and critical revision of the manuscript. Deepak Srivastava helped with conception and design, financial support, critical revision and final approval of manuscript.

2.2 Abstract

We previously identified two families with aortic valve disease caused by *NOTCH1* mutations, but the mechanism by which premature valve calcification occurs remains unknown. We carried out mRNA-seq using normal Human Aortic Valve Endothelial Cells (HAVECs) with siRNA knockdown of NOTCH1 to mimic the diseased state and found a decrease in epiphyseal plate associated genes including *Matrix GLA Protein* (*MGP*). MGP is highly expressed in aortic valves and inhibits calcification of soft tissue by sequestering bone morphogenetic proteins (BMPs). Altering NOTCH1 levels specifically affected MGP mRNA and protein in HAVECs but not in valve interstitial cells. Furthermore, laminar flow activated NOTCH signaling and MGP expression in a NOTCH1-dependent manner in HAVECs. In addition, we have identified a novel endothelial enhancer 20kb upstream of the MGP gene that is bound by NOTCH1 and its DNA binding partner CSL. Our studies reveal a novel regulatory pathway in endothelial cells that may function to repress aortic valve calcification.

2.3 Introduction

Calcific Aortic Stenosis affects roughly 2% of the U.S. population and is the leading cause for valve transplants (Akat et al., 2008). This percentage climbs to 13% when looking at patients between 75 and 85 years of age (Akat et al., 2008). In addition, 25% of patients with bicuspid aortic valves typically develop valve calcification

(Roberts, 1970). While valve transplants can successfully cure this disease, the procedure is invasive, expensive and replacement valves don't last forever. The late onset and progressive nature of this disease make it an ideal candidate for therapeutic intervention. In order to develop an effective therapy, we must continue to interrogate the molecular events that lead to aortic valve calcification.

Aortic valve calcification is associated with multiple risk factors including age, gender, height, hypertension, smoking and cholesterol levels in older patients (Stewart et al., 1997). The hallmarks of valve stenosis include inflammation, extracellular matrix remodeling including fibrosis, valve thickening, angiogenesis and ultimately aberrant osteoblast gene expression leading to calcification (Bossé et al., 2008). In addition, blood flow, or hemodynamic shear stress has been implicated in the progression of aortic valve disease (Butcher and Nerem, 2007). Laminar shear stress seems to be a protective anti-atherosclerotic force that is sensed by the endothelial lining of the arterial system, with regions of disturbed flow more likely to calcify. The endothelium senses shear forces and responds by altering the expression of many genes involved in inflammation and monocyte adhesion. Areas of turbulent or oscillatory blood flow result in an activated endothelium that expresses higher levels of monocyte, leukocyte and T-cell receptors, in addition to increased fenestration of the endothelial barrier (Ghaisas et al., 2000) (Butcher and Nerem, 2007). Calcification of the aortic valve occurs most frequently on the aortic side in the fibrosa layer, which is subject to little if any shear stress (Weinberg et al., 2010).

While there are many factors associated with and leading to valve calcification, the keystone of the disease process is the conversion of interstitial cells to osteoblast-like cells. The aortic valve consists of endothelial cells, mesenchymal interstitial cells and the ECM components collagen, elastin and glycosaminoglycans, which provide strength and flexibility (Schoen, 2008). During valve calcification, inflammation activates valve interstitial cells, leading to their expression of α-smooth muscle actin and subsequent transformation into bone progenitor or osteoblast-like cells. These cells express the osteoblast master regulator RUNX2 and other calcification promoting genes like ALP (alkaline phosphatase), IBSP (bone sialoprotein) and SPARC (osteonectin) (Akat et al., 2008) (Bossé et al., 2008). While many cellular pathways including TGFβ, NOTCH and WNT result in the activation of RUNX2 *in vitro*, the molecular mediators of this activation are unknown (Akat et al., 2008).

NOTCH1 is a transmembrane protein that is cleaved upon binding to it's ligands (Delta-like 1,3,4 and Jagged 1,2), which are expressed on neighboring cells (Bray, 2006). Upon cleavage, the intracellular domain translocates to the nucleus and binds to the DNA binding adaptor protein CSL (Bray, 2006). Then, co-activators MAML and histone acetyl transferases are recruited to the CSL complex, resulting in chromatin modification and target gene activation (Bray, 2006). We have identified two families with aortic valve disease attributed to mutations in NOTCH1, resulting in a range of developmental valve defects and severe, early calcification of the aortic valve (Garg et al., 2005). Affected members of these families have mutations that

create premature stop codons, leading to non-sense mediated decay of the mRNA and ultimately haploinsufficiency of NOTCH1 (Garg et al., 2005).. A candidate approach looking at known NOTCH targets showed that decreased *in vitro* expression of the NOTCH targets HRT1 and HRT2 in COS7 cells resulted in de-repression of RUNX2. However, NOTCH1 is likely to affect numerous targets leading to gene disregulation *in vivo*.

In order to understand the role of NOTCH1 in valve disease, we used a multi-omics approach. mRNA-seq was carried out using normal Human Aortic Valve Endothelial Cells (HAVECs), with and without NOTCH1 siRNA to mimic the diseased state. In addition, fluid flow, or shear stress was applied to the cells to test its effect on endothelial gene expression in the context of the diseased state. Many genes within the endochondral ossification pathway were regulated by NOTCH1 and shear stress including SOX6, PLAT, PTHrP, FGF18, and MGP. ChIP-seq of the NOTCH1 intracellular domain (NICD) identified the genome wide occupancy and potential direct targets of NOTCH1. In addition, our ChIP-seq data suggests that NOTCH1 may be targeting many regions of the genome through a non-canonical interaction with Ets family members. Cross referenceing our RNA-seq and ChIP-seq datasets identified potential targets including genes important for bone and epiphyseal or growth plates (*ITGA1, PLAT, SOX6, MGP, CALU*) and genes that play important roles in atherosclerosis, vascular calcification and angiogenesis (*MGP, CALU, GJA5 and SAT1*). The regulation of MGP by NOTCH1 and shear stress was more deeply

interrogated because the MGP knockout mouse has the most severe arterial/valve calcification phenotype of any knockout mouse (Luo et al., 1997).

MGP inhibits calcification of soft tissues by binding free calcium and BMPs (Akat et al., 2008). Patients treated long term with vitamin K agonists (Warfarin), develop aortic valve calcification through a mechanism thought to involve MGP, which is activated by a vitamin K dependent carboxylase (Schurgers et al., 2004). Our data suggest that MGP is activated by shear stress in a NOTCH1 dependent manner. In addition, NOTCH1 may be directly activating MGP through a novel endothelial enhancer 20 kb upstream of the gene.

2.4 Results

2.4.1 Shear Stress and NOTCH1 Signaling

Normal human aortic valves sections where stained with an antibody specific to NOTCH1 intracellular domain, in order to identify the cellular compartment of active NOTCH1 signaling. There was strong expression in both the valve interstitial cells and endothelial cells lining the valve (Figure 2.1A). NOTCH signaling is important for arterial endothelial cell development and is activated by shear stress from blood flow. Shear stress also seems to be atheroprotective and must be functioning through the endothelium as it senses and responds to these forces. To test the interplay between NOTCH1 signaling and shear stress forces, human aortic valve endothelial cells were isolated and transfected with either control or NOTCH1

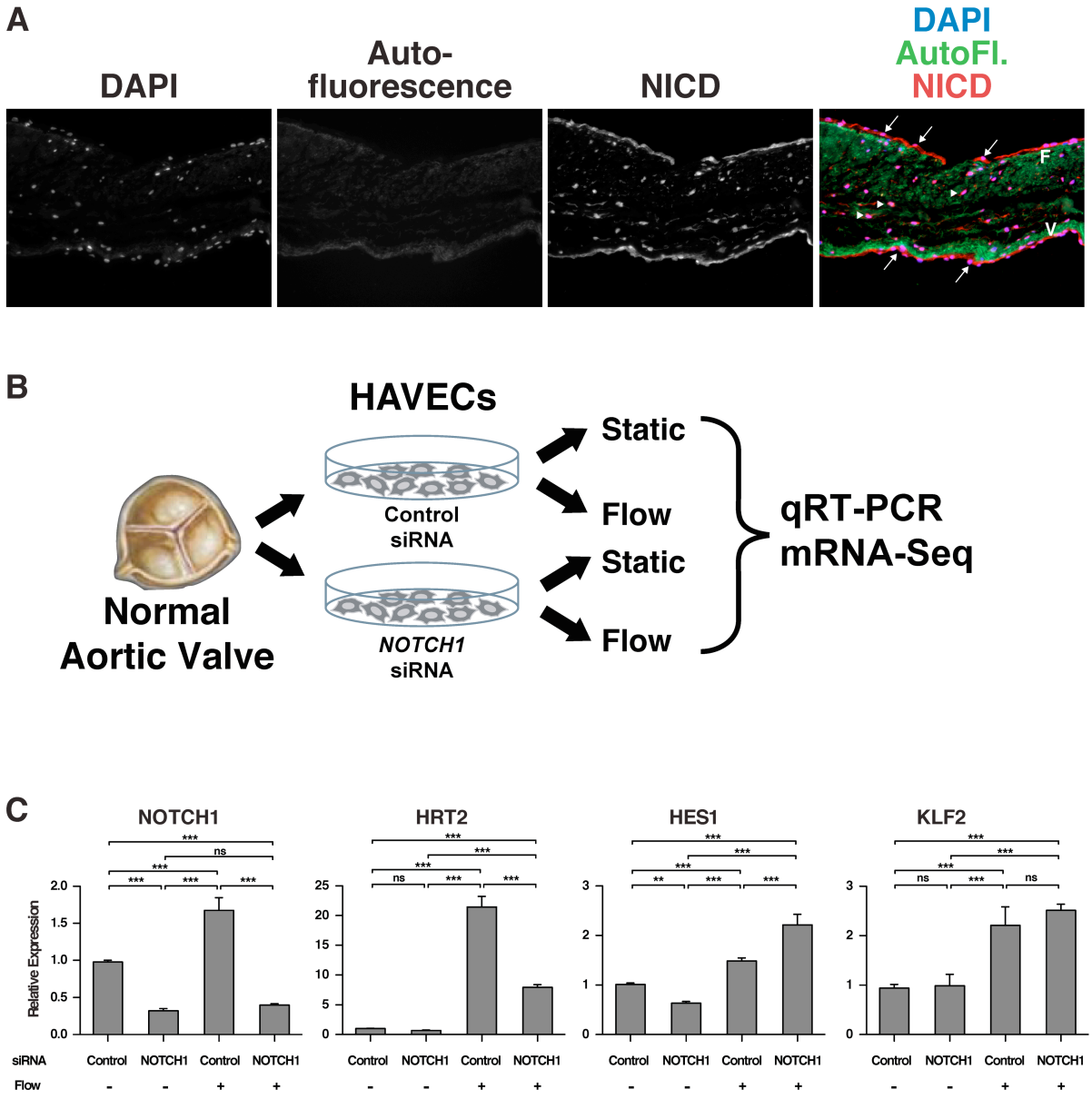

Figure 2.1 NOTCH1 intracellular domain (NICD) is expressed in valve cells and is flow dependent. (A): Normal human aortic valve section stained with an antibody specific to the active form of NOTCH1, NICD (red). NICD is found in both cell types of the valve: endothelial (arrows) and interstitial cells (arrowheads). Autofluorescence (green) shows collagen in the fibrosa layer (F) and elastin fibrils in

the ventricularis layer (V). Nuclei are stained with DAPI (blue). **(B):** Schematic of experimental procedure. NOTCH1 receptor was knocked down in normal HAVECs, which were then placed in static of fluid flow conditions. Cells were harvested and RNA was extracted and analyzed by qRT-PCR or mRNA-seq. **(C):** qRT-PCR analysis of HAVECs from four conditions. NOTCH1 receptor, two canonical direct targets, HES1 and HRT2 and a known flow responsive gene, KLF2, were analyzed. Graphs show mean gene expression relative to the no flow no siRNA condition with error bars representing standard deviation. Statistical significance was determined using one-way ANOVA with Tukey's multiple comparison post hoc test (** $P < 0.01$, *** $P < 0.001$).

---

specific siRNAs. Then, cells from these two treatments were split into static or 15 dynes/cm^2 media flow conditions for a total of four conditions (Figure 2.1B). qRT-PCR confirmed that the *NOTCH1* receptor is indeed activated by shear stress and can be knocked down by siRNA (Figure 2.1C). In addition, canonical NOTCH1 targets, *HRT2* and *HES1,* and a known shear responsive gene *KLF2,* are activated by shear stress conditions (Figure 2.1C).

2.4.2 Transcriptome Profiling of HAVECs

RNA-seq was performed on pools of RNA from biological replicates of each of the four conditions to understand how shear stress and NOTCH1 signaling may be controlling gene regulation on a transcriptome-wide level. Because regions of the

arterial system with laminar blood flow are calcification resistant, including the ventricular side of the aortic valve, and NOTCH1 is thought of as an activator, genes that were activated by flow in a NOTCH1 dependent manner were identified in the RNA-seq data. Pathways overrepresented in this data set were identified with GO-Elite and GenMAPP-CS and included Heart Development, Complement Activation and Endochondral Ossification (Tables 2.1, 2.2). The genes involved in heart development include important valve development regulators TWIST1, HEY1 & 2, FOXC1 and BMP2. The endochondral ossification pathway members include many genes important for maintaining epiphyseal plates, such as SOX6, PLAT, PTHrP, FGF18, and MGP (Figure 2.2).

Table 2.1 Pathways Associated with Genes Activated by Flow by 2 Fold.

MAPP Name	# Changed	# Measured	# on MAPP	Z Score	Adjusted P	Gene symbols
GPCRs	20	59	261	5.94	0.05	CNR1|CXCR4|EDNRA|F2R|F2RL2|F2RL3|GPR173|GPR21|GPR37|GPR4|GPR52|GPR75|HTR2B|LPAR5|OPN1SW|OR10A4|P2RY1|P2RY2|P2RY6|TBXA2R
Endochondral Ossification	14	41	64	4.99	0.05	ADAMTS1|ADAMTS4|ALPL|CHST11|FGF18|FGFR3|GHR|MGP|PLAT|PTHLH|SLC38A2|SOX6|TGFB1|VEGFA
Heart Development	11	30	44	4.71	0.05	BHLHE40|BMP2|BMPR2|FOXC1|GATA6|HEY1|HEY2|SHH|TBX20|VEGFA|VEGFC
Vitamin A Metabolism	7	17	39	4.14	0.05	BCMO1|CYP26B1|DHRS3|RARB|RARG|RDH10|RXRB
Complement and Coagulation	7	19	62	3.76	0.07	C9|F2R|MASP1|PLAT|PLAUR|SERPIN

						E1|THBD
Complement Activation	3	5	17	3.62	0.13	C9|CD55|MASP1
Matrix Metalloproteinases	6	16	31	3.54	0.08	MMP1|MMP10|MMP2|MMP24|MMP25|TIMP1
Nucleotide GPCRs	3	6	11	3.16	0.18	P2RY1|P2RY2|P2RY6
Nuclear Receptors	7	24	38	3.00	0.13	NR4A1|NR4A2|PGR|RARB|RARG|RXRB|VDR
TGF Beta Signaling	10	43	54	2.76	0.16	ENG|INHBA|JAK1|LIF|SERPINE1|SMAD6|SMAD7|SMAD9|TGFB1|TGFBR1
Id Signaling	8	35	52	2.40	0.24	ACVRL1|BMP2|BMPR2|FLT1|ID1|MSC|NGF|VEGFA

Table 2.2 Pathways Associated with Genes Activated by Flow by 2 Fold and are NOTCH1 Dependent.

MAPP Name	# Changed	# Measured	# on MAPP	Z Score	Adjusted P	Gene symbols
Heart Development	8	30	44	7.03	0.02	BHLHE40|BMP2|FOXC1|GATA6|HEY1|HEY2|SHH|VEGFA
Complement Activation	3	5	17	6.95	0.02	C9|CD55|MASP1
Endochondral Ossification	9	41	64	6.56	0.02	ALPL|FGF18|FGFR3|MGP|PLAT|PTHLH|SOX6|TGFB1|VEGFA
Complement and Coagulation Cascades	5	19	62	5.49	0.02	C9|F2R|MASP1|PLAT|THBD
GPCRs	7	59	261	3.60	0.08	F2R|F2RL2|F2RL3|GPR173|LPAR5|OR10A4|P2RY6
Adipogenesis	7	84	131	2.51	0.97	BMP2|EGR2|GATA3|LIF|PTGIS|TGFB1|TWIST1

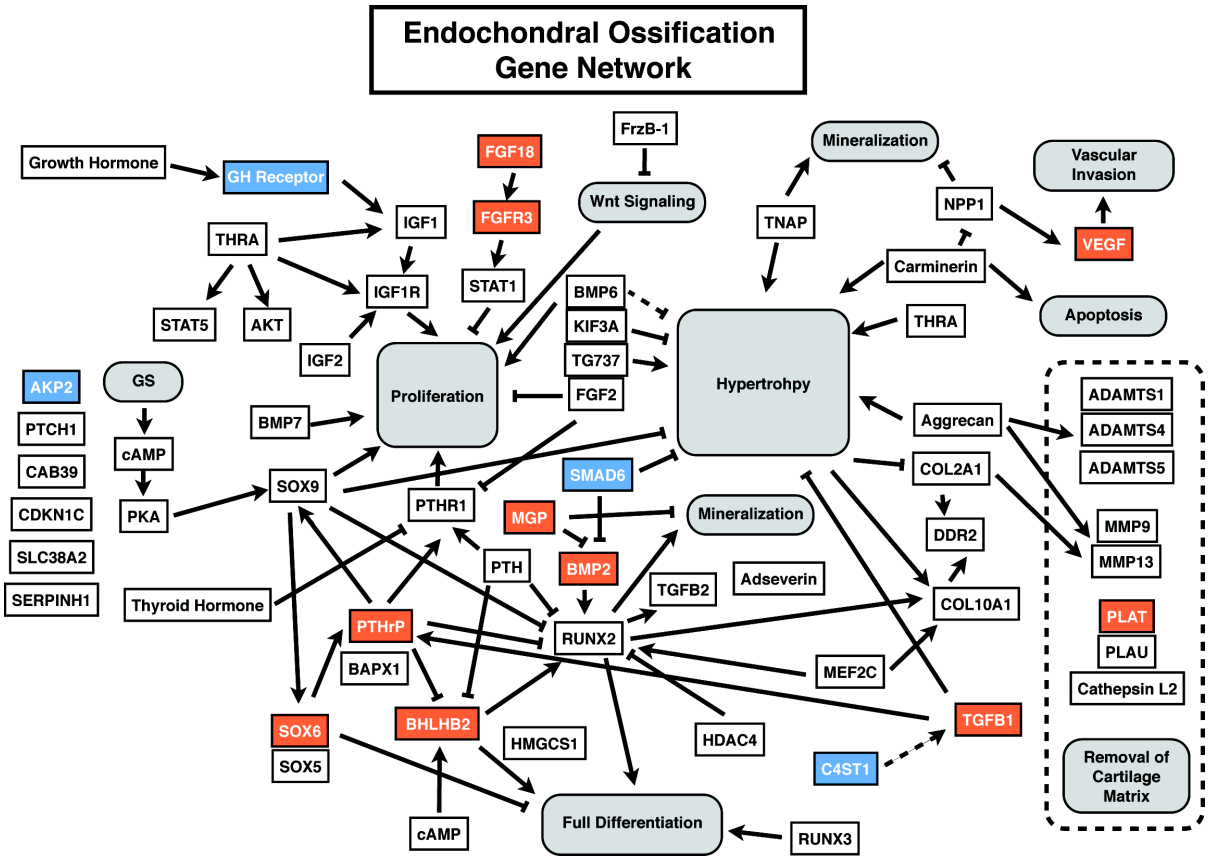

Figure 2.2 Endochondral Ossification Gene Network. Genes highlighted in blue are activated by flow (≥ 2 fold change control vs. flow) and those in orange are activated by flow (≥ 2 fold change control vs. flow) and NOTCH1 dependent (≤ 0.5 control flow vs NOTCH1 siRNA flow).

2.4.3 Genomewide NOTCH1 Binding in HAVECs

In addition to RNA-seq, ChIP-seq was performed using human aortic valve endothelial cells infected with a lentivirus containing a CMV promoter driving myc tagged NICD. Attempts to perform ChIP-seq with NICD antibodies and endogenous levels of NICD were unsuccessful. Roughly 6400 peaks were identified to fall within

20kb of a gene transcriptional start site. Enriched transcription factor binding motifs were predicted with various algorithms for each peak.

2.4.4 NOTCH1 Binding Site Motif Analysis

Transcription factor binding motif prediction was used to identify potential DNA binding partners and regulators of NOTCH1 throughout the genome. Surprisingly, the canonical DNA binding adaptor protein CSL was only predicted in 15% of the peaks identified. 45% of the peaks contained motifs similar to the Ets family of proteins. There are 18 Ets family members expressed in HAVECs, with *ERG*, *ELK4*, *ETS1* and *FLI1* being the most highly expressed.

2.4.5 Direct NOTCH1 Target Prediction

The NOTCH1 ChIP-seq data was then combined with the RNA-seq data to begin to build a list of potential direct targets of NOTCH1 in endothelial cells. In order to find genes that are impacted by shear stress and NOTCH1 signaling, we focused on two patterns of gene expression. Pattern 1 contained genes activated by shear stress in a NOTCH1 dependent manner and Pattern 2 contained genes repressed by shear stress in a NOTCH1 dependent manner (Figure 2.3 and Table S2.3). These two patterns can then we broken down into potential NOTCH1 targets (Figure 2.3 A & B)

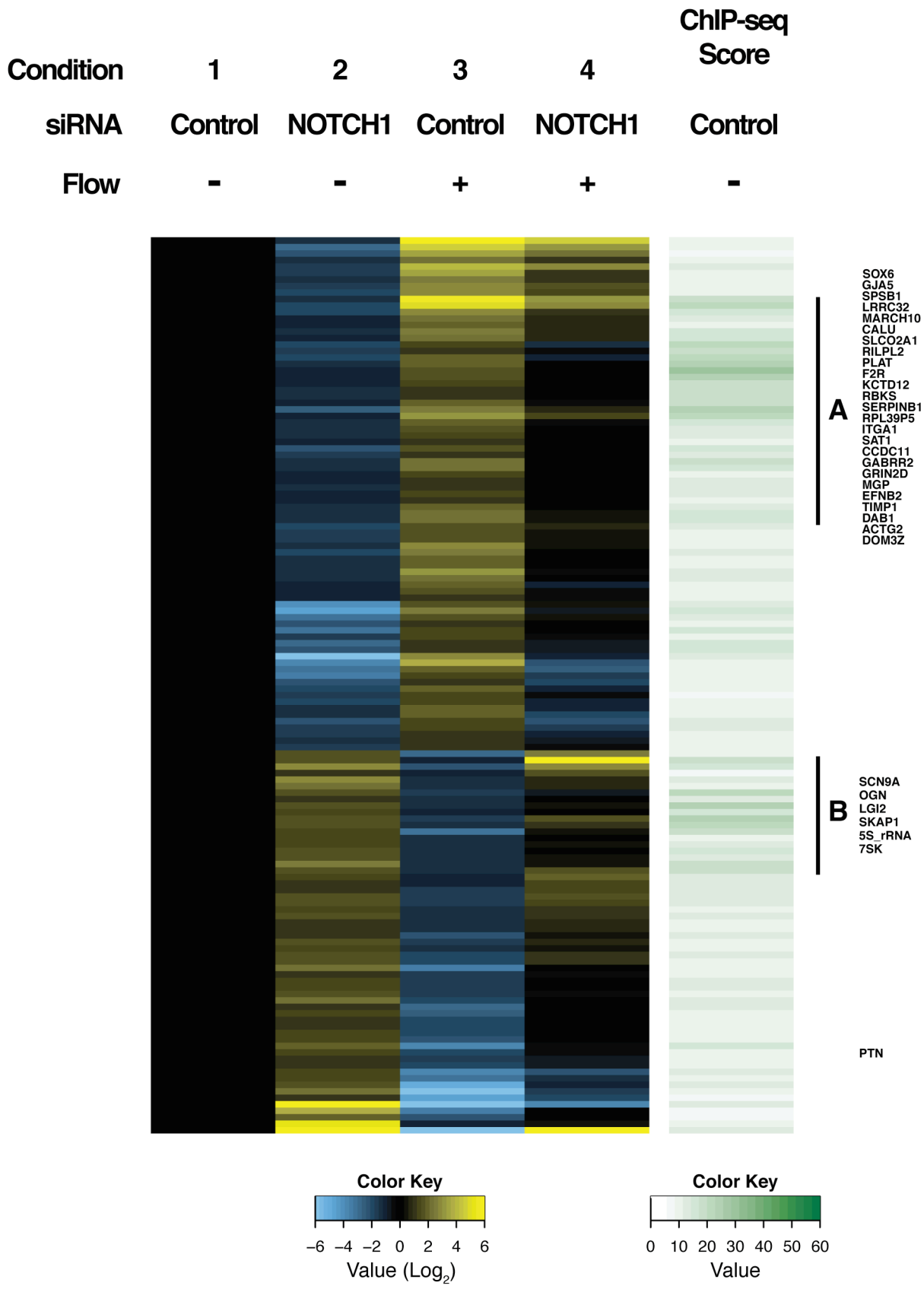
Condition
1
2
3
4
ChIP-seq Score
siRNA
Control
NOTCH1
Control
NOTCH1
Control
Flow
-
-
+
+
-
SOX6
GJA5
SPSB1
LRRC32
MARCH10
CALU
SLCO2A1
RILPL2
PLAT
F2R
KCTD12
RBKS
SERPINB1
RPL39P5
ITGA1
SAT1
CCDC11
GABRR2
GRIN2D
MGP
EFNB2
TIMP1
DAB1
ACTG2
DOM3Z
A
SCN9A
OGN
LGI2
SKAP1
5S_rRNA
7SK
B
PTN
Color Key
−6 −4 −2 0 2 4 6
Value (Log2)
Color Key
0 10 20 30 40 50 60
Value

Figure 2.3 Heatmap and clustering analysis of gene expression and ChIP-seq score. The expression of each gene was normalized to the siRNA control, no flow condition and then Log_2 transformed. Displayed genes were identified by matching to two patterns: 1) at least 2 fold down upon NOTCH1 siRNA knockdown in both static and flow conditions, and at least 2 fold up in flow control siRNA condition compared to static, or 2) at least 2 fold up in NOTCH1 siRNA knockdown in both static and flow conditions, and at least 2 fold down in flow control siRNA condition compared to static. ChIP-seq score shows the value for the highest ChIP peak +/- 20 kb from the TSS of each gene. Groups A and B indicate genes that may be direct targets of NOTCH1 based on ChIP-seq score.

and non-targets. Potential targets directly repressed by NOTCH1 and shear stress include *Osteoglycin* or *Osteo Inductive Factor* (*OGN or OIF*), a glycoprotein that inhibits osteoclasts and is known to induce ectopic bone formation along with TGFβ1. *Pleiotrophin* (*PTN*) is also repressed by NOTCH1 and shear stress, though it doesn't seem to be a direct NOTCH1 target. Potential targets activated directly by NOTCH1 and shear stress include genes important for bone and growth plates (*ITGA1, PLAT, SOX6, MGP, CALU*) and genes that play important roles in atherosclerosis, vascular calcification and angiogenesis (*MGP, CALU, GJA5 and SAT1*) (Figure 2.4, 2.5 and Table S2.2). The *MGP* knockout mouse has the most

severe ectopic calcification phenotype of any knockout mouse, with epiphyseal plates and the arterial system including valves turning to bone within weeks of birth (Luo et al., 1997). For this reason, the regulation of MGP by NOTCH1 was explored in greater detail.

2.4.6 Matrix Gla Protein Characterization

Localization of MGP protein expression in human aortic valves has not been reported to date, so both uncarboxylated, inactive (ucMGP) and λ-carboxylated, active MGP (cMGP) protein expression levels were assayed via immunofluorescence using conformation specific antibodies. Both forms of MGP are expressed in the valve endothelial and interstitial cells, though the active form seems higher in the endothelium and the inactive form more prevalent in the interstitial cells (Figure 2.6A). MGP binds BMP2, a protein that activates SMAD signaling leading to phosphorylation of SMADs 1, 5 and 8 (pSMAD1/5/8). Active BMP signaling as shown by pSMAD1/5/8 staining was present in both endothelial and interstitial cells, though the highest expression was on the aortic side of the valve similar to Ankeny et al. (Ankeny et al., 2011) (Figure 2.6A). qRT-PCR validation in HAVECs showed that *MGP* expression levels were activated by shear stress in a NOTCH1 dependent manner (Figure 2.6B). Furthermore, chemical inhibition of NOTCH1 with DAPT showed a dose dependent decrease in the active cMGP isoform (Figure 2.6C). In addition, lentiviral over-expression of NICD1 induced higher levels of cMGP in endothelial cells but not in interstitial cells (Data not shown).

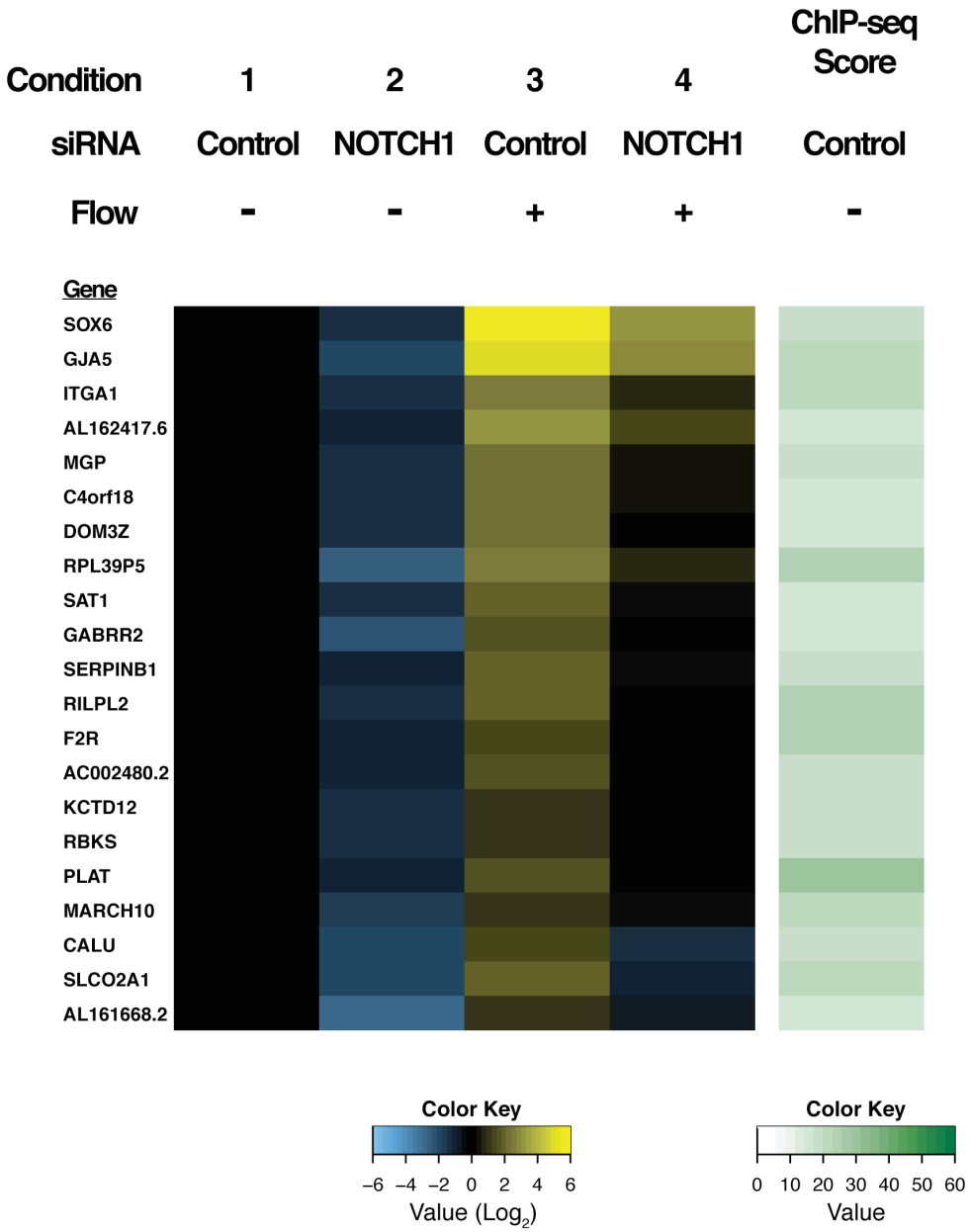

Figure 2.4 Heatmap and clustering analysis of gene expression and ChIP-seq score Cluster A. The expression of each gene was normalized to condition 1 and then Log_2 transformed. Displayed genes were identified by at least 2 fold down upon NOTCH1 siRNA knockdown in both static and flow conditions, at least 2 fold up in flow control siRNA condition compared to static and a ChIP-seq score above 13.

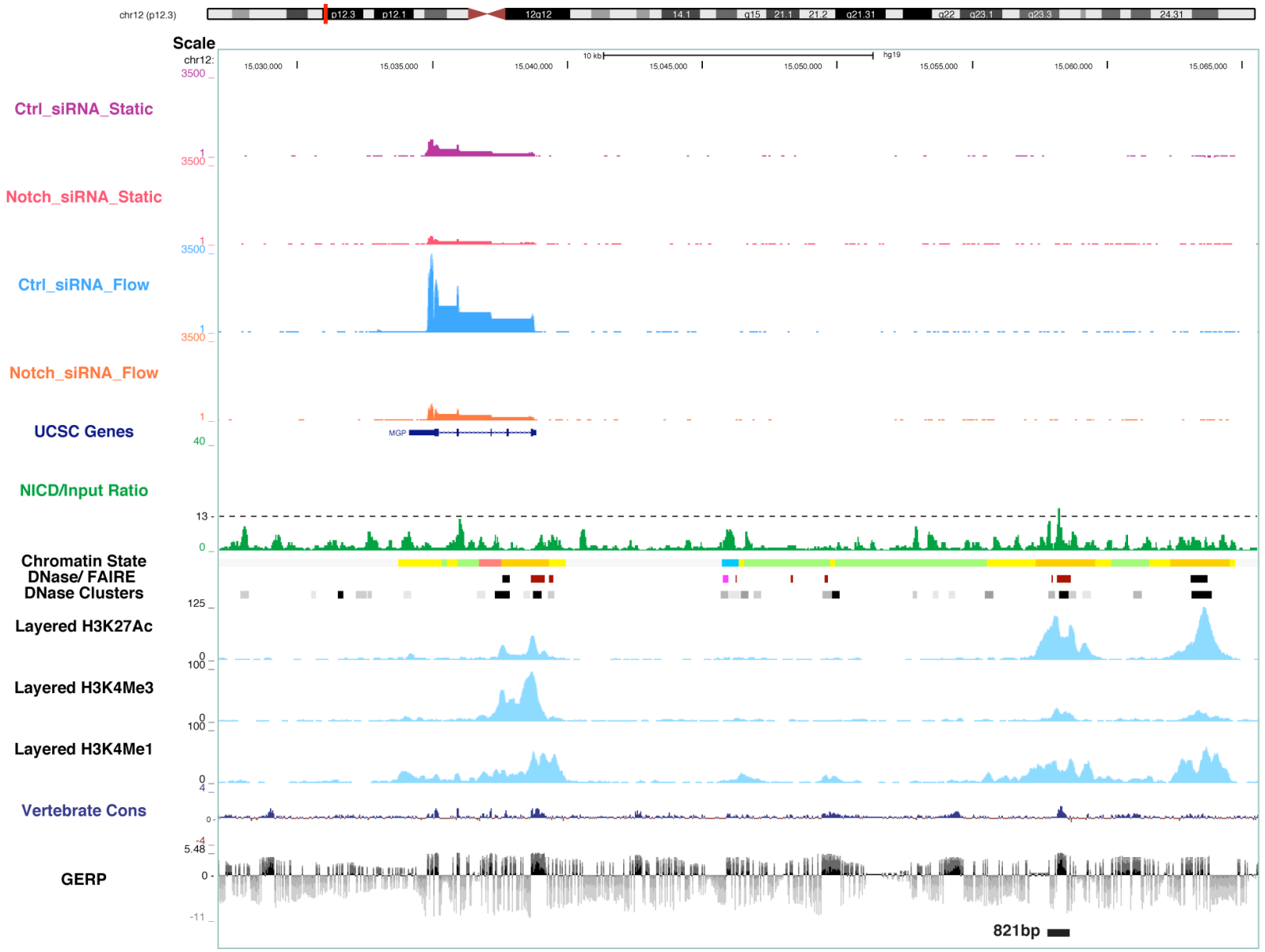
chr12 (p12.3)
p12.3
p12.1
12q12
14.1
q15
21.1
21.2
q21.31
q22
q23.1
q23.3
24.31
Scale
chr12:
15,030,000
15,035,000
15,040,000
10 kb
hg19
15,045,000
15,050,000
15,055,000
15,060,000
15,065,000
Ctrl_siRNA_Static
Notch_siRNA_Static
Ctrl_siRNA_Flow
Notch_siRNA_Flow
UCSC Genes
MGP
NICD/Input Ratio
Chromatin State
DNase/ FAIRE
DNase Clusters
Layered H3K27Ac
Layered H3K4Me3
Layered H3K4Me1
Vertebrate Cons
GERP
821bp

Figure 2.5 Overview of genomic region containing the MGP gene locus.

Purple/Red/Blue/Orange Histogram Tracks show RNA-seq reads for MGP and are labeled with the four culture conditions. **NICD/Input Ratio** shows a histogram of NICD-myc ChIP-seq results with a threshold of 13 as the cutoff between background and real called peaks. Data from HUVEC cell lines in UCSC genome browser and the ENCODE project are labeled as follows: **Chromatin State** colors indicate types of regulatory regions such as strong enhancer (orange), weak/poised enhancer (yellow), insulator (blue), transcriptional transition/elongation (green) and active promoter regions (red); **DNAse/FAIRE** displays open chromatin and transcription factor binding sites with black bars representing peaks identified by both DNase1 hypersensitivity and FAIRE assay and red bars representing lower significance peaks; **DNAse Clusters** indicate open chromatin (grey boxes) and intensity of signal strength is indicated by the box darkness; **H3K27Ac** indicates active regulatory elements, **H3K4Me3** is often found near promoters and **H3K4Me1** is often found near regulatory elements. **Vertebrate conservation** shows measurements of sequence conservation using the *phyloP* method from human to zebrafish with blue peaks showing more conservation. Genomic Evolutionary Rate Profiling (GERP) shows evolutionary constraint with positive scores indicating a substitution deficit.

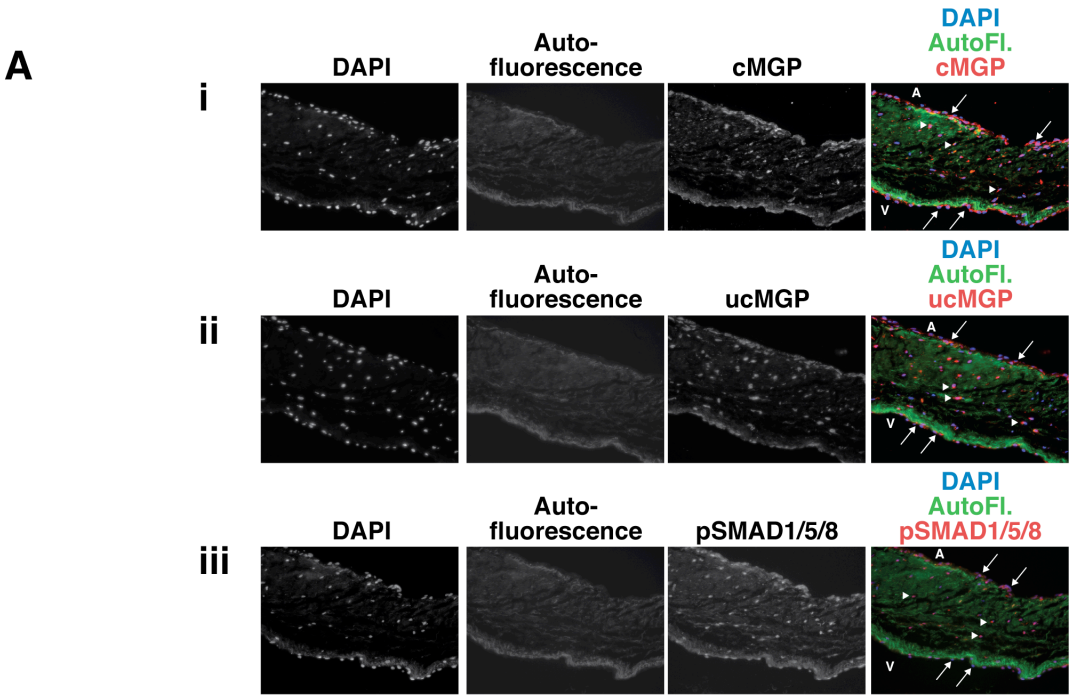
A
i
DAPI
Auto-
fluorescence
cMGP
DAPI
AutoFl.
cMGP
A
V
ii
DAPI
Auto-
fluorescence
ucMGP
DAPI
AutoFl.
ucMGP
A
V
iii
DAPI
Auto-
fluorescence
pSMAD1/5/8
DAPI
AutoFl.
pSMAD1/5/8
A
V

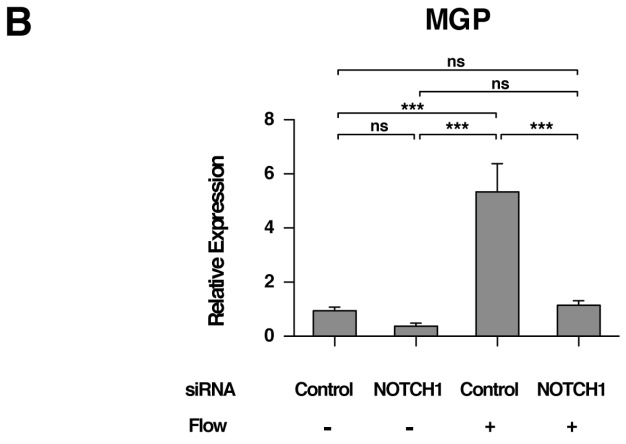
B
MGP
ns
ns
***
ns
***
***
Relative Expression
8
6
4
2
0
siRNA
Control
NOTCH1
Control
NOTCH1
Flow
-
-
+
+

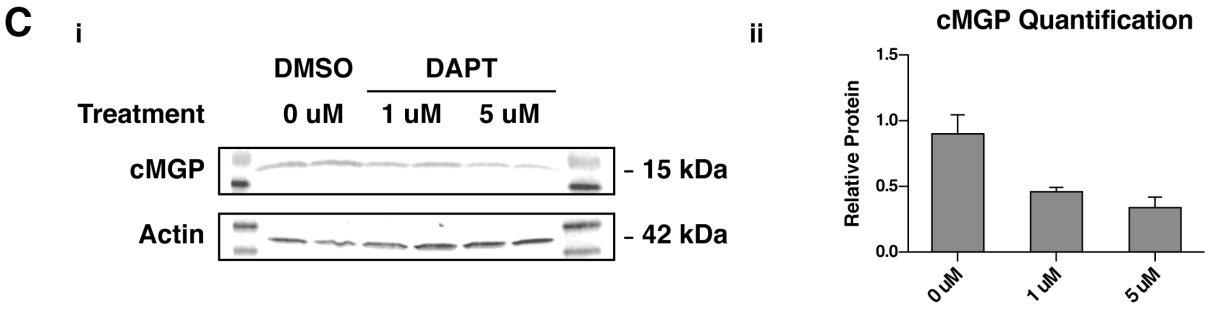
C
i
DMSO
DAPT
Treatment
0 uM
1 uM
5 uM
cMGP
- 15 kDa
Actin
- 42 kDa
ii
cMGP Quantification
Relative Protein
1.5
1.0
0.5
0.0
0 uM
1 uM
5 uM

Figure 2.6 MGP is NOTCH1 dependent. (A): Normal human aortic valve section stained with an antibody specific to: i. cMGP, the active, carboxylated form of MGP; ii. ucMGP, the inactive, uncarboxylated form of MGP; and iii. phosphoSMAD 1/5/8 (pSMAD1/5/8), an indicator of active BMP signaling. cMGP, ucMGP and pSMAD1/5/8 (red) are found in both cell types of the valve: endothelial (arrows) and interstitial cells (arrowheads). pSMAD1/5/8 may have stronger expression on the aortic side of the valve (A). Autofluorescence (green). Nuclei are stained with DAPI (blue). **(B):** qRT-PCR analysis of MGP gene expression in HAVECs from four conditions was analyzed. Graph shows mean gene expression relative to the no flow no siRNA condition with error bars representing standard deviation. Statistical significance was determined using one-way ANOVA with Tukey's multiple comparison post hoc test (* $P < 0.05$). **(C):** Western Blot of active MGP. (i): The active form of MGP shows a does dependent decrease in protein expression in HAECs upon addition of the γ-secretase inhibitor DAPT, which degreases NOTCH signaling. (ii): Quantification of cMGP protein expression level adjusted to the loading control β-actin. Error bars show standard deviation.

2.4.7 Potential Direct Activation of MGP

The gene and protein expression level changes and the ChIP-seq data suggest that NOTCH1 may be directly activating MGP. The only significant NOTCH1 ChIP-seq peak identified lies 20kb upstream of MGP between MGP and its closest gene

ERP27 (Figure 2.7A). This ChIP-seq peak lies within a region of the genome from an endothelial cell line (HUVEC) that displays many markers of an active regulatory region. These include markers of accessible open chromatin (DNAse1 hypersensitivity, FAIRE) and H3K27ac/H3K4me1 histone marks, which both show a pattern with a dip, indicating a region bound by transcription factors that displace nucleosomes (Ernst et al., 2011). This data is used to predict a “strong enhancer” chromatin state for this region, marked by an orange bar. In addition, this region is conserved throughout vertebrate evolution from human to zebrafish and Genomic Evolutionary Rate Profiling (GERP) shows evolutionary constraint with a substitution deficit. Finally, the NICD DNA binding partner, CSL, is predicted to bind to a pair of strong CSL motifs 6bp apart and a third weaker site 15bp upstream in the potential enhancer. ChIP followed by qRT-PCR validated this region as enriched for NICD signal to a similar degree as a canonical, validated HES1-NICD/CSL binding site (Figure 2.7B). In addition, electrophoretic mobility shift assays indicate that CSL is capable of binding both strong CSL sites (Fig 2.7C). In order to test the activity of the putative enhancer, we generated transient transgenic mice containing a wildtype (Wt) or 3X CSL Mutant (3X Mut), 821 base pair enhancer region with a minimal promoter driving LacZ (Fig 2.7D). Strong expression of the LacZ reporter in the large vessels of the arterial system including the aorta, branching arteries, pulmonary artery and aortic valve of the Wt enhancer mice (2/6 mice) was the only consistent pattern of expression and was completely absent in the 3X Mut enhancer mice (0/6) (Figure 2.7D).

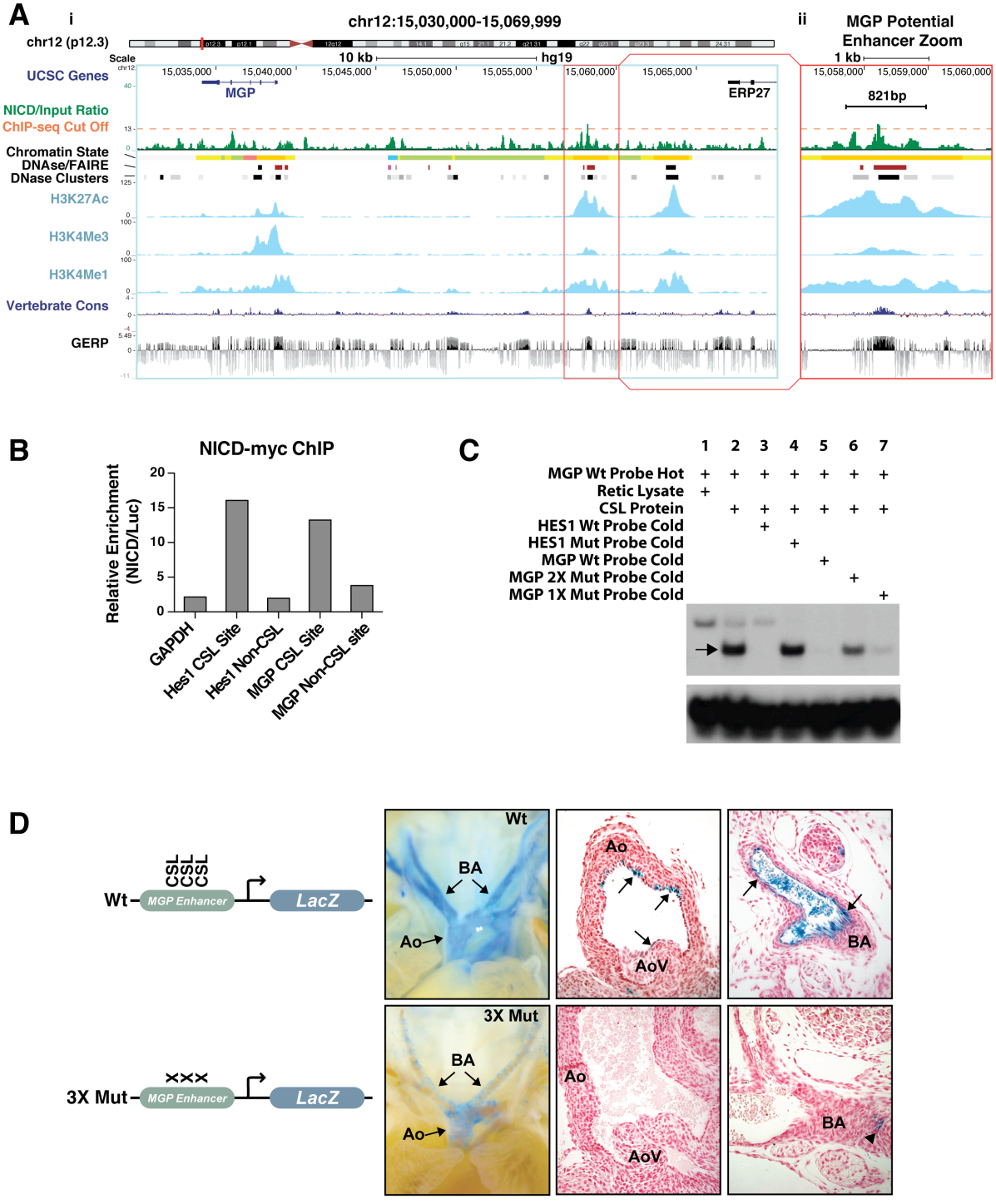
A
i
chr12:15,030,000-15,069,999
chr12 (p12.3)
Scale
10 kb
hg19
UCSC Genes
MGP
ERP27
NICD/Input Ratio
ChIP-seq Cut Off
Chromatin State
DNAse/FAIRE
DNase Clusters
H3K27Ac
H3K4Me3
H3K4Me1
Vertebrate Cons
GERP
ii
MGP Potential
Enhancer Zoom
1 kb
821bp
B
NICD-myc ChIP
Relative Enrichment
(NICD/Luc)
GAPDH
Hes1 CSL Site
Hes1 Non-CSL
MGP CSL Site
MGP Non-CSL site
C
MGP Wt Probe Hot
Retic Lysate
CSL Protein
HES1 Wt Probe Cold
HES1 Mut Probe Cold
MGP Wt Probe Cold
MGP 2X Mut Probe Cold
MGP 1X Mut Probe Cold
D
Wt
CSL
CSL
CSL
MGP Enhancer
LacZ
3X Mut
BA
Ao
AoV

Figure 2.7 Potential MGP Endothelial Enhancer. (**A):** Overview of genomic region containing the MGP gene locus. **NICD/Input Ratio** shows a histogram of NICD-myc ChIP-seq results with a threshold of 13 as the cutoff between background and real called peaks. Data from HUVEC cell lines in UCSC genome browser and the ENCODE project are labeled as follows: **Chromatin State** colors indicate types of regulatory regions such as strong enhancer (orange), weak/poised enhancer (yellow), insulator (blue), transcriptional transition/elongation (green) and active promoter regions (red); **DNAse/FAIRE** displays open chromatin and transcription factor binding sites with black bars representing peaks identified by both DNase1 hypersensitivity and FAIRE assay and red bars representing lower significance peaks; **DNAse Clusters** indicate open chromatin (grey boxes) and intensity of signal strength is indicated by the box darkness; **H3K27Ac** indicates active regulatory elements, **H3K4Me3** is often found near promoters and **H3K4Me1** is often found near regulatory elements. **Vertebrate conservation** shows measurements of sequence conservation using the *phyloP* method from human to zebrafish with blue peaks showing more conservation. Genomic Evolutionary Rate Profiling (GERP) shows evolutionary constraint with positive scores indicating a substitution deficit. The region boxed in orange indicates the potential endothelial enhancer region of MGP where NICD1 may bind and the black bar indicates the 821bp cloned for further enhancer studies. **(B):** ChIP-qRT-PCR with NICD1-myc. Relative enrichment is shown for each site: positive control HES1 NOTCH1/CSL binding site, negative controls GAPDH transcriptional start site and HES1 non-CSL binding site, and MGP

test sites at the predicted CSL binding sites within the 821bp potential binding site and a negative control site. The HES1 and MGP non-CSL binding sites are located approximately 2kb from the CSL binding sites. **(C):** EMSA showing CSL binding to MGP potential enhancer. A 46bp double stranded oligo surrounding the NICD1-myc ChIP-seq peak was labeled with ^{32}P-dCTP and mixed with CSL protein and the indicated non-radiolabeled (cold) competitor probes. Wt indicates the wild type CSL binding sequence and Mut indicates the CSL binding site or sites have been mutated. Arrow indicates the shifted oligo when CSL is added. Reticulocyte lysate only causes a higher, non-specific shift band. **(D):** An 821bp region surrounding the potential MGP endothelial enhancer was cloned into a construct with an Hsp68 minimal promoter driving LacZ and then, the three predicted CSL binding sites were mutated. Both construct were delivered via pronuclear injection into FVB/N mice, which were harvested at e16.0. Mice containing the Wt enhancer had strong endothelial cell expression of LacZ (blue) in the large vessels of the arterial system and some weak expression in the aortic valve (arrows) (2/6 PCR positive animals) and the only expression observed in this region in the mutant enhancer was weaker expression in the smooth muscle layer (arrowhead) (1/6 PCR positive embryos). Sections were counterstained with Eosin (red). Aorta (**Ao**), Branching arteries (**BA**), Aortic Valve (**AoV**).

2.4.8 Retinoic Acid Activation of MGP

Retinoic acid, a natural metabolite of Vitamin A, has been shown to activate Matrix Gla Protein expression in chondrocytes, osteblasts, osteosarcoma cells and fibroblasts and repress expression in breast cancer and rat kidney cell lines (Cancela and Price, 1992) (Kirfel et al., 1997). When treated with retinoic acid, human aortic endothelial and aortic valve interstitial cells activate MGP gene expression by two fold (Figure 2.8).

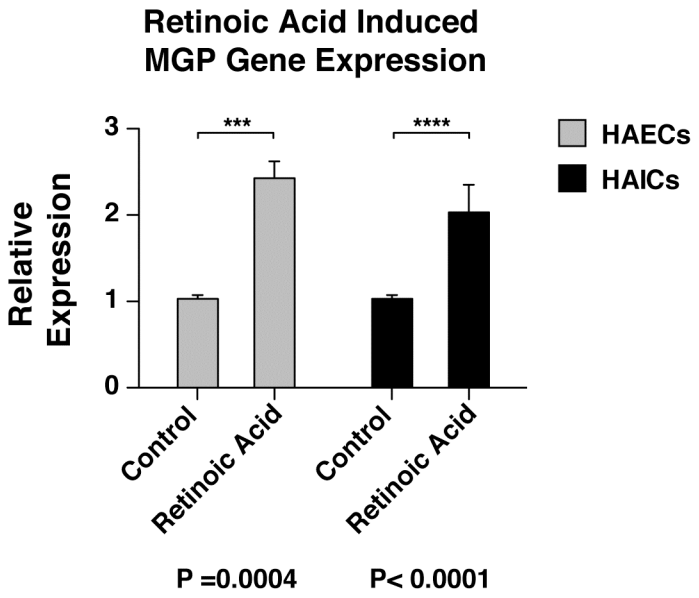

Figure 2.8 Retinoic acid induced MGP gene expression. Mean expression of MGP compared to GAPDH with error bars representing standard deviation is shown in two cell lines, HAECs and HAICs. 30 mg/mL retinoic acid was added to media for 24 hours. Mean values are statistically different between untreated and retinoic acid

treated conditions when compared with two-tailed unpaired t test (*** P= 0.0004, **** P< 0.0001).

2.5 Discussion

2.5.1 Discussion Summary

In order to develop effective treatments capable of preventing or even reversing valve calcification, we must define the detailed molecular mechanisms that occur in both cell types of the aortic valve during the disease process. Valve interstitial cells have been extensively studied due to their activation and subsequent differentiation into osteoblasts, the cell type responisible for matrix mineralization. On the other hand, the valve endothelium's role in valve calcification beyond inflammatory modulation is less well understood. This study provides the first genome wide survey of the role of NOTCH1 and shear stress in human aortic valve endothelium. Whole transcriptome profiling coupled with ChIP-seq provide evidence that members of the gene network responsible for maintaining a non-calcified region of proliferating chondrocytes in long bones, known as the eiphyseal or growth plate, are responsive to shear stress in a NOTCH1 dependent manner. Included in this list is MGP, the most potent inhibitor of ectopic calcification in mice.

2.5.2 NOTCH1 Binding Site Motif Analysis

Our study is the first to profile the genome wide occupancy of NOTCH1 in endothelial cells. One surprising outcome of the motif enrichment analysis of our NICD peaks is the lack of CSL binding sites. We predicted a CSL binding motif in only 15% of our NICD peaks, while 45% of the peaks have an Ets family member binding site such as ELK1 or Ets1. The presence of Ets family motifs in NOTCH ChIP-seq data has been described in Wand et al. (Wang et al., 2011). These transcription factors play an intimate role in the development and maintenance of endothelial cells. In the context of NOTCH1 binding, Ets factors may simply mark activate euchromatin as this family of transcription factors activates most endothelial specific genes. On the other hand, they may provide a DNA binding partner, allowing NOTCH1 to activate cell type specific gene networks independent of CSL binding. Indeed, NOTCH1 has been shown to physically interact with cell type specific transcription factors in T-ALL cells, potentially leading to co-operative cell type specific gene activation (Yatim et al., 2012).

2.5.3 Shear Stress and the Endothelial Regulation of Osteogenesis

The endothelium functions as a selectively permeable physical barrier between blood and tissue that can react to stimuli. In addition, endothelial cells directly help prevent vascular calcification. In valve and arterial calcification, it is thought that the primary function of the endothelium is to modulate immune cells and the molecules they secrete. A breakdown of this endothelial barrier leads to progressive

inflammation, triggering calcification. Recently, however, the endothelium has been implicated in playing a more active and direct role in modulating the phenotype of underlying cells such as the interstitial and vascular smooth muscle cells in the valve and arterial system respectively (Cola et al., 2004). Shear stress is also sensed by the endothelium and seems to alter not only the inflammatory properties of the endothelium, but also a host of other gene programs. This study shows that the endothelium reacts to shear stress in a NOTCH1 dependent manner, resulting in altered expression of many genes important for maintaining the growth plates of long bones. Many genes in this group include secreted factors that may act non-cell autonomously on underlying cell populations. Indeed, the endothelium has been shown to effect the osteogenesis of vascular smooth muscle cells undergoing calcification (Shin et al., 2004) and can signal to valve interstitial cells to maintain a quiescent phenotype characterized by lower expression levels of smooth muscle actin (Butcher and Nerem, 2006).

2.5.4 NOTCH1 and Shear Stress Repress OGN and PTN

Two important bone-stimulating proteins, osteoglycin (OGN) and pleiotrophin (PTN), are repressed by shear stress in a NOTCH1 dependent manner. Osteoglycin is a proteoglycan involved in collagen I fibrilogenesis and has been implicated in enhancing osteoblast mineralization (Ge, 2004) (Tanaka et al., 2012). Pleiotrophin is pro-angiogenic secreted growth factor that can trigger inflammation and fibrosis, and induces osteoblast proliferation and differentiation (Perez-Pinera et al., 2008) (Yokoi

et al., 2011) (Zhou et al., 1992) (Yang et al., 2003). In addition, periostin knockout mice have loss of NOTCH1 signaling and increased PTN expression, which leads to osteocalcin activated valve mineralization (Tkatchenko et al., 2009).

2.5.5 NOTCH1 and Shear Stress Control Calcification Regulators

Many shear stress activated genes contained in our data set are NOTCH1 dependent and play important roles in regulating calcification processes. FGF18 is expressed by the perichondrial cells lining the growth plate and signals to all layers of developing chondrocytes in the epiphyseal plate (Kronenberg, 2003). FGF18 acts through FGFR3 to inhibit chondrocyte proliferation and via FGFR1 and 2 to inhibit differentiation of hypertrophic chondrocytes to osteoblasts (Kronenberg, 2003). Perichondrial cells and chondrocytes at the end of long bones secrete parathyroid hormone-related protein (PTHrP), which helps maintain chondrocytes in a proliferative, anti-hypertrophic state (Suda et al., 1999). Intriguingly, the valve endothelium may act in a similar manner to the perichondrial cell layer of the growth plate, secreting cytokines to control the proliferation and differentiation of an underlying cell type. SOX6 is a critical transcription factor that is thought to delay terminal differentiation of chondrocytes into osteoblasts, and down regulates IHH, FGFR3 and RUNX2 in addition to activating BMP6 (Smits et al., 2001), while tissue plasminogen activator (PLAT) knockout mice have increased bone mass. Interestingly, connexin 40 (GJA5) is shear responsive, activated by NOTCH over-expression and modulates arterial endothelial cell identity (Brütsch et al., 2010)

(Buschmann et al., 2010). In addition, endothelial cell specific knockout of connexin 40 results in increased levels of atherosclerosis in mice (Chadjichristos et al., 2010). Our data is the first to show that the activation of GJA5 by shear stress is dependent on the direct activation by NOTCH1. Taken together, this co-option of the endochondral ossification gene network by NOTCH1 in the valve endothelium may be critical for the prevention of aortic valve calcification.

2.5.6 Shear Stress Regulated Valve Development Genes

The endochondral gene network is also important for the development and patterning of the endocardial cushion and their subsequent remodeling into mature valves, though the cell type responsible has yet to be studied in depth (Chakraborty et al., 2008) (Lincoln et al., 2006). In addition, the endothelial cells of the endocardium play a critical role in the development of the valve and give rise to valve interstitial cells through the process of epithelial to mesenchymal transition. Furthermore, the endothelial cells of the cushion intimately signal to the underlying valve mesenchymal cells and help direct their ultimate fate. Indeed, when we alter shear stress and NOTCH1, we find genes involved in heart development to be overrepresented. This gene list includes many genes critical for endocardial cushion formation and valve development such as TWIST1, HEY1 & 2, VEGF, FOXC1 and BMP2 (Combs and Yutzey, 2009). It seems that genes from both of these pathways are involved not only in helping pattern the developing valve, but may also play a role in the maintenance and homeostasis of the valve via the endothelium.

2.5.7 Shear Stress and BMP Signaling

It is widely accepted that interstitial cells become activated myofibroblasts and then trans-differentiate into RUNX2 positive osteoblast like cells. Ectopic gene expression of the bone master regulator, RUNX2, is thought to occur via Bone Morphogenic Protein (BMP) expression signaling through the SMAD 1/5/8 pathway. Normal aortic valve endothelial and interstitial cells have active BMP-SMAD signaling as shown by phosphorylated SMAD 1/5/8 immunofluorescence. This signaling pathway is most likely necessary for normal maintenance of these cell types and indeed, BMP2 promotes survival and migration of endothelial cells (Teichert-Kuliszewska, 2006). Therefore, it seems that endothelial cells have also evolved ways of modulating the BMPs they express, via expression of BMP inhibitors such as MGP and BMPER, in order to prevent some of the detramental effects of these potent growth factors. Interestingly, BMPER seems to be a direct NOTCH1 target with an NICD peak in one intron, but is not activated by shear stress.

2.5.8 Matrix Gla Protein and Valve Calcification

Based on knockout mouse phenotypes, Matrix Gla Protein is the most potent inhibitor of calcification in the arterial system. We have identified patients with mutations in the NOTCH1 receptor that suggest a decreased ability to activate NOTCH1 signaling. Interestingly, these patients have only presented with

calcification of the aortic valve and have yet to show signs of ectopic calcification in other regions of the vasculature or elsewhere. We have shown that NOTCH1 signaling is active in aortic valve endothelial and interstitial cells in vivo and endothelial cells in vitro. Aortic Vascular Smooth Muscle Cells (AVSMCs) show lower expression of NICD in vivo and *NOTCH1* in vitro (data not shown). In addition, MGP expression level is unaffected by NOTCH signaling knockdown with DAPT in vascular smooth muscle. Therefore, we propose that in the disease setting, the vascular smooth muscle expression of MGP is less affected by NOTCH1 receptor mutations and is able to compensate for decreased endothelial MGP expression in the arteries. In addition, the endothelium of the arterial system experiences more shear stress, even at branch points and the inner curvature of the aorta, than the aortic side of the valve, which experiences little to no shear stress. Thus, the set point of the NOTCH1-MGP pathway is the lowest on the aortic side of the valve. In addition, gene expression analysis the four valves in the heart show that the aortic valve expresses the lowest levels of MGP of any of the valves, again suggesting the lowest set point of this anti-calcific factor occurs in the aortic valve (Bouchard-Martel et al., 2009). Furthermore, Warfarin treatment to prevent clotting events has a side effect of inactivating MGP and Periostin due to its Vitamin K inactivation mechanism. This leads to an increase in the incidence of aortic valve calcification in hemodialysis patients (Holden et al., 2007), again indicating the susceptibility of the aortic valve to calcify before the other three valves of the heart. Together, this suggests that even without the NOTCH1 receptor mutation, if we accept that MGP is the most important

anti-calcific factor in the arterial system, the backside of the valve is the most likely to be affected by alterations in the balance of BMP-MGP antagonism. Thus, a simple haploinsuffuciencey of NOTCH1 resulting in decreased MGP expression is able to tip the balance towards ectopic activation of RUNX2 only in the aortic valve. The other valves and arterial vessels may have a high enough set point of MGP expression to resist this process, or can may compensate with expression for cells in a different domain such as the smooth muscle.

2.5.9 Prevention of Valve Calcification

As we begin to think about treating this disease, ensuring that systemic Matrix Gla Protein is present in its active carboxylated form is imperative. The western diet is deficient in menaquinone, or Vitamin K2, which is required by the γ-glutamyl carboxylase enzyme GGC, for MGP activation (Danziger, 2008). A large epidemiological trial known as the Rotterdam Study, showed an inverse relationship between high levels of dietary Vitamin K2 and all cause mortality, coronary heart disease and atherosclerosis (Geleijnse et al., 2004). To date, there are no interventional studies addressing whether Vitamin K2 could prevent onset or progression of calcification diseases (Shea and Holden, 2012). In addition, our data shows that Vitamin A or retinoic acid can induce MGP expression in both endothelial and interstitial valve cells types. Therefore, we suspect that in patients with lower set points of MGP expression, increased dietary or supplemented Vitamin A and Vitamin K2 could be used to induce and activate higher levels of the carboxylated, active

form of the MGP protein. Careful testing using double-blinded, randomized controlled trials will be imperative to determine if such interventions may yield a positive effect on preventing vascular calcification.

2.6 Materials and Methods

2.6.1 Primary Cell Culture

Human Aortic Endothelial cells (HAECs)(Sciencell, San Diego, CA) and Human Aortic Valve Endothelial cells were plated on plates coated with 10 μg/mL fibronectin from bovine plasma (Sigma, St Loius, MO) and grown in Endothelial cell media (ECM)(Sciencell) at 5% CO2. Media was changed every other day and cells were passaged with 0.05% Trypsin EDTA when confluent until. All experiments were performed with cells less than 7 passages. Cells were cultured in “Flow” or pulsatile shear stress conditions using μSlide I 0.8 Luer channel slides and flow kit (Ibidi, Verona, WI) and a L/S® Modular brushless digital dispensing drive peristaltic pump with 6-roller cartridge pump head (Cole Parmer, Vernon Hills, IL). Shear stress conditions were between 13 and 15 dynes/cm2.

2.6.2 Isolating Human Valve Cells

Normal Aortic valves were obtained from patients undergoing heart lung transplants for pulmonary hypertension according to the IRB at Stanford and UCSF. Leaflets were removed from the discarded hearts and placed on ice in PBS. One leaflet was

divided between Trizol reagent and RIPA buffer for later RNA and Protein studies. One half of a leaflet was fixed in formalin for paraffin embedding and sectioning and the remaining leaflet pieces were processed for live cell isolation. The valves were rinsed five times in ice cold PBS and then digested in 2.5 mg/ml collagenase type IV (C5138, Sigma, St. Louis, MO) in M199 media (Lonza Biosciences, Walkersville, MD) at 37 degrees C for 30 minutes. The valve tissue was vortexed to remove valve endothelial cells, supernatant was removed and spun at 500 x g for 2 min and then endothelial cells were plated in ECM on fibronectin. The remaining valve tissue was digested further with 0.8 mg/ml collagenase in M199 for 3 hours at 37 degrees C with vortexing every 30 min. The tissue was vortexed and pipetted repeatedly to break up the tissue mass and then spun at 500 x g for 2 min. The supernatant containing freed cells was transferred to a new tube and spun down at 1100 x g for 8 minutes at 4 degrees C. The cells were resuspended in M199 containing 10% heat inactivated FBS and 1X pen/strep, and plated onto two t75s. After 3 to 4 days, endothelial cells were purified using anti-CD31 labeled magnetic beads (Miltenyi Biotec, Auburn, CA). To check cell type purity, cells were stained with mouse anti-human CD31-488 and anti-human CD144-PE conjugated antibodies (BD Bioscences) and checked by fluorescence activated cell analysis on an LSR II (BD Bioscences, San Jose, CA).

2.6.3 siRNA Delivery

siRNAs were delivered into endothelial cells using RNAiMax (Life Technologies, Carlsbad, CA). The siRNAs used were NOTCH1 siRNA (cat# 4392422 s9633 and control scrambled siRNA (cat# 4390843) (Ambion/Life Technologies). Endothelial cell media was changed to optimem with no suplements (Gibco/Life Technologies), siRNA/RNAiMax was added for 4 hours. Then, the media was changed to full ECM and the cells were harvested for analysis 48 hours later.

2.6.4 DAPT Treatment

For gene expression experiments, cells were treated with 5μM DAPT (Sigma) in DMSO and control treated cells were treated with an equivalent amount of DMSO. Cells were harvested in Trizol reagent 48 hours after addition of DAPT. For Western blots, endothelial cells were treated for 48 hours in DMSO or DAPT and then trypsinized, washed with PBS, and re-plated for 96 hours before harvesting in RIPA buffer (Sigma, St. Louis, MO) + 1X Complete Mini protease inhibitors (Roche, Madison, WI).

2.6.5 RNA-seq and Analysis Pipeline

RNA from HAVECs from each condition was purified using trizol extraction followed by RNeasy MinElute Cleanup Kit with on column DNAse digestion (Qiagen, Valencia, CA). Then, biological triplicates were pooled prior to library generation. 50

ng of RNA was used with the Ovation® RNA-Seq System (7100-08)(NuGEN, San Carlos, CA) and manufacturer's protocol to synthesize and SPIA amplify cDNA, which was then sheared with a covaris S-series. After end repair, purification and P1 P2 adaptor ligation, templated beads were generated with the EZ beads system, and libraries where then paired end sequened (50bp forward, 35bp reverse) on a SOLiD4 DNA sequencing system (Life Technologies). RNA-seq reads were aligned to the human hg19 genome using TopHat (Langmead et al., 2009). TopHat was supplied with GTF-format annotation of known exon positions. Novel exon discovery was disallowed—only exons and splice junctions that were already present in the annotation were included. Duplicate reads (reads mapping to the exact same start / stop position) were removed using the Picard tool MarkDuplicates (http://picard.sourceforge.net/). Secondary mapping locations were discarded. For each read, only the top alignment was retained. For paired-end reads, any "singleton" reads (where both ends did not map successfully) were discarded. Cufflinks was used to obtain a reads-per-gene total and provide normalized expression levels, reported as RPKM (reads mapped to a gene per thousand bases of the gene, per million mapped reads) (Roberts et al., 2011). Differentially expressed genes were identified using Cuffdiff, part of the Cufflinks suite. Only genes with RPKMs > 1 and CuffDiff output of "OK" were included in subsequent analysis. Relative expression levels for heatmaps were normalized to the control, no flow condition and values were transformed to a log base 2 scale. UCSC Genome

Browser tracks were generated using wiggle tracks and indicate the number of fragments that mapped to a particular locus.

2.6.6 ChIP-seq and ChIP-qRT-PCR

ChIP-seq was performed according to a protocol from the Bruneau Lab (Wamstad et al., 2012). Briefly, 2.5 million HAVECs were infected with either Luciferase-myc tag or NICD1-myc tag lentivirus and fixed with formaldehyde after 48 hours. All myc tag ChIPs were done with a Goat polyclonal to Myc tag-ChIP grade antibody (ab9132, Abcam, Cambridge, MA). ChIPs were done in triplicate with Protein G magnetic beads and then pooled for subsequent ChIP-seq library preparation with the standard Illumina ChIP-seq library protocol. High-throughput sequencing was performed on an Illumina GAIIxs machine. Tags were mapped back to the genome using the bowtie aligner (Langmead et al., 2009) and ChIP tag densities were calculated using bedops (Neph et al., 2012). Peaks in ChIP signal were identified using SPP (Kharchenko et al., 2008). Genome feature enrichment analysis was implemented in perl and R, utilizing bedops in conjunction with Ensemble annotations (Hubbard et al., 2002). Motif discovery was performed using Transfac (Matys, 2006) and Uniprobe (Newburger and Bulyk, 2009) motif weight matrices in conjunction with the Fimo motif discovery algorithm (Bailey et al., 2009). Statistical analysis of motif enrichments was performed using permutation tests of genomic sequence at sites of notch binding. Custom Taqman probes (Life Technologies) were designed with the following sequences as targets (primer

sequences were not provided by Life Technologies): GAPDH TSS (GRCh37/hg19) chr12:6,643,459-6,643,659; HES1 CSL (GRCh37/hg19) chr3:193,853,706-193,854,009; HES1 non-CSL (GRCh37/hg19) chr3:193,845,818-193,846,315. Custom PrimeTime qRT-PCR primers (IDT, Coralville, IA) were designed with the following sequences: MGP CSL- Primer 1- 5'-GGG CTT TTG GGA ACA GAT TTG-3', Primer 2- 5'-GTT CAG GAA GTT AGG GCA GG-3', Probe- 5'-/56-FAM/AGT GAA AAG /ZEN/GAA GCA AGC AGG AGG A/3IABkFQ/-3'; MGP non-CSL, Primer 1- 5'-GAA GGG AAG AGG CTA AGT CAG-3', Primer 2- 5'-GTC AAC ATC ACATTATCA CCC AC-3', Probe-5'-/56-FAM/CCC TCC CAT /ZEN/GAA CAC CTA ACATTA CCA C/3IABkFQ/-3'.

2.6.7 Bioinformatic Analysis

Gene lists were generated based on differential expression and ChIP-seq data. Then, GO Elite and GenMAPP-CS were used to predict GO terms and pathways overrepresented in the data sets (Zambon et al., 2012) (Salomonis et al., 2007).

2.6.8 Electrophoretic mobility shift assays (EMSAs)

DNA binding assays were carried out as previously described (Dodou et al., 2003). Oligos were annealed, labeled with 32P-dCTP, and gel purified on a 40% acrylamide gel. CSL protein was generated with a TNT T7/Sp6 Coupled Reticulocyte Lysate System (Promega, Madison, WI). Each DNA binding reaction was performed in

40mM KCL, 15mM HEPES pH7.9, 1mM EDTA, 5mM DTT and 5% Glycerol and then run on a 6% acrylamide gel before film exposure to visualize the 32P. Oligos used for the EMSA were as follows: HES1 Wt For, 5′-GGATTACTATTTCCCACACATCTT-3′; HES1 Wt Rev, 5′-GGTAAGATGTGTGGGAAATAGTAAT-3′; HES1 Mut For, 5′-GGATTACTATTAACCACACATCTTA-3′; HES1 Mut Rev, 5′-GGTAAGATGTGTGGTTAATAGTAAT-3′; MGP WT For, 5′-GGTCCAAGGGCTTTTGGGAACAGATTTGTGAGAAAAGAGTGAAAAG-3′; MGP WT Rev, 5′-GGCTTTTCACTCTTTTCTCACAAATCTGTTCCCAAAAGCCCTTGGA-3′; MGP 2X Mut For, 5′-GGTCCAAGGGCTTTGTCGAACAGATTTGGTCGAAAAGAGTGAAAAG-3′; MGP 2X Mut Rev, 5′- GGCTTTTCACTCTTTTCGACCAAATCTGTTCGACAAAGCCCTTGGA-3′.

MGP 1X Mut For, 5′-GGTCCAAGGGCTTTTGGGAACAGATTTGTGTCAAAAGAGTGAAAAG-3′.

MGP 1X Mut Rev, 5′-GGCTTTTCACTCTTTTGACACAAATCTGTTCCCAAAAGCCCTTGGA-3′.

2.6.9 qRT-PCR

RNA was purified from cells in Trizol reagent and cDNA was generated from 1 μg of RNA using Superscript III First Strand Synthesis Supermix (Life Technologies).

Gene expression analysis was performed by quantitative reverse transcriptase-PCR (qRT-PCR) using standard Taq-Man primer sets and Taqman Gene Expression Mastermix on an ABI-7900 HT (Applied Biosystems).

2.6.10 Immunohistochemistry

Human aortic valves were fixed with 10% formalin overnight at 4 degrees C, paraffin embedded, and sectioned. Valve sections were subjected to antigen retrieval under heat and pressure for 2 minutes in antigen retrieval buffer (10 mM Tris, 1 mM EDTA, and 0.05% tween). The sections were permeabilized with PBS Triton (0.1%) and blocked with serum from the secondary antibody source. Primary antibodies were diluted 1:50 in PBS Triton (0.1%) and were incubated at 4 degrees C overnight. The sections were thoroughly washed with PBS and incubated with secondary antibody diluted in PBS triton (0.1%) 1:200 for 2 hours at room temperature. Sections were thoroughly washed in PBS, nuclei stained with DAPI or Hoescht and sections were then mounted under coverslips and imaged on a Leica upright fluorescent microscope. Primary antibodies used were NOTCH1 intracellular domain (ab8925, Abcam), cMGP (clone G8A#1) and ucMGP (clone B11#1, VitaK BV, Maastricht, The Netherlands), phospho-SMAD 1/5/8 (#9511, Cell Signaling Technology, Danvers, MA).

.

2.6.11 Lentiviral Production

Expression of NICD was achieved by OmicsLink expression construct Lv140 (GeneCopoeia, Rockville, MD) with a CMV promoter driving NICD1 (UniProtKB/Swiss-Prot: P46531.4, aa1769- 2555 2364bp) with a myc tag and IRES mCherry to check the percent of cells infected. A control lentivirus contained a Luciferase gene in place of NICD in the same LV140 construct. Additionally, the myc tag was replaced by a 3X FLAG tag for the IP-Mass Spec pipeline. Lentiviral particles were produced using the Lenti-Pac HIV expression packaging kit (Genecopoeia) and HEK-293t cells.

2.6.12 Western Blot

Western blots were performed using according to the Licor quantitative western blot protocol and visualized on an Odyssey Fc (Licor, Lincoln, NE). Antibodies used were anti-FLAG M2 antibody (F1804, Sigma), anti-β-Actin clone AC-15 (A1978, Sigma), anti-GAPDH (ab8245, Abcam), anti-cMGP (clone G8A#1) and anti-ucMGP (clone B11#1, VitaK BV, Maastricht, The Netherlands).

2.6.13 Transgenic Animals

The wildtype (Wt) 800 bp MGP putative enhancer region was TOPO cloned into pCR2.1-TOPO vector (Life Technologies) using the following primers: MGP-Wt-800bp For, 5′- aatgccataagggtccttcc-3′; MGP-Wt-800bp Rev, 5′-

tgaagaagcgagccacatc-3′. The pCR2.1-MGP-800bp enhancer region was then cut with Nhe1 (New England Biolabs, Ipswich, MA), blunted with T4 DNA polymerase and then cut with Not1-HF (New England Biolabs). The MGP-800bp enhancer was then ligated into the plasmid pENTR1A (Life Technologies), which was cut with Xmn1 and Not1-HF. The pENTR1A-MGP-Wt-800bp plasmid was cut with BglII and SanD1(Thermo Scientific, Waltham, MA) and Cold Fusion Cloning Kit was used to introduce a double stranded oligo containing mutations in the CSL binding sites: MGP-3XMut-800bp For 5′-AAGTGGTCAGGTGTAGTACAGAGATCTGGGGCAATCATTGCATGTTGGAGTCGACGATTCCAAGGGCTTTGTCGAACAGATTTGGTCGAAAAGAGTGAAA-3′. The MGP Wt- and 3XMut-800bp enhancers were then subcloned into an hsp68 lacZ-DV minimal promoter plasmid using LR clonase (Life Technologies). These final plasmids were cut with HindIII and NaeI before pronuclear injection in FVB/N mice. LacZ transgenes were detected in pups by PCR from tail biopsies (Transnetyx, Cordova, TN). All experiments using animals were reviewed and approved by the UCSF Institutional Animal Care and Use Committee and complied with all institutional and federal guidelines.

2.6.14 Sequences

ChIP-seq primers

Custom Taqman probes (Life Technologies) were designed with the following seuquences as target: GAPDH (GRCh37/hg19) chr12:6,643,459-6,643,659; HES1 CSL (GRCh37/hg19) chr3:193,853,706-193,854,009; HES1 Non-CSL (GRCh37/hg19) chr3:193,845,818-193,846,315. Custom PrimeTime qRT-PCR primers (IDT, Coralville, IA) were designed with the following sequences: MGP CSL- Primer 1- 5'-GGG CTT TTG GGA ACA GAT TTG-3', Primer 2- 5'-GTT CAG GAA GTT AGG GCA GG-3', Probe- 5'-/56-FAM/AGT GAA AAG /ZEN/GAA GCA AGC AGG AGG A/3IABkFQ/-3'; MGP non-CSL, Primer 1- 5'-GAA GGG AAG AGG CTA AGT CAG-3', Primer 2- 5'-GTC AAC ATC ACATTATCA CCC AC-3', Probe-5'-/56-FAM/CCC TCC CAT /ZEN/GAA CAC CTA ACATTA CCA C/3IABkFQ/-3'.

Cloning Sequences

MGP-Wt-800bp For, 5′- AATGCCATAAGGGTCCTTCC-3′;

MGP-Wt-800bp Rev, 5′-TGAAGAAGCGAGCCACATC-3′;

MGP-3XMut-800bp For

5′AAGTGGTCAGGTGTAGTACAGAGATCTGGGGCAATCATTGCATGTTGGAGTC

GACGATTCCAAGGGCTTT**GTC**GAACAGATTTG**GTC**GAAAAGAGTGAAA-3.

siRNA Sequences

NOTCH1 siRNA- Ambion 4392422 s9633

Control siRNA- Ambion 4390843

Lentiviral Sequences-

Notch 1- UniProtKB/Swiss-Prot: P46531.4 aa1769- 2555

atgcctgagggcttcaaagtgtctgaggccagcaagaagaagcggcgggagcccctcggcgaggactccgtggg

cctcaagcccctgaagaacgcttcagacggtgccctcatggacgacaaccagaatgagtgggggacgaggacc

tggagaccaagaagttccggttcgaggagcccgtggttctgcctgacctggacgaccagacagaccaccggcagt

ggactcagcagcacctggatgccgctgacctgcgcatgtctgccatggcccccacaccgccccagggtgaggttga

cgccgactgcatggacgtcaatgtccgcgggcctgatggcttcaccccgctcatgatcgcctcctgcagcgggggcg

gcctggagacgggcaacagcgaggaagaggaggacgcgccggccgtcatctccgacttcatctaccagggcgc

cagcctgcacaaccagacagaccgcacgggcgagaccgccttgcacctggccgcccgctactcacgctctgatgc

cgccaagcgcctgctggaggccagcgcagatgccaacatccaggacaacatgggccgcaccccgctgcatgcg

gctgtgtctgccgacgcacaaggtgtcttccagatcctgatccggaaccgagccacagacctggatgcccgcatgca

tgatggcacgacgccactgatcctggctgcccgcctggccgtggagggcatgctggaggacctcatcaactcacac

gccgacgtcaacgccgtagatgacctgggcaagtccgccctgcactgggccgccgccgtgaacaatgtggatgcc

gcagttgtgctcctgaagaacggggctaacaaagatatgcagaacaacagggaggagacacccctgtttctggcc

gcccgggagggcagctacgagaccgccaaggtgctgctggaccactttgccaaccgggacatcacggatcatatg

gaccgcctgccgcgcgacatcgcacaggagcgcatgcatcacgacatcgtgaggctgctggacgagtacaacctg

gtgcgcagcccgcagctgcacggagccccgctgggggcacgcccaccctgtcgcccccgctctgctcgcccaac

ggctacctgggcagcctcaagcccggcgtgcagggcaagaaggtccgcaagcccagcagcaaaggcctggcct

gtggaagcaaggaggccaaggacctcaaggcacggaggaagaagtcccaggacggcaagggctgcctgctgg

acagctccggcatgctctcgcccgtggactccctggagtcaccccatggctacctgtcagacgtggcctcgccgcca

ctgctgccctccccgttccagcagtctccgtccgtgcccctcaaccacctgcctgggatgcccgacacccacctgggc

atcgggcacctgaacgtggcggccaagcccgagatggcggcgctgggtgggggcggccggctggcctttgagact

ggcccacctcgtctctcccacctgcctgtggcctctggcaccagcaccgtcctgggctccagcagcggaggggccct

gaatttcactgtgggcgggtccaccagtttgaatggtcaatgcgagtggctgtcccggctgcagagcggcatggtgcc

gaaccaatacaaccctctgcgggggagtgtggcaccaggccccctgagcacacaggccccctccctgcagcatg
gcatggtaggcccgctgcacagtagccttgctgccagcgccctgtcccagatgatgagctaccagggcctgcccag
cacccggctggccacccagcctcacctggtgcagacccagcaggtgcagccacaaaacttacagatgcagcagc
agaacctgcagccagcaaacatccagcagcagcaaagcctgcagccgccaccaccaccaccacagccgcacc
ttggcgtgagctcagcagccagcggccacctgggccggagcttcctgagtggagagccgagccaggcagacgtg
cagccactgggccccagcagcctggcggtgcacactattctgccccaggagagccccgccctgcccacgtcgctg
ccatcctcgctggtcccacccgtgaccgcagcccagttcctgacgcccccctcgcagcacagctactcctcgcctgtg
gacaacacccccagccaccagctacaggtgcctgagcacccccttcctcaccccgtcccctgagtcccctgaccagt
ggtccagctcgtccccgcattccaacgtctccgactggtccgagggcgtctccagccctcccaccagcatgcagtccc
agatcgcccgcattccggaggccttcaagtaa

2.6.15 Statistical Analysis

All experiments were performed at least three times unless otherwise stated. All statistical analysis was completed using GraphPad Prism software. Two-way analysis was completed with two-tailed unpaired t tests with a 95% confidence interval. Multiple comparison tests were performed by one-way ANOVA with Tukey's multiple comparison post test.

Chapter 3

Limited Gene Expression Variation in Human Embryonic Stem Cell and Induced Pluripotent Stem Cell Derived Endothelial Cells

3.1 Contributions

The author has contributed significantly to the work described in this chapter. The author is responsible for the conception and design, provision of study material or patients, collection and/or assembly of data, data analysis and interpretation, writing and critical revision of the manuscript. Rufaihah J Abdul helped with collection and/or assembly of data, data analysis and interpretation, manuscript writing and critical revision of manuscript. Lei Liu performed most of the cell differentiations.

Kathryn N. Ivey helped with conception and design, and critical revision of manuscript. John P. Cooke provided financial support and critical revision of manuscript/experimental design. Deepak Srivastava helped with conception and design, financial support and final approval of manuscript.

3.2 Abstract

Recent evidence suggests human embryonic stem (ES) and induced pluripotent stem (iPS) cell lines have differences in their epigenetics marks and transcriptomes, yet the impact of these differences on subsequent terminally differentiated cells is less well understood. Comparison of purified, homogeneous populations of somatic

cells derived from multiple independent human iPS and ES lines will be required to address this critical question. Here, we report a differentiation protocol based on embryonic development that consistently yields large numbers of endothelial cells (EC) derived from multiple human ES or iPS cells. Mesoderm differentiation of embryoid bodies was maximized and defined growth factors were used to generate KDR^+ EC progenitors. Magnetic purification of a KDR^+ progenitor subpopulation resulted in an expanding, homogeneous pool of ECs that expressed EC markers and had functional properties of ECs. Comparison of the transcriptomes revealed limited gene expression variability between multiple lines of human iPS–derived ECs, or between lines of ES– and iPS–derived ECs. These results demonstrate a method to generate large numbers of pure human EC progenitors and differentiated ECs from pluripotent stem cells, and suggest individual lineages derived from human iPS cells may have significantly less variance than their pluripotent founders.

3.3 Introduction

Induced pluripotent stem (iPS) cells have recently emerged as a promising alternative to embryonic stem cells for modeling disease and developing therapeutics (Robinton et al., 2012). While seemingly equivalent, many recent studies suggest subtle differences between these two pluripotent cell types, including specific culture-derived genetic abnormalities, propensity to differentiate towards a specific lineage, and somatic epigenetic memory (Leeper et al., 2010). In

contrast, the impact of the putative differences between iPS and ES cells on fully differentiated cell states after *in vitro* directed differentiation has not been explored to the same extent, especially in human cell types where cell-type specific reporter lines have been difficult to generate. Well-defined cell surface markers make endothelial cells (ECs) a useful platform to systematically profile a homogeneous cell population derived from pluripotent stem cells without the requirement for reporter cell lines.

The endothelium is a monolayer that invests the luminal surface of all blood and lymphatic vessels. ECs composing this diaphanous film of tissue modulate the growth and reactivity of the underlying smooth muscle, control the interaction of the vessel wall with circulating blood elements, and regulate vascular responses to hemodynamic forces (Cooke et al., 2003) Transplanted human ES or iPS derived ECs lead to increased function and vascularization in multiple animal disease models including hind limb perfusion and myocardial infarction in addition to stably carrying blood up to 150 days after transplantation with no safety issues as yet reported (Cho etal., 2007; Wang et al., 2007; Rufaihah et al., 2007; Descamps et al., 2012).

Several methods for generating ECs from human pluripotent stem cells have been reported. Original embryoid body differentiation methods supplemented with high VEGF generated 5–8% CD31 positive cells after two weeks in culture (Nourse et al., 2010; Kane et al., 2011). Recent improvements claim efficiencies from 15–57% CD31 positive cells by day 14, however, these methods have been difficult to

consistently replicate across multiple pluripotent stem cell lines either because of protocol complexity, batch variation in required reagents, or other unexplained factors Kane et al., 2010; James et al., 2010). Independent pluripotent stem cell lines may require optimization of conditions for each cell line due to inherent variation amongst lines (Kattman et al., 2011). Most importantly, a comprehensive genome-wide analysis of gene expression variability in human ECs, or any other specific human lineage, among multiple different ES or iPS lines has not been reported (Li et al., 2011; Tatsumi et al., 2011).

Here, we report a differentiation protocol that recapitulates normal development and consistently yielded large numbers of relatively pure ECs derived from multiple independent human ES or iPS cell lines. Comprehensive profiling of this well-defined cell population revealed remarkably few gene expression differences between ECs derived from multiple hiPSCs or hESCs, as well as ECs derived with different differentiation protocols. These findings suggest that differentiated cell types derived from hES and hiPS cells lines, and from multiple hiPS cell lines, may have limited transcriptome variance, increasing the likelihood of successful disease-modeling using iPS-based technology.

3.4 Results

3.4.1 Generation of KDR+ precursors

Large numbers of cardiac myocytes have been efficiently generated from mouse and human stem cells by inducing pre-cardiac mesoderm cells marked by

KDR and PDGFR-a cell surface receptors, then biasing toward the cardiac muscle fate (Kattman et al., 2006; Yang et al. 2008). Since the pre-cardiac mesoderm cells are multipotent and give rise to endothelial and smooth muscle cells in addition to cardiac myocytes, we searched for approaches to bias these precursors into the EC lineage (Yamashita et al., 2000). hESCs and hiPSCs were grown in feeder-free conditions and aggregated to form embryoid bodies (EBs). KDR^+ cells were induced from day 1–4 (D1–D4) (stage 1) with defined medium containing bFGF (5 ng/mL), Activin A (6 ng/mL) and a range of BMP4 (4–14 ng/mL) in a manner similar to a reported protocol for directed differentiation of ESCs into cardiac myocytes (Yang et al., 2008) (Fig. 3.1A).

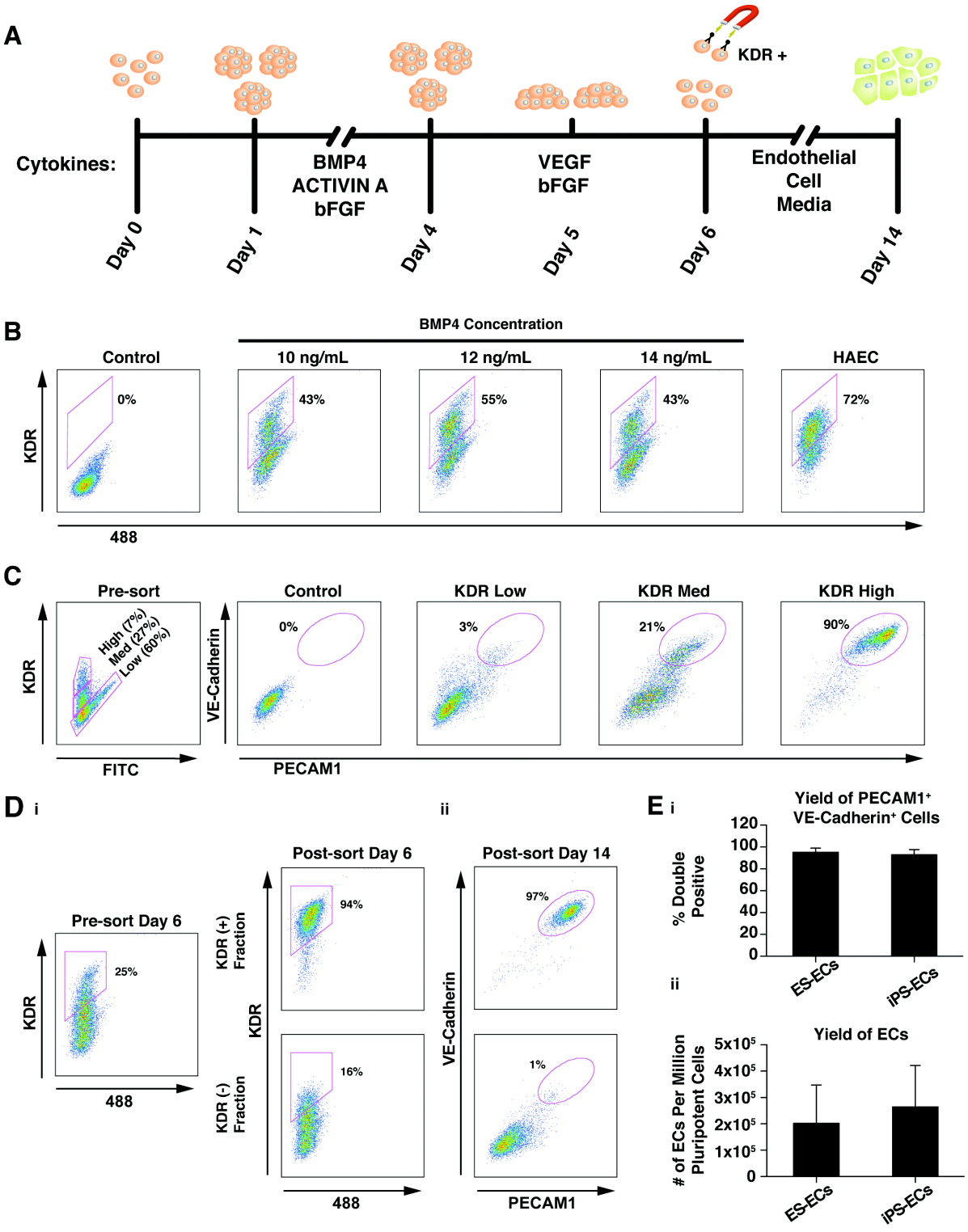
A
KDR +
Cytokines:
BMP4
ACTIVIN A
bFGF
VEGF
bFGF
Endothelial
Cell
Media
Day 0
Day 1
Day 4
Day 5
Day 6
Day 14
B
BMP4 Concentration
Control
10 ng/mL
12 ng/mL
14 ng/mL
HAEC
0%
43%
55%
43%
72%
KDR
488
C
Pre-sort
Control
KDR Low
KDR Med
KDR High
High (7%)
Med (27%)
Low (60%)
0%
3%
21%
90%
KDR
VE-Cadherin
FITC
PECAM1
D i
ii
Pre-sort Day 6
Post-sort Day 6
Post-sort Day 14
25%
94%
97%
16%
1%
KDR
KDR (+) Fraction
KDR (-) Fraction
VE-Cadherin
488
PECAM1
E i
Yield of PECAM1+ VE-Cadherin+ Cells
% Double Positive
120
100
80
60
40
20
0
ES-ECs
iPS-ECs
ii
Yield of ECs
# of ECs Per Million Pluripotent Cells
5x10^5
4x10^5
3x10^5
2x10^5
1x10^5
0
ES-ECs
iPS-ECs

Figure 3.1 KDR^{high} cells differentiate into mature endothelial cells. (A): Endothelial cell differentiation protocol. Human ES or iPS cells were induced to form cardiac mesoderm using BMP, Activin A, and bFGF. Embryoid bodies were placed into conditions promoting endothelial cell formation at day 4, plated on fibronectin at day 5 and then KDR^{high} endothelial precursor cells were magnetically sorted on day 6. The precursors were plated in endothelial cell maintenance conditions and expanded until day 14 when they were frozen. **(B)**: Flow cytometric analysis of the effects of various BMP4 concentrations on KDR expression. The control population consisted of cells labeled with isotype control antibodies (IgG). The experiment was repeated three times and representative data from one experiment is displayed. **(C)**: Analysis of the EC differentiation potential of three cell sub-populations with varying KDR expression levels. Three populations were sorted by FACS at day 6 and then analyzed for expression of the mature human endothelial cell-surface markers VE-Cadherin and PECAM1 on day 14. The control population consisted of cells labeled with isotype control antibodies (IgG). The experiment was repeated three times and representative data from one experiment is displayed. **(D)**: i. Analysis of KDR expression before and after magnetic sorting of KDRhigh cells at day 6. ii. Two KDR fractions (+ and –) were replated after magnetic sorting and reanalyzed on day 14 for expression of VE-Cadherin and PECAM1. The experiment was repeated three times and representative data from one experiment is displayed. **(E)**: i. Mean

percentage of cells expressing both PECAM1 and VE-Cadherin at Day 14 of differentiation from ES or iPS cells from 4 different cell lines in 4 separate experiments for each group. Error bars represent standard deviation. Mean values were not statistically different when compared with two-tailed unpaired t test. ii. Mean yield of ECs from 1 million pluripotent stem cells from 4 different cell lines in 4 separate experiments for each group. Error bars represent standard deviation. Mean values were not statistically different when compared with two-tailed unpaired t test.

We attempted to further differentiate pre-cardiac mesoderm into endothelial precursors from D4–D5 (stage 2) with VEGF (10 ng/mL) and bFGF (10 ng/mL), two cytokines critically important for angiogenesis (Olsson et al., 2006; Cross et al., 2001). At D5.4, EBs were plated on fibronectin-coated plates which promote attachment and proliferation of endothelial cells (Grant et al., 1990). On D6, single-cell suspensions were generated using Accutase and subsequently stained for KDR. Expression of KDR ultimately becomes restricted to the endothelial lineage (Yamashita et al., 2000; Olsson et al., 2006), so we tested a range of BMP4 concentrations (BMP 4-14 ng/ml) (Fig. 3.2A) for the ability to generate KDR^{+} cells at

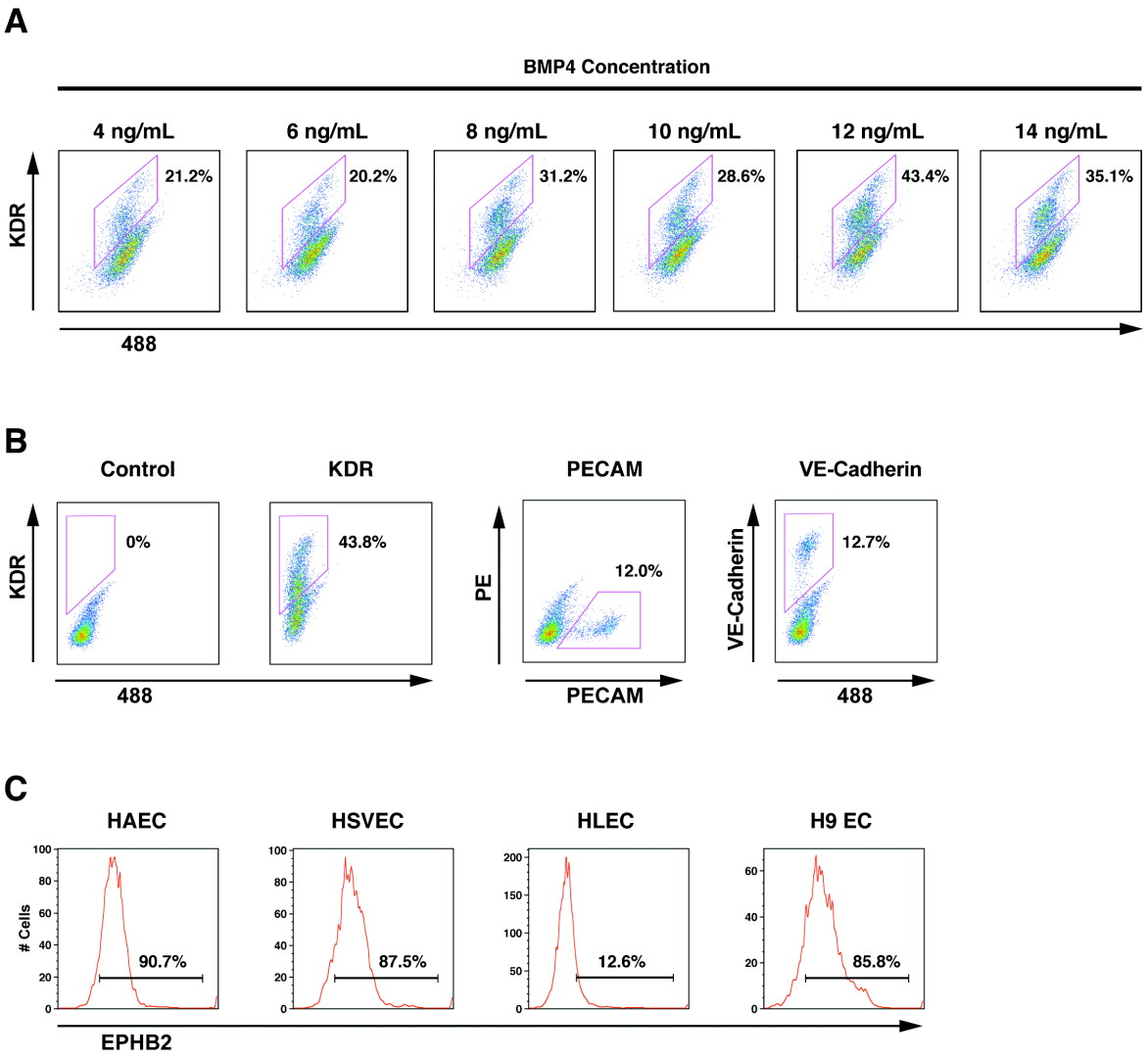

Figure 3.2 Extended analysis of EC differentiation. (A): Flow cytometric analysis of the effects of various BMP4 concentrations on KDR expression on day 6 of differentiation. **(B)**: Flow cytometric analysis of the mature EC differentiation state on day 6 before KDR+ cell sorting using PECAM and VE-Cadherin. The control population consisted of cells labeled with isotype control antibodies. **(C)**: Flow cytometric analysis for EPHB2 staining on PECAM / VE-Cadherin double positive

cells on day 14. HAEC, HSVEC, and HLEC were used as positive and negative controls and H9 ECs were differentiated from ES cells.

D6. BMP4 administered at 12 ng/mL from D1–4 resulted in maximal KDR expression (55%) at D6, as detected by flow cytometry (Fig. 3.1B). This concentration of BMP4 was used for subsequent differentiations of all pluripotent cell lines, though optimization for each line may further maximize EC yield. In order to determine the level of commitment to the endothelial lineage at D6 we used flow cytometric analysis to profile the surface markers PECAM1 (CD31) and VE-Cadherin (CD144), which are highly expressed in mature human ECs. While 44% of the cells were KDR^{+}, only 12% or 13% of the cells were $CD31^{+}$ or $CD144^{+}$, respectively (Fig. 3.2B).

3.4.2 Endothelial Cell Differentiation Potential of KDR+ Populations

Cells expressing KDR at D6 could be divided into three sub-populations based on KDR expression level: KDR^{low}, KDR^{med}, KDR^{high}. To investigate their potentials to differentiate into ECs, the three sub-populations were sorted by fluorescence activated cell sorting (FACS) and re-plated on fibronectin-coated plates in EC medium commonly used to maintain primary EC lines. We used PECAM1 (CD31) and VE-Cadherin (CD144) cell surface staining at D14 to monitor and optimize the EC differentiation. The KDR^{high} population resulted in greater than 90% CD31/CD144 double positive ECs ($CD31^{+}/CD144^{+}$) (Fig. 3.1C). The KDR^{med} or KDR^{low} populations generated 20% or 3% $CD31^{+}/CD144^{+}$ ECs, respectively. Interestingly, a mixture of

$KDR^{high/med}$ cells resulted in greater than 90% $CD31^{+}/CD144^{+}$ ECs, while a mixture of $KDR^{med/low}$ cells generally resulted in fewer than 10% $CD31^{+}/CD144^{+}$ ECs (data not shown). This may indicate that the KDR^{med} sub-population is a plastic precursor cell responsive to non-cell autonomous differentiation cues from surrounding cells. The KDR^{low} fraction's inhibition of EC differentiation may represent a dominant effect over the KDR^{high} population or may be due to more rapid proliferation of the KDR^{low} derivatives that then become the dominant cell type.

Isolating large numbers of $KDR^{high/med}$ cells that could ultimately become ECs required a more efficient method than FACS, which is time consuming and destructive to cells needing further culture and expansion. Therefore, we employed magnetic cell sorting (MACS) to isolate $KDR^{high/med}$ cells using a combination of a KDR antibody conjugated to Phycoerythrin (PE) and an anti-PE antibody conjugated to a magnetic bead. We purified $KDR^{high/med}$ cells by MACS and quantified the KDR-expressing cells by FACS from the pre- and post- magnetic sort populations. By MACS at D6, we recovered a KDR^{+} population that was 94% $KDR^{high/med}$ cells (Fig. 3.1D). The percent $KDR^{high/med}$ of the total cell population varied widely between cell lines and between differentiations of the same cell line with a range of 6.78 to 72.7% (Table 3.1).

Table 3.1 Summary of KDR$^{high/med}$ yield on day 6 of differentiation.

Pluripotent Cell Line	KDR$^{high/med}$
H1	6.78
H1	12.8
H7	43.8
H9	33.6
H9	43.4
H9	44.8
H9	59.1
H9	76.2
iPS2	9.79
iPS2	19.6
iPS2	30.5
iPS2	72.7

Data are displayed as percentage of total cell population staining positive for KDR at d6 of differentiation. Duplicate lines indicate independent differentiations done on separate days. Percentages from same cell line are arranged in ascending order.

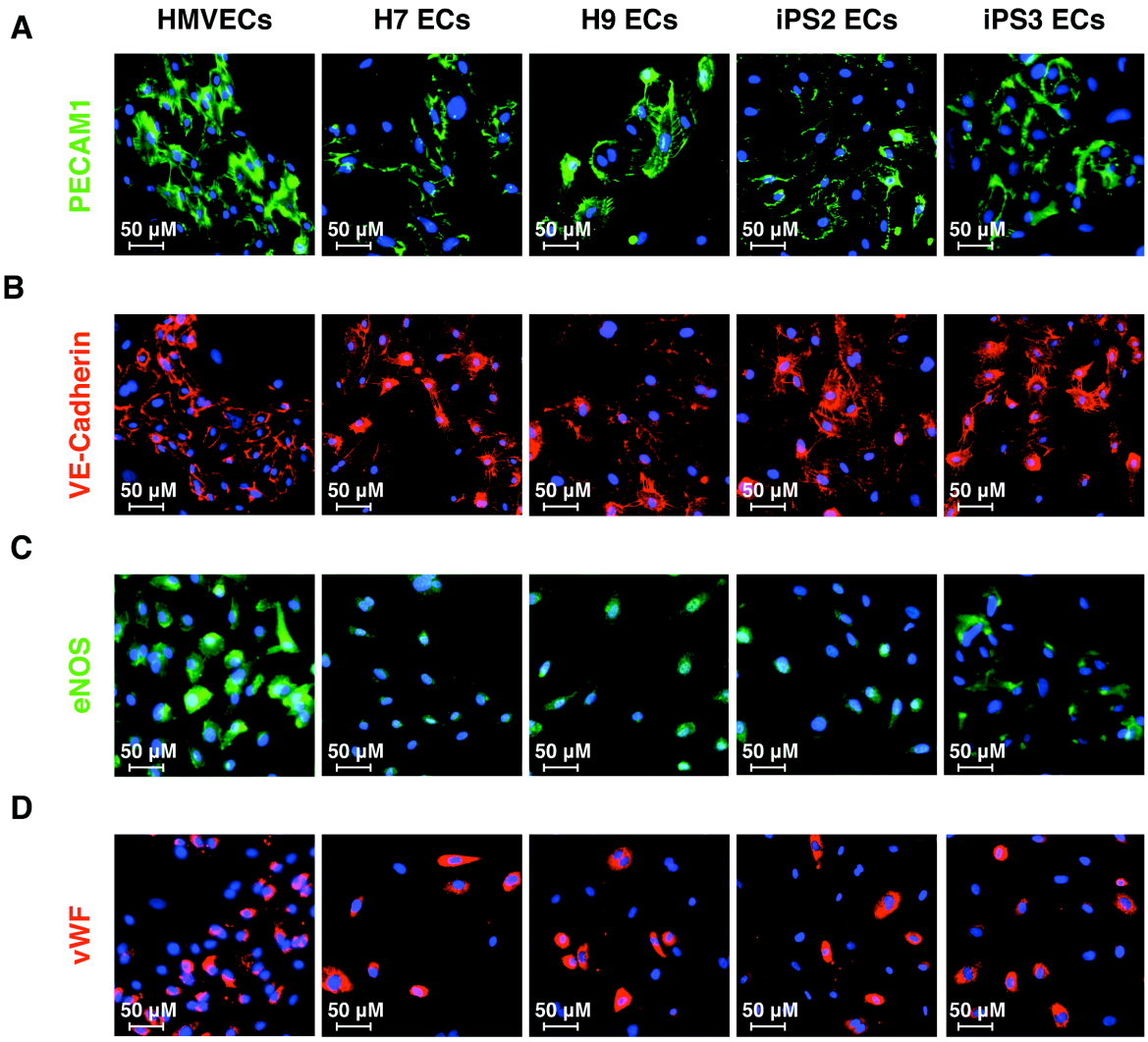

Figure 3.3 Morphology and protein expression of endothelial cells derived from pluripotent stem cells. Immunofluorescent staining for PECAM1 **(A)**, VE-Cadherin **(B)**, eNOS **(C)**, and vWF **(D)** in ECs derived from pluripotent stem cells at day 21 of differentiation protocol. Control cells are human microvascular endothelial cells (HMVECs). Nuclei were visualized with DAPI (blue).

Once replated on fibronectin in EC medium, the $KDR^{high/med}$ endothelial precursor cells had a high proliferative capacity and were allowed to grow to 80–90%

confluence and then were split 1:3 by using 0.05% trypsin. Endothelial cells round up and can be tapped off of the plate before other contaminating cell types release from the culture dish when using 0.05% trypsin, which helped maintain nearly pure populations of $CD31^+/CD144^+$ ECs. All differentiations with adequate enrichment of 95% ± 3.7 $CD31^+/CD144^+$ cells at day 14 for ES cells and 93% ± 4.8 for iPS cells (Fig. 3.1D and E). The $CD31^+/CD144^+$ ECs were frozen at D14 and could be thawed and expanded again. The yield of ECs varied among batches and lines, but ranged from 1.5 X 10^5 to 4.0 X 10^5 cells per million pluripotent cells and correlated with the proliferation rate of the $KDR^{high/med}$ cells after sorting rather than the percentage of $KDR^{high/med}$ cells at the time of sorting (Fig. 3.1E). It should be noted that this calculation is based on the number of starting ES cells on day 0 and not the number of cells present at D1 after aggregation (~50% of starting population) as was reported in James et al., 2010.

3.4.3 Biological and Functional Characterization

$CD31^+/CD144^+$ cells were derived from various hiPS (iPS1, iPS2, iPS3) and hES cell lines (H1, H7, H9) and used for genome-wide gene expression analysis. Two lines of each EC type (hiPS or hES) were randomly selected for full characterization and were subjected to a comprehensive series of standard endothelial characterization tests, including immunostaining, fluorescent acetylated LDL (Dil-Ac-LDL) uptake assays, and Matrigel assays. Both hiPS-ECs and hES-ECs developed cobblestone morphology and stained positive for the endothelial markers PECAM-1 (CD31), VE-cadherin (CD144), endothelial nitric oxide (eNOS), and von Willebrand factor (vWF)

(Fig. 3.3, 3.4). These cells also formed vascular network-like structures when placed on Matrigel (Fig. 2.5A) and were able to incorporate 1,1'-dioctadecyl-3,3,3',3'-tetramethlyindocarbocyanine perchlorate-acetylated-low density lipoprotein (Dil-Ac-LDL) (Fig. 3.5B). hiPS-ECs and hES-ECs also migrated in response to VEGF (Fig. 3.5C). When compared to a hESC line, all EC lines tested produced significantly higher levels of nitric oxide, which is a fundamental determinant of vascular homeostasis (Fig. 3.5D).

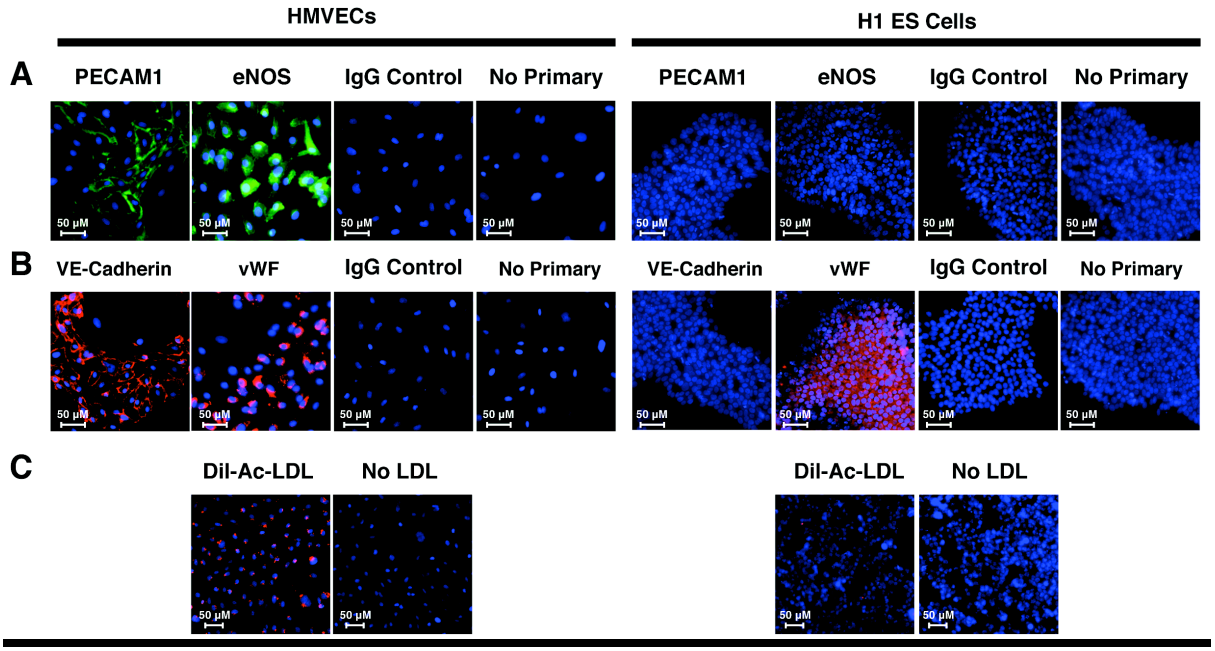

Figure 3.4 Control immunofluorescence staining. (A): Staining of positive control (HMVECs) and negative control (H1 ES) with PECAM1 and eNOS primary antibodies (green). The same alexa-488 secondary was used to visualize both primary antibodies. Negative control no primary wells were stained with secondary antibody only. **(B):** Staining for VE-Cadherin or vWF (red). The same alexa-594 secondary was used to visualize both primary antibodies. **(C):** Dil-Ac-LDL alexa 594 uptake (red) in positive control (HMVEC) or negative control (H1 ES) cells. Negative

control cells received no Alexa 594 conjugated LDL. Nuclei in all panels visualized with DAPI (blue).

An *in vivo* Matrigel plug assay was used to evaluate the angiogenic capabilities of $CD31^+/CD144^+$ pluripotent cell derived ECs. When ECs are mixed with Matrigel and injected subcutaneously in a mouse, they organize into functional capillaries that link with the endogenous circulatory system and carry red blood cells. All of the hiPS-ECs and hES-ECs were able to form functional blood capillaries in a similar fashion to primary ECs, as indicated by the robust staining for human CD31 and the presence of blood cells within some lumens (Fig. 3.5E).

3.4.4 Gene Expression Analysis of Pluripotent Cell-Derived Endothelial Cells

Global gene expression of the pluripotent cell–derived endothelial cells (ES/iPS) and primary human ECs was profiled by microarrays and 32 genes with the highest differential gene expression between various groups were subsequently analyzed by qRT-PCR (Figures 3.8, 3.10, 3.11, 3.12). Human aortic ECs (HAECs), human saphenous vein ECs (HSVECs), and human lymphatic ECs (HLECs) were chosen as representative primary cell lines of the three major EC types of the body: arterial, venous, and lymphatic. The primary ECs were grown *in vitro* in EC medium until passage 3, while still actively dividing, and the cells were collected for total RNA extraction.

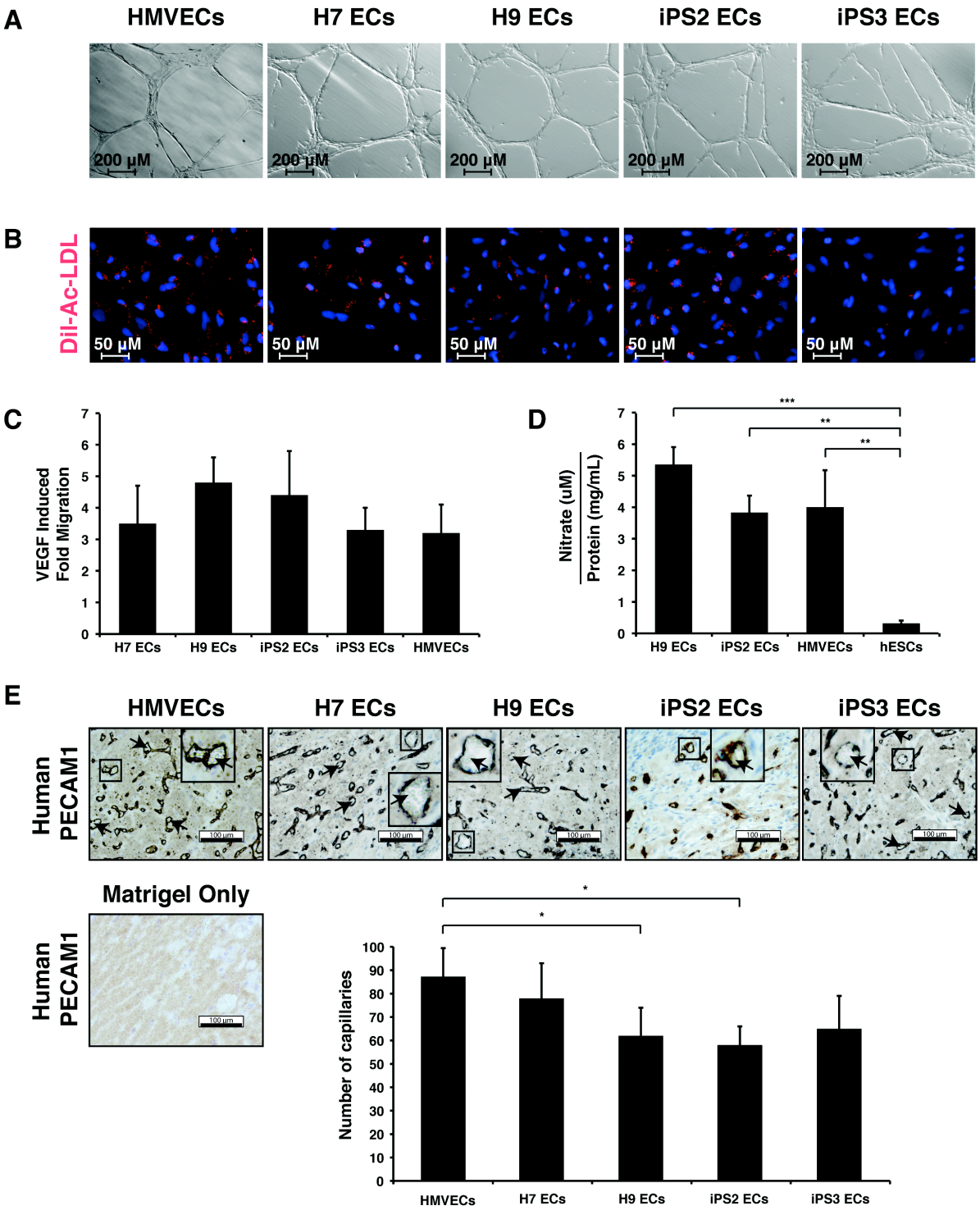
A
HMVECs
H7 ECs
H9 ECs
iPS2 ECs
iPS3 ECs
200 μM
B
DiI-Ac-LDL
50 μM
C
VEGF Induced Fold Migration
H7 ECs
H9 ECs
iPS2 ECs
iPS3 ECs
HMVECs
D
Nitrate (uM) / Protein (mg/mL)
***
**
**
H9 ECs
iPS2 ECs
HMVECs
hESCs
E
HMVECs
H7 ECs
H9 ECs
iPS2 ECs
iPS3 ECs
Human PECAM1
100 μm
Matrigel Only
Human PECAM1
*
*
Number of capillaries
HMVECs
H7 ECs
H9 ECs
iPS2 ECs
iPS3 ECs

Figure 3.5 Functional characterization of endothelial cells derived from pluripotent stem cells. (A): Bright-field microscopy of Matrigel tube formation assay showing *in vitro* angiogenesis potential. **(B):** Fluorescent microscopy of Dil-Ac-LDL uptake (red) and nuclei (blue) in endothelial cells derived from pluripotent stem cells. **(C):** Quantification of endothelial cell migration induced by VEGF. The graph shows fold migration, which refers to migration rate when stimulated with VEGF divided by migration rate without VEGF. All measurements were performed in triplicate and were not statistically different from one other using one-way ANOVA with Bonferroni's multiple comparison post hoc test. **(D):** Quantification of nitric oxide production. Cells were grown for 24 hr. in serum free media in the presence of 50ng/mL VEGF at which time nitrite concentration was measured in the conditioned media by HPLC. The nitrite concentration was adjusted for cell number by measuring the protein concentration of the cell lysate, resulting in arbitrary units of nitric oxide production. All measurements were performed using one-way ANOVA with Bonferroni's multiple comparison post hoc test (* $P< 0.05$, ** $P< 0.01$, *** $P< 0.001$). **(E):** Bright field microscopy of representative sections from *in vivo* Matrigel plug angiogenesis assay. Human PECAM1 staining is shown in brown. Blood cells are indicated (arrowheads). Scale bars represent 100 μm. Quantification of average capillary number from 6 fields of view per cell line is displayed ± standard deviation. Statistical significance was determined using one-way ANOVA with Bonferroni's multiple comparison post hoc test (* $P< 0.05$). No human PECAM1 positive cells or

capillaries were observed in animals injected with matrigel only and this condition was excluded from subsequent graphing and statistical analysis.

D14 ES- or iPS-derived ECs were thawed and matured until D21, at which point cell proliferation had decreased, as expected. All lines were collected for RNA at full confluence when the ECs were contact inhibited and displayed cobblestone morphology.

We compared three human ES–derived ECs (H1, H7, and H9 ECs) to three genetically independent human iPS–derived EC lines (iPS1, iPS2, and iPS3 ECs), as well as one of the same iPS cell line differentiated on two separate days (iPS2 Day X and iPS2 Day Y). In addition, we compared ES- and iPS-derived EC lines differentiated with two independent methods (H9 EC-A, H9 EC-B, iPS3 EC-A, and iPS3 EC-B). Method A represents the new differentiation method described here and Method B is an embryoid body + VEGF method.

When comparing array $\log_2$ intensity values from all ESC– and iPSC–derived ECs pair wise, Pearson's R^2 values were >0.97 for all pairs (Fig. 3.6A and Fig 3.7A). Clustering analysis of all genes with twofold or greater difference in gene expression between any two samples clearly revealed a single cluster containing all three primary ECs and a second cluster that included all ES– or iPS–derived ECs (Fig. 3.6B).

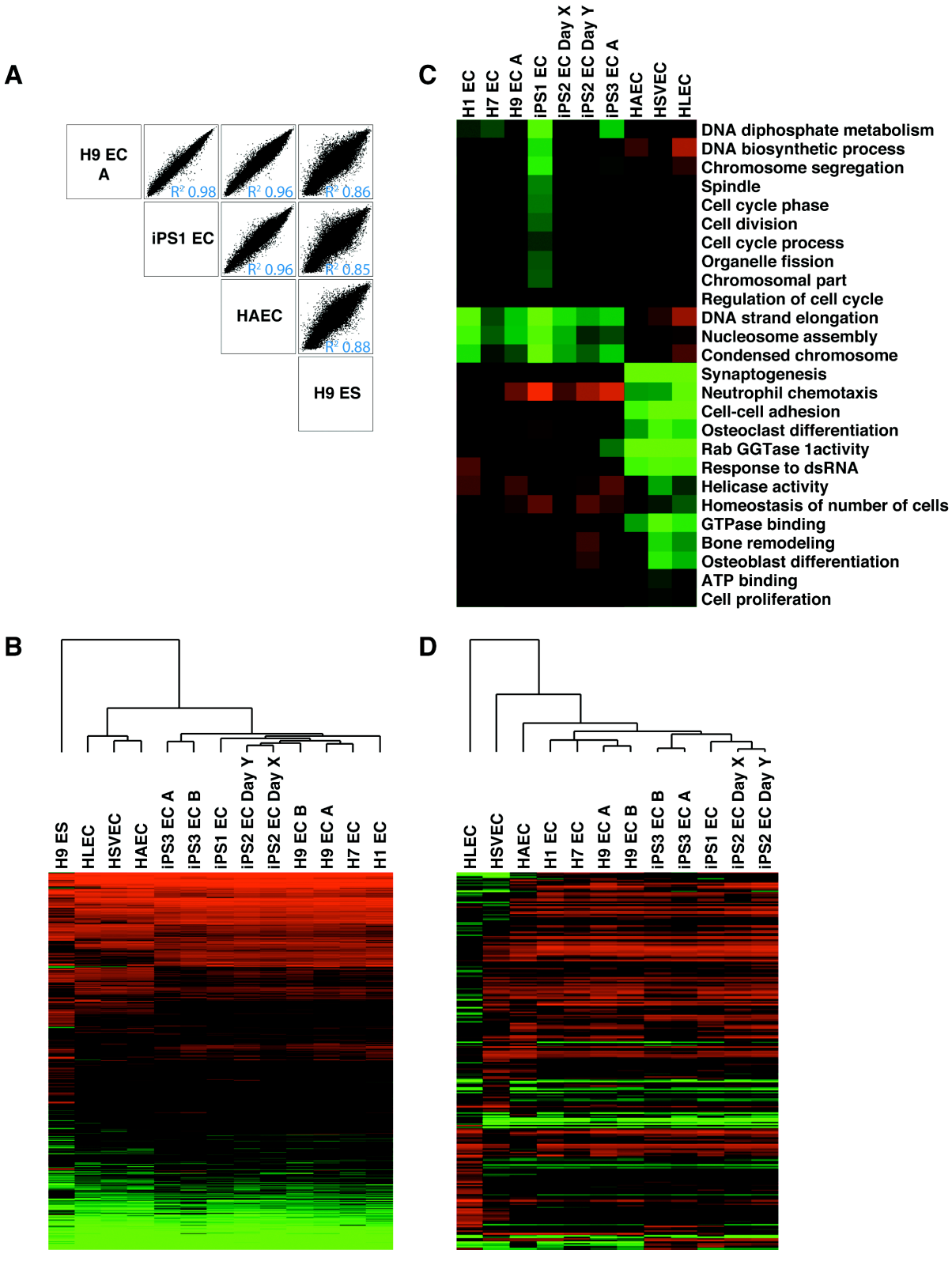
A
H9 EC A
iPS1 EC
HAEC
H9 ES
R² 0.98
R² 0.96
R² 0.86
R² 0.96
R² 0.85
R² 0.88
B
H9 ES
HLEC
HSVEC
HAEC
iPS3 EC A
iPS3 EC B
iPS1 EC
iPS2 EC Day Y
iPS2 EC Day X
H9 EC B
H9 EC A
H7 EC
H1 EC
C
H1 EC
H7 EC
H9 EC A
iPS1 EC
iPS2 EC Day X
iPS2 EC Day Y
iPS3 EC A
HAEC
HSVEC
HLEC
DNA diphosphate metabolism
DNA biosynthetic process
Chromosome segregation
Spindle
Cell cycle phase
Cell division
Cell cycle process
Organelle fission
Chromosomal part
Regulation of cell cycle
DNA strand elongation
Nucleosome assembly
Condensed chromosome
Synaptogenesis
Neutrophil chemotaxis
Cell-cell adhesion
Osteoclast differentiation
Rab GGTase 1activity
Response to dsRNA
Helicase activity
Homeostasis of number of cells
GTPase binding
Bone remodeling
Osteoblast differentiation
ATP binding
Cell proliferation
D
HLEC
HSVEC
HAEC
H1 EC
H7 EC
H9 EC A
H9 EC B
iPS3 EC B
iPS3 EC A
iPS1 EC
iPS2 EC Day X
iPS2 EC Day Y

Figure 3.6 Global gene expression in endothelial cells derived from multiple pluripotent stem cell lines and primary endothelial cells. (A): Log2 intensity plots of representative samples from four groups of cells: ESC-ECs (H9 EC-A), iPS-ECs (iPS1-EC), Primary ECs (HAEC), and ESCs (H9 ES). **(B)**: Heat map and clustering analysis of genes displaying at least two fold differential expression between any sample (15,740 genes). Scale extends from 2.5 to 13. Red indicates log2 intensity >7.0, and green <7.0. iPS2 EC Day X and iPS2 EC Day Y indicate the same iPSC line differentiated in two independent experiments. iPS3 EC A and iPS3 EC B refer to the same iPSC line differentiated by two different methods. **(C)**: Heat map of GO analysis terms that differentiate pluripotent-cell derived ECs from primary ECs. Genes with threefold difference in expression between pluripotent cell derived ECs and primary ECs and P value < 0.05 were selected (968 genes) and GO Elite was used to group them by GO category with an adjusted P value < 0.05. Red indicates average log2 intensity of genes in each category that are higher than 8.75, and green lower than 8.75. **(D)**: Heat Map and clustering analysis of genes with at least four fold differential expression between any two of the primary endothelial cell lines, not considering X and Y chromosome genes (240 genes). Red indicates log2 intensity >7.0 and Green <7.0. All Array data available from Gene Expression Omnibus (accession number GSE37631).

Genes differentially expressed between these two clusters included mainly those involved in cell cycle and adhesion, likely reflecting the nature of the 6 day primary

culture vs. longer-term differentiation of the pluripotent stem cells (day 21). Importantly, when comparing ECs from the same pluripotent cell line differentiated in two separate experiments (iPS2 Day X ECs and iPS2 Day Y ECs) or ECs from the same pluripotent cell line differentiated with two separate methods (iPS3 EC-A:iPS3 EC-B or H9 EC-A:H9 EC-B), differences in gene expression were very small: Pearson's R = 0.99 for all comparisons and only 7 protein coding genes were differentially regulated by more than 2 fold between the two different methods (Fig. 3.7A and Table S3.1). Expression of cell cycle genes were similar under all conditions and protocols.

When comparing ES– and iPS–derived endothelial cells, only 17 protein coding genes were differentially expressed by more than threefold and 147 genes showed greater than twofold differences (P value ≤0.05) (Tables S3.2 and S3.3 and Fig. 3.8). Genes upregulated in iPS-ECs showed significant overlap with genes reported to be upregulated in iPS derived beating clusters or iPS cells in an undifferentiated state when compared to ES counterparts, whereas genes downregulated in iPS-ECs did not show overlap with genes downregulated specifically in iPS cells or iPS derived beating clusters compared to their ES counterparts (Table S3.4) (Gupta et al. 2010; Chin et al., 2009; Marchetto et al., 2009). When analyzed with GO-Elite, iPS-ECs had reduced expression of genes involved in cell division/cell cycle and higher expression levels of genes involved in cell adhesion, chemotaxis, and proteolysis compared to ES-ECs, potentially indicating a difference in growth and senescence (Fig. 3.9).

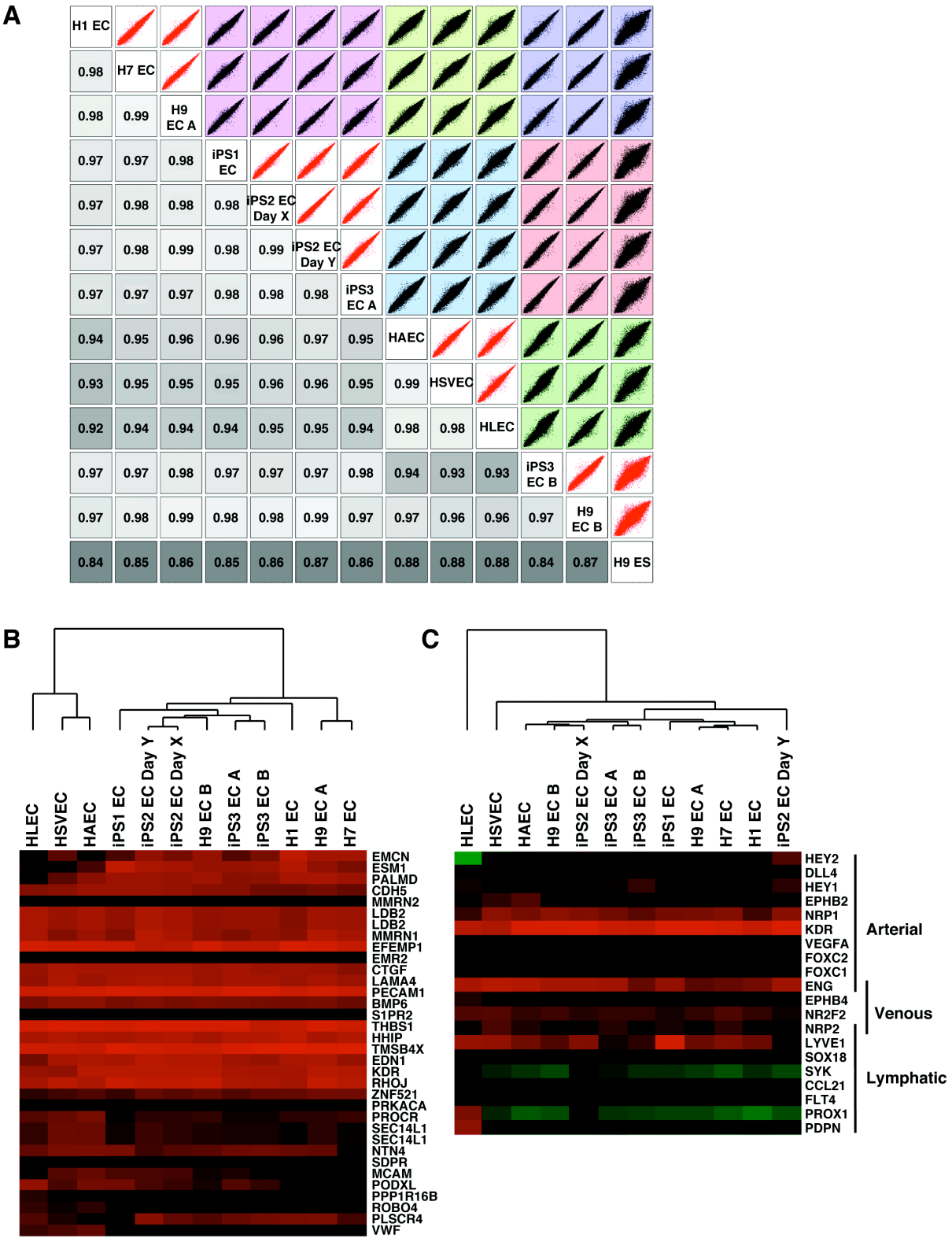
A
H1 EC
0.98 H7 EC
0.98 0.99 H9 EC A
0.97 0.97 0.98 iPS1 EC
0.97 0.98 0.98 0.98 iPS2 EC Day X
0.97 0.98 0.99 0.98 0.99 iPS2 EC Day Y
0.97 0.97 0.97 0.98 0.98 0.98 iPS3 EC A
0.94 0.95 0.96 0.96 0.96 0.97 0.95 HAEC
0.93 0.95 0.95 0.95 0.96 0.96 0.95 0.99 HSVEC
0.92 0.94 0.94 0.94 0.95 0.95 0.94 0.98 0.98 HLEC
0.97 0.97 0.98 0.97 0.97 0.97 0.98 0.94 0.93 0.93 iPS3 EC B
0.97 0.98 0.99 0.98 0.98 0.99 0.97 0.97 0.96 0.96 0.97 H9 EC B
0.84 0.85 0.86 0.85 0.86 0.87 0.86 0.88 0.88 0.88 0.84 0.87 H9 ES
B
HLEC
HSVEC
HAEC
iPS1 EC
iPS2 EC Day Y
iPS2 EC Day X
H9 EC B
iPS3 EC A
iPS3 EC B
H1 EC
H9 EC A
H7 EC
EMCN
ESM1
PALMD
CDH5
MMRN2
LDB2
LDB2
MMRN1
EFEMP1
EMR2
CTGF
LAMA4
PECAM1
BMP6
S1PR2
THBS1
HHIP
TMSB4X
EDN1
KDR
RHOJ
ZNF521
PRKACA
PROCR
SEC14L1
SEC14L1
NTN4
SDPR
MCAM
PODXL
PPP1R16B
ROBO4
PLSCR4
VWF
C
HLEC
HSVEC
HAEC
H9 EC B
iPS2 EC Day X
iPS3 EC A
iPS3 EC B
iPS1 EC
H9 EC A
H7 EC
H1 EC
iPS2 EC Day Y
HEY2
DLL4
HEY1
EPHB2
NRP1
KDR
VEGFA
FOXC2
FOXC1
ENG
EPHB4
NR2F2
NRP2
LYVE1
SOX18
SYK
CCL21
FLT4
PROX1
PDPN
Arterial
Venous
Lymphatic

Figure 3.7. Extended microarray analysis. (A): Log_2 intensity plots of all samples from four groups of cells; ESC ECs (H1, H7, H9, H9 cont.), iPSC ECs (iPS1, iPS2A, iPS2B, iPS3, iPS3 Cont.), primary ECs (HAEC, HSVEC, HLEC)and ESCs (H9 ES). Red points are between group comparisons. Values in lower left are Pearson's R values of log transformed values. **(B):** Heat map and clustering analysis of genes specifically expressed in endothelial cells. Scale extends from 2.5 to 13. Red indicates log_2 intensity higher than 7.5, and green lower than 7.5. **(C):** Heat map and clustering analysis of genes culled from the literature that are specifically expressed in different endothelial cell subtypes. Overlapping bars indicate genes expressed in two of the three primary cell lines. Scale extends from 2.5 to 13. Red indicates log_2 intensity higher than 7.5, and green lower than 7.5.

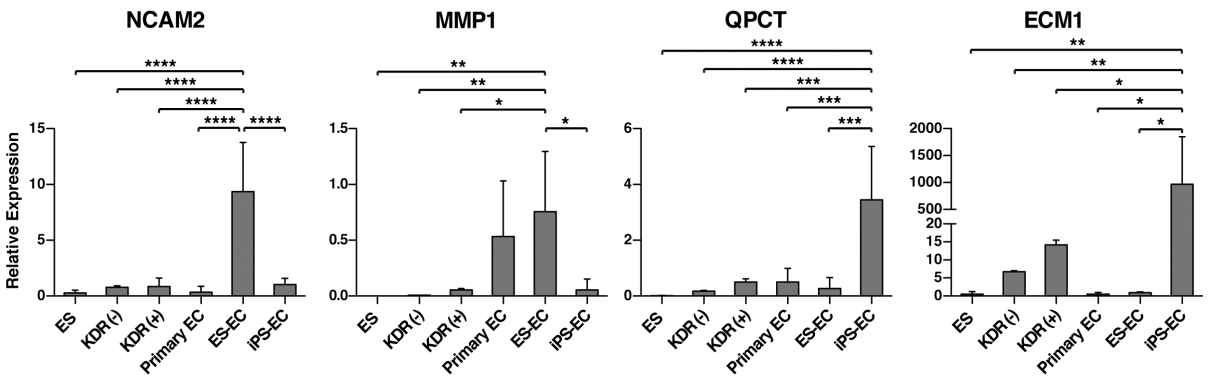

Figure 3.8 Microarray data validation by qRT-PCR of genes differentially expressed between ES-ECs and iPS-ECs by at least 4 fold. Average gene expression from three biological replicates is plotted and error bars show standard deviation. Primary EC bar is average of HAECs, HSVECs and HLECs. RNA samples from H9 hES cells (ES), day 6 H9 differentiated cells (KDR^{-}), or endothelial precursors (KDR^{+}), are included for reference. Statistical significance was determined using one-way ANOVA with Bonferroni's multiple comparison post hoc test(* $P< 0.05$, ** $P< 0.01$, *** $P< 0.001$, **** $P< 0.0001$).

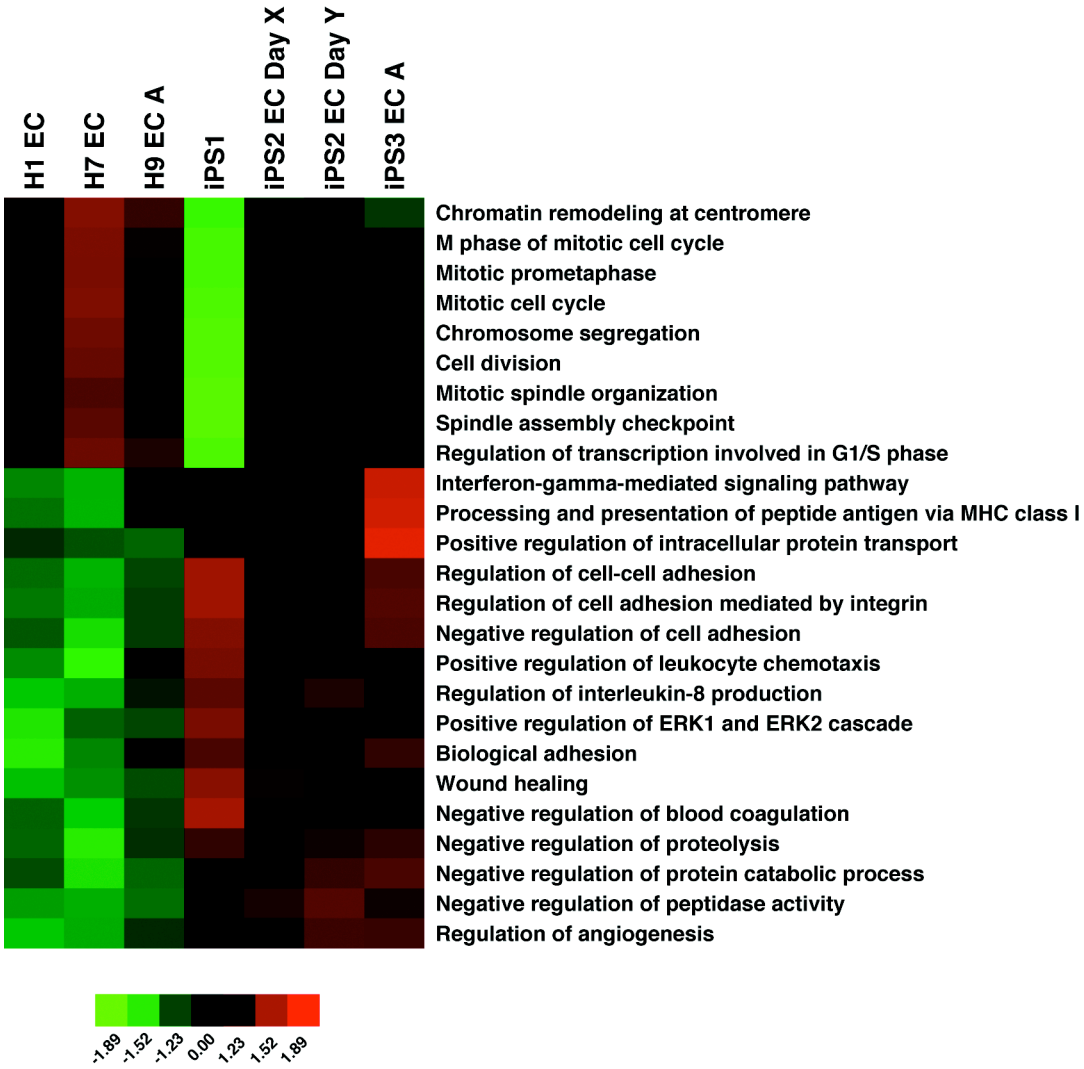

Figure 3.9. Gene ontology differences between ES-ECs and iPS ECs. Heat map of GO analysis terms that differentiate iPS-ECs from ES-ECs. Genes with twofold difference in expression between iPS-ECs and ES-ECs and P value < 0.05 were selected (147 genes) and GO Elite was used to group them by GO category with an adjusted P value < 0.05.

To calculate the difference in gene expression variance across all genes between hES– and hiPS–derived ECs, the non-parametric Wilcoxon signed rank test was used. This test calculates and determines which group of ECs (hES– or hiPS–derived) has higher variance in gene expression for each individual gene on the microarray (28,439 genes).Then, each group is assigned a percentage corresponding to the number of individual genes across the entire microarray that are more variable. If hES or hiPS cells have a fundamental difference in their ability to generate endothelial cells or a certain type of endothelial cells, then one might expect global gene expression to be more highly variable between different lines in one of the types of pluripotent derived ECs. For example, if hiPS cells stochastically have incomplete epigenetic remodeling during reprogramming and thus more heterogeneity between pluripotent lines, one might expect more variation in expression when comparing each gene individually across the transcriptome. 54% of the genes showed higher variance in hiPS–ECs, while 46% were more variant in hESC–ECs, indicating iPS– and ES–derived ECs have similar variance in gene expression and implying a lack of fundamental difference between the ability of hES and iPS cells to generate ECs.

The limited gene expression variation between the ES– or iPS–derived ECs allowed us to group them together for further comparisons with primary culture of ECs. Pairwise comparisons between ES– or iPS–derived ECs and primary ECs resulted in a range of Pearson's R^2 values of 0.92–0.97. Grouping all of the pluripotent cells together and comparing them to primary ECs, we found 839 genes

with at least threefold change up or down (P value ≤0.05). When analyzed with GO Elite, ES– and iPS–derived ECs had reduced expression of genes involved in cell division/cell cycle and higher expression levels of genes involved in integrin-mediated cell adhesion and chemotaxis compared to primary ECs, including CDK2, CDK6, FAT1, RGS5 AND PCDHB5 (Fig. 3.6C and Fig. S3.10). This difference likely reflects the fact that primary cells were analyzed after only 3 passages and 6 days of culture, while pluripotent cell-derived ECs were passaged 7-8 times and cultured for 21 days prior to analysis; both cell types are known to decrease their proliferative rate with prolonged culture

Limiting the comparisons to endothelial-specific genes (Ho et al., 2003), the ES– or iPS–derived ECs and primary cells all expressed high levels of KDR, PECAM1, CDH5 (VE-cadherin), LAMA4, MCAM, and THBS1. ES– or iPS–derived ECs expressed lower levels of vWF, PRKACA, and ROBO4 and higher levels of PLSCR4 when compared to primary ECs (Fig. 3.7B). qRT-PCR showed lower expression levels of Nitrtic Oxide Synthase 3 and Von Willebrand Factor and higher expression of VEGF receptor 2 in pluripotent derived ECs compared to primary ECs (Fig. 3.11). Using a set of known EC type–specific genes to perform cluster analysis, ES– and iPS–derived ECs lacked expression of canonical lymphatic specific genes PROX1, PDPN, and SOX18 (Fig. 3.7C). Cluster analysis indicated ES– and iPS–derived ECs were most similar to arterial cells *in vitro*.

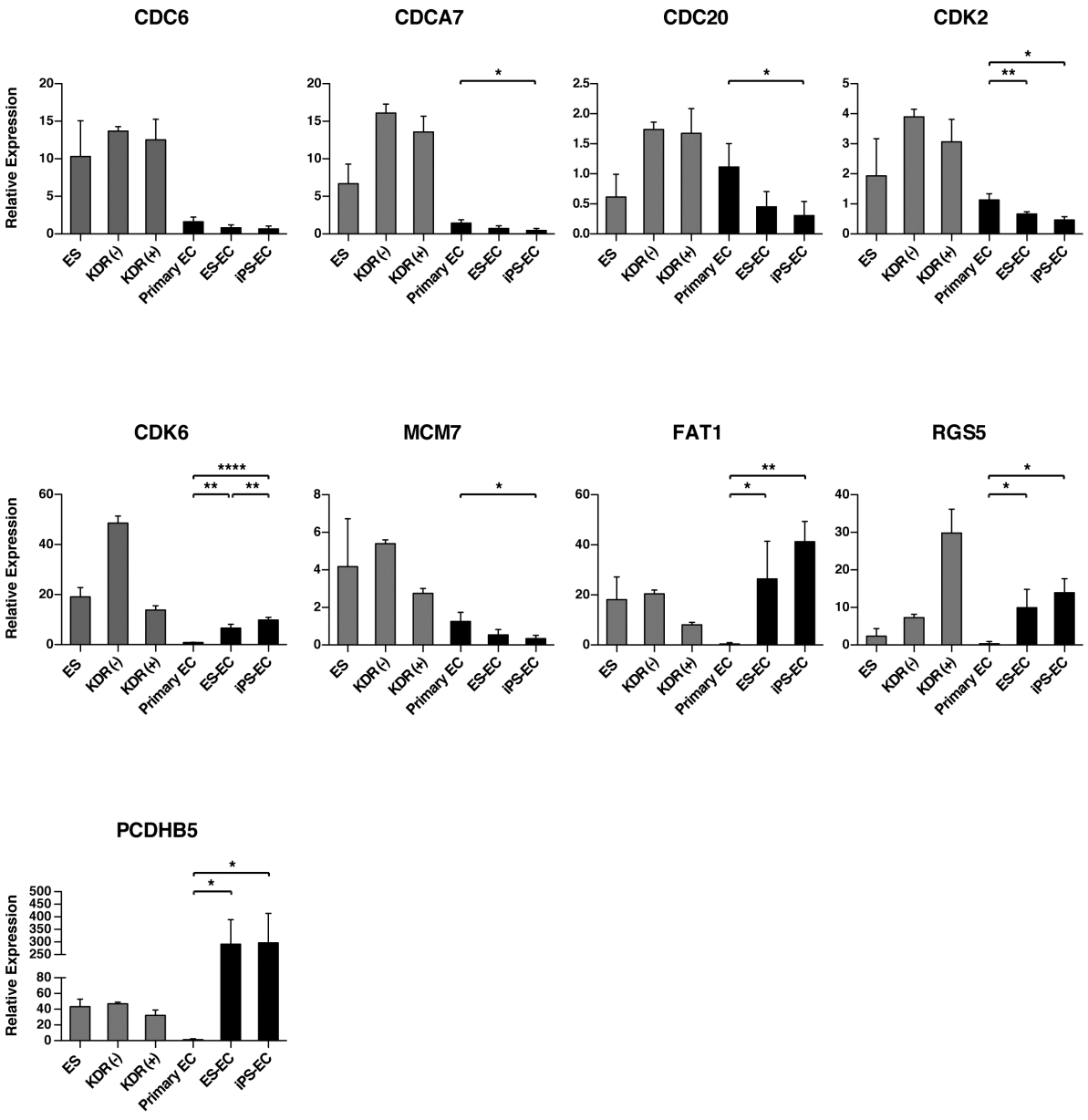

Figure 3.10 Microarray data validation by qRT-PCR of genes differentially expressed between primary-ECs and pluripotent derived-ECs (ES-ECs and iPS-ECs). Average gene expression from three biological replicates is plotted and

error bars show standard deviation. RNA samples from H9 hES cells (ES), day 6 H9 differentiated cells (KDR^{-}), or endothelial precursors (KDR^{+}), are included for reference but were not included in the statistical analysis because of the null hypothesis being tested, i.e., that there is no difference in expression between primary ECs and pluripotent derived ECs. Statistical significance was determined using one-way ANOVA with Bonferroni's multiple comparison post hoc test(* $P< 0.05$, ** $P< 0.01$, **** $P< 0.0001$).

To perform an unbiased cluster analysis, the top 250 genes differentially expressed between the three primary endothelial cell types were identified and genes with X and Y chromosome locations were removed to control for sex of primary cell source. Then, gene expression analysis and clustering was extended to the ES– or iPS–derived ECs. This impartial clustering analysis also indicated ES– or iPS–derived ECs, by the method described here, are most similar to primary arterial cells *in vitro* (Fig. 3.6D, Fig. 3.12). In addition, FACS analysis showed that 86% of pluripotent cell-derived ECs were positive for expression of the arterial EC marker, EPHB2, although the levels of VEGF in the media could also induce EPHB2 expression in venous derived cells (Fig. 3.2C).

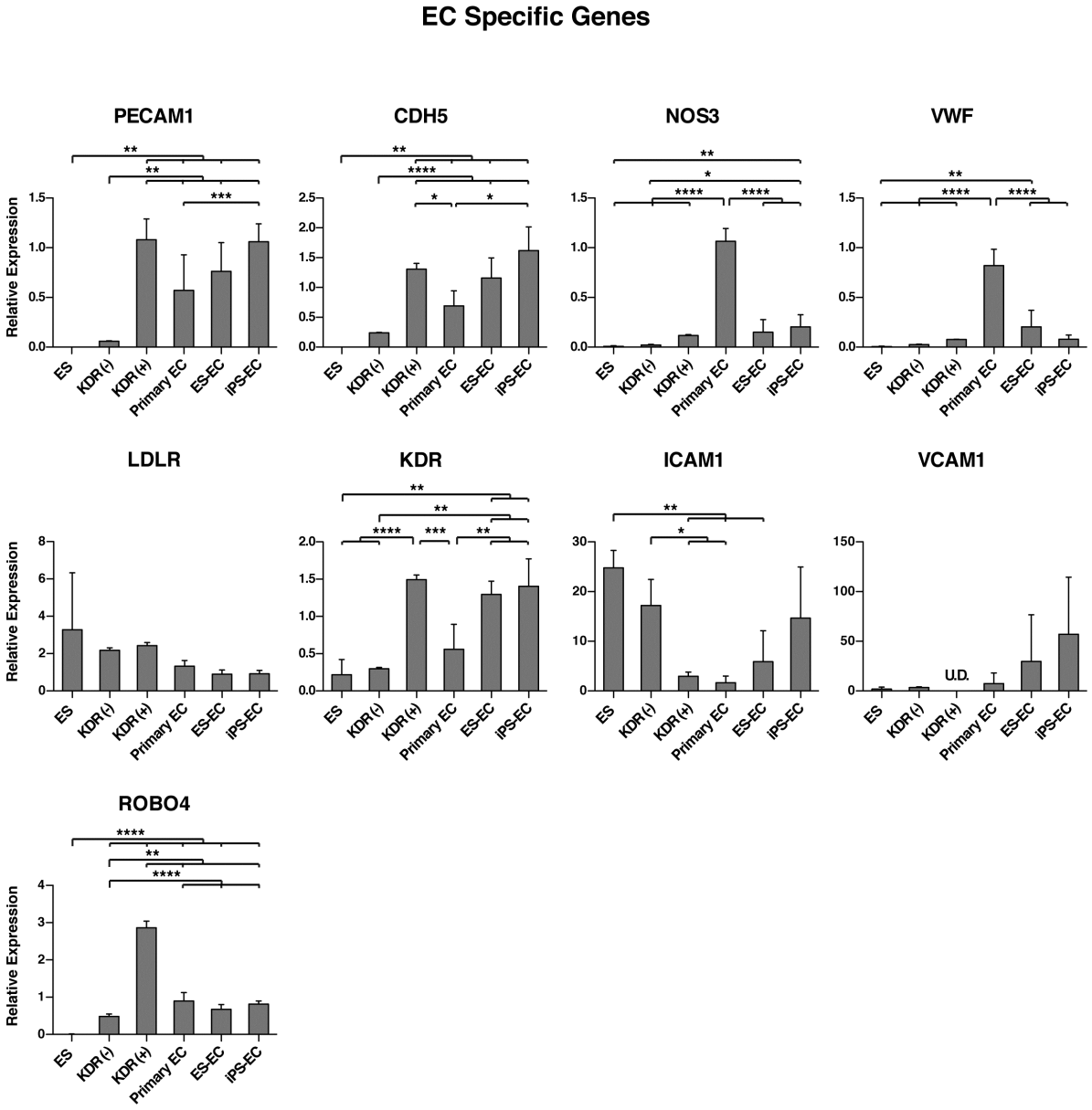

Figure 3.11 EC specific genes expressed in indicated cell types. Average gene expression from three biological replicates is plotted and error bars show standard deviation. Statistical significance was determined using one-way ANOVA with Bonferroni's multiple comparison post hoc test(* $P < 0.05$, ** $P < 0.01$, *** $P < 0.001$, **** $P < 0.0001$).

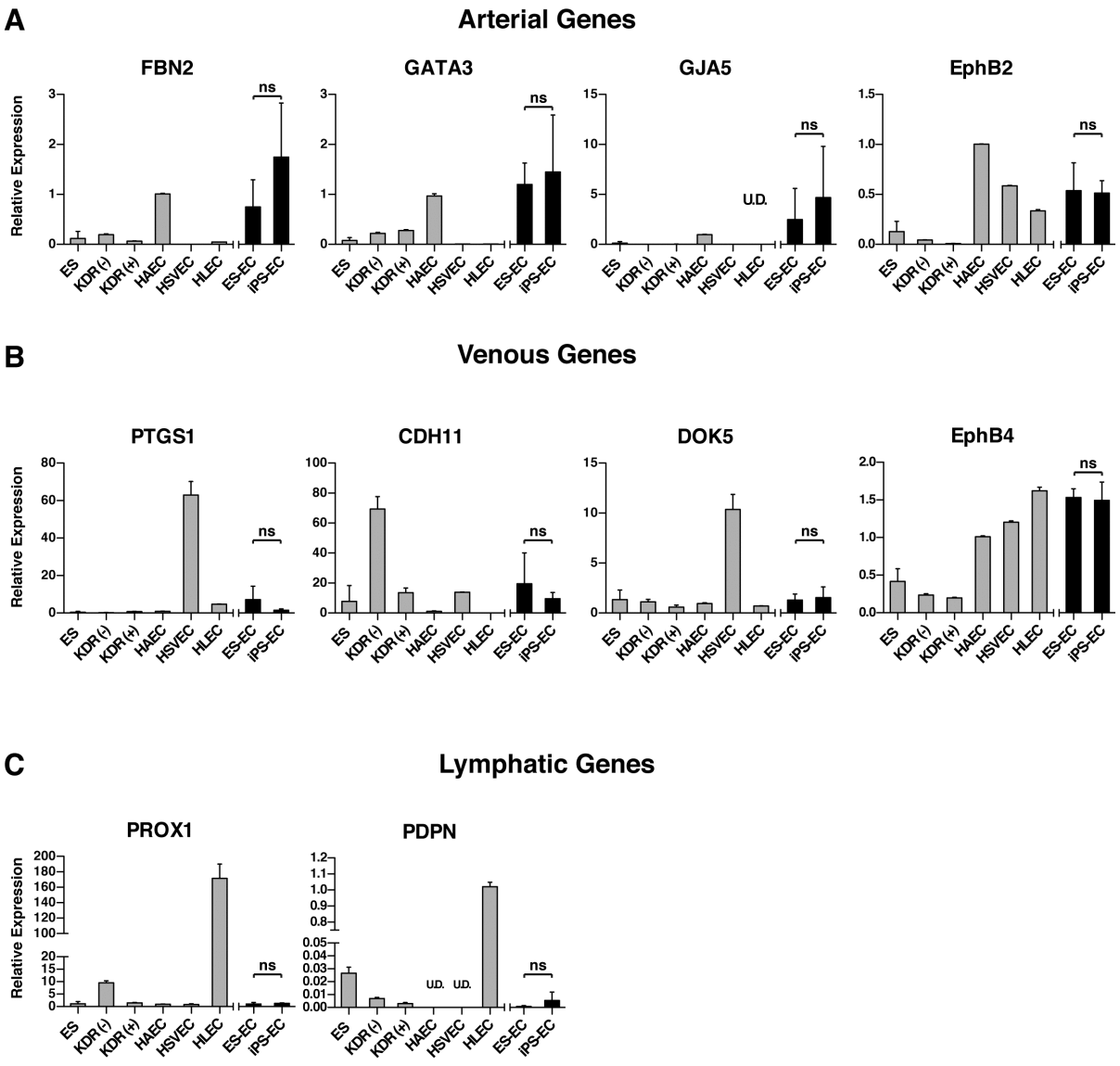

Figure 3.12 Microarray data validation by qRT-PCR of genes differentially expressed between (A) Arterial (B) Venous and (C) Lymphatic EC subtypes. Grey bars show the mean expression level from each of the primary EC types and error bars show technical standard deviation as a reference to compare the pluripotent derived ECs. Black bars show the average of three biological replicates of each EC type (ES or iPS derived) and error bars show standard deviation. RNA

samples from H9 hES cells (ES), day 6 H9 differentiated cells (KDR-), or endothelial precursors (KDR+), are included for reference but were not included in the statistical analysis. ES-ECs and iPS ECs were compared with students t test and no genes showed statistical differences in expression between these two pairs.

3.5 Discussion

3.5.1 Discussion Summary

This study describes a simple method for differentiating human pluripotent stem cells into ECs amenable to multiple pluripotent cell lines, which revealed limited gene expression variability among multiple human iPS- and ES-derived ECs. In this method, stem cells were guided through cell fate decisions mimicking their EC development in vivo, and the intermediate progenitors could be isolated, unlike previously described approaches. This advancement provides a platform for investigating novel aspects of human EC fate commitment, including chromatin remodeling and gene expression changes. Furthermore, the limited variance in gene expression of a defined human iPS-derived cell type supports the potential for successful detection of meaningful transcriptome alterations in iPS-based disease models.

3.5.2 EC Subtype

Of the EC subtypes, ECs derived using this differentiation method most closely resembled arterial cells, as previously reported for in vitro derived ECs (Yamamizu et

al., 2010). Future functional studies such as monocyte adhesion assays could further define the EC subtype. The medium used for the growth and expansion of the KDR+ precursors contains relatively high concentration of human-VEGF, which promotes the arterial fate by inducing NOTCH signaling (Lanner et al., 2007). Immature ECs show plasticity and can switch between arterial and venous fates (Oliver et al., 2010). Further maturation into fully differentiated arterial cells may require higher levels of VEGF, cAMP, or induction of NOTCH signaling by shear stress. Based on our knowledge of EC development in vivo, NOTCH signaling inhibition or retinoic acid treatment might induce ECs to venous or lymphatic fates, respectively (Lanner et al., 2007; Marino et al., 2011). Isolation of significant numbers of human KDR+ endothelial precursors, uniquely enabled by the approach we describe, will permit interrogation of early EC-type fate determination through high-throughput screening or candidate approaches, taking cues from zebrafish and mouse development.

3.5.3 Primary EC comparison

The gene expression of the pluripotent derived ECs resembles the primary derived ECs, though they express lower levels of NOS3 and vWF than the primary cells, which may indicate incomplete maturation. Importantly, the in vivo Matrigel plug angiogenesis assays indicate that the endothelial cells produced from ES or iPS derived sources are capable of organizing into functional capillaries that link with the endogenous circulatory system and carry red blood cells, though further studies are

necessary to determine if the cells from this protocol can functionally rescue a disease model such as hind limb ischemia or myocardial infarction.

3.5.4 ES and iPS derived EC Comparison

This study is the first comprehensive analysis of ECs derived from multiple hESC and hiPSC lines. The wide variation in percent KDRhigh/med cells derived from the same pluripotent cell line during separate differentiations is quite surprising and seems to be influenced by the state of pluripotent cells in combination with reagent variability, which is a major problem for directed differentiation protocols. This variation may impede interrogation of the role genetic mutations play in affected and unaffected iPS cell differentiation potential and requires the use of multiple cell lines from each group. It seems that the health and purity of the starting ES or iPS cell line on the first day of differentiation played a larger role in the success of the differentiation than the passage number of the pluripotent cell line, as some of the most successful differentiations were from ES cells with a passage number over 200. Fortunately, after purification using a cell surface marker, the resulting cell populations were seemingly more homogeneous, allowing for more accurate comparisons between different pluripotent cell lines. Our data indicate some significant disparity in gene expression between pluripotent cell–derived ECs and primary ECs. Many of these differences are related to cell cycle and adhesion. One possible explanation is that the primary cells were collected at passage 3 (day 6 of culture) to minimize in vitro gene expression changes and, thus, were in a more

proliferative state. In contrast, the pluripotent cell–derived ECs were grown to day 21 (7–8 passages), and their proliferation rates had greatly decreased by that time, indicating a shift towards a senescent state, as expected. Senescent primary ECs at high passage numbers display higher levels of integrin β4 signaling, similar to our pluripotent cell–derived ECs, indicating a shared characteristic of senescence at high passage number between the two EC types (Sun et al., 2010). The addition of the TGFb-inhibitory molecule, SB431542, during EC differentiation seems to promote cell proliferation and inhibit senescence and could be a useful tool for expanding pure populations of ECs (James et al., 2010).

Our data indicate that despite gene expression heterogeneity between undifferentiated hESC and hiPSC lines as a whole (Bock et al., 2011), ECs derived from both pluripotent cell types are very similar. While there are some iPS-specific upregulated genes, most of the gene expression differences between ES-ECs and iPS-ECs were related to cell cycle and adhesion. These gene programs seem to be mutually exclusive in our data sets and most likely reflect differences between proliferation genes (high cell cycle, low adhesion) and senescence genes (low cell cycle, high adhesion) that would be expected in endothelial cells maintained in long-term culture. In addition, the high concordance of gene expression between ECs derived from the same pluripotent cell line via separate experiments or differentiation methods indicates that in a well-defined differentiated cell type, such as CD31+/CD144+ ECs, gene expression differences are most likely due to the inherent differentiation capacity of the originating cell line. These findings are

relevant as we consider bioengineering vascularized tissues or creating vascular grafts for ischemic repair using hiPSCs. In addition, given the limited variability, ECs derived from patient-specific iPSCs should be useful in modeling diseases caused by defects in EC differentiation or maintenance, enabling the identification of molecular mechanisms underlying such ailments. Successful modeling of endothelial diseases with limited gene expression "noise" will enable drug-screening strategies using iPSC–derived ECs to identify novel therapeutics.

3.6 Materials and Methods

3.6.1 Human PSC Culture and Differentiation into Endothelial Cells

hESCs (H1, H7, and H9) and hiPSCs (iPS1, iPS2, and iPS3) were cultured according to WiCell Protocols under feeder-free conditions on matrigel-coated plates in mTeSR®1 (Stem Cell Technologies, Vancouver, BC) in a hypoxic environment (5% CO_2, 5% O_2). hiPSC lines were all derived by reprogramming fibroblasts with four factors (Oct4, Sox2, Klf4, and c-Myc) and were fully characterized for pluripotency. iPS1 is the iPSC line K23F (Shinya Yamanaka & Kiichiro Tomoda , unpublished), iPS2 is 3S5F, and iPS3 is Huf5 (Nakamura et al., 2009; Byrne et al., 2009). To induce differentiation, hESCs and hiPSCs were detached with Dispase (Gibco, Carlsbad, CA) and scraped with a cell lifter and then placed into StemPro-34 (Invitrogen) supplemented with 10 ng/mL pen/strep, 2 mM L-glutamine, 150 mg/mL Transferrin, 1 mM ascorbic acid, and $4X10^{-4}$ M monothioglycerol (MTG) (Sigma, St.

Louis, MO). All cytokines, including human-bFGF, human-Activin A, human-BMP4 (R&D Systems, Minneapolis, MN) and human-VEGF (Calbiochem, Gibbstown, NJ), were added at the indicated time points and concentrations. Pluripotent stem cells were cultured in a hypoxic environment (5% CO_2, 5% O_2, 90% N_2) until D6 of differentiation. After D6, MACS was performed according to the manufacturers protocol and KDR^+ cells were plated on fibronectin (Sigma) in a normoxic environment (5% CO_2, 20% O_2, 75% N_2) in ECM medium (ScienCell, Carlsbad, CA) with 5% FBS, pen/strep and ECGS (10 mg/ml BSA, 10 mg/ml apo-transferrin, 5 mg/ml insulin, 10 ng/ml EGF, 2 ng/ml bFGF, 2 ng/ml VEGF, 2 ng/ml IGF-1, 1 mg/ml hydrocortisone and 30 ng/mL retinoic acid). KDR^+ cells were allowed to grow to 80–90% confluence and were then split 1:3 using 0.05% trypsin. Control differentiations consisted of EB formation followed by addition of 10 ng/mL VEGF from D1 to D14 and then $CD31^+$ cell sorting on D14.

3.6.2 Flow Cytometry and Magnetic Cell Sorting

Accutase (Millipore, Bellerica, MA) was used to generate single-cell suspensions from EBs plated overnight on fibronectin. The cells were stained with KDR-PE-conjugated antibodies (R&D Systems) and FACS sorted on a FACS ARIA 2 or MACS sorted on a midi column (Miltenyi Biotec, Auburn, CA) according to the manufacturer's protocol. CD31 antibodies conjugated to magnetic beads (Miltenyi Bio) were used with midi columns to further purify cultures contaminated with more than 10% non-ECs. Characterization of fully differentiated endothelial cells was

determined by PECAM-1-488-conjugated primary antibody (CD31, R&D Systems) or VE-cadherin-PE-conjugated antibody (CD144; R&D Systems) staining. EPHB2 staining was performed with recombinant mouse EphB4 Fc chimera protein (R&D Systems). Fluorescent intensity was determined for 10,000 cells total and percentages shown in all Figures are the percent of live single cells that fall within the gate shown. Gates were determined using a negative control (isotype specific IgG) stained cell population.

3.6.3 Immunocytochemical Staining

To characterize the phenotype of ECs, purified cells were stained with antibodies against endothelial markers, including PECAM-1 (CD31, R&D Systems), VE-cadherin (CD144; R&D Systems), endothelial nitric oxide synthase (eNOS; BD Pharmingen, San Diego, CA, USA), von Willebrand factor (vWF; Abcam, Cambridge MA). Briefly, the cells were fixed with paraformaldehyde (4%), permeabilized with Triton X-100 (0.1%), and blocked with either normal goat or donkey serum (1%) for 30 minutes, followed by overnight incubation with the primary antibodies at 4°C. The cells were washed with 1x PBS and incubated with Alexa Fluor-488 or -594 secondary antibodies for 1 hour at room temperature. Cells were washed with 1x PBS, and the nuclei were stained with Hoechst 33342 dye (Invitrogen, Carlsbad, CA).

3.6.4 Acetylated LDL Uptake

Cells were incubated with Dil-labeled Ac-LDL (10 μg/ml; Invitrogen) for 4 hours at 37°C. After incubation, the cells were washed with 1x PBS before being visualized and photographed under a fluorescent microscope.

3.6.5 In Vitro Matrigel Assay

Cells (2.5 x 10^5) were seeded on 24-well plates pre-coated with growth factor-reduced Matrigel (BD Discovery Labware, Bedford, MA) and incubated for 24 hours at 37°C. Images were taken using a light microscope.

3.6.6 In Vivo Matrigel Injection

To determine if hiPSC– and hESC–derived ECs formed functional blood vessels *in vivo*, a Matrigel plug assay was performed using immunodeficient SCID mice. Matrigel was mixed with bFGF (50 ng/ml; Peprotech, Rocky Hill, NJ) and ECs (5×10^5). The mixture was subcutaneously injected into SCID mice. After 14 days, the animals were euthanized and the Matrigel plugs were removed. Paraffin-embedded matrigel sections were stained with human CD31. The number of capillaries formed by the ECs was counted under 200x magnification from 6-7. All animals were treated in accordance with an approved protocol from the Stanford Administrative Panel on Laboratory Animal Care.

3.6.7 Endothelial Cell Migration Assay

EC migration was measured using BD Biocoat Angiogenesis System and the manufacturer's protocol. Briefly, a cell suspension of 4.0 x 10 cells/ml was prepared for each EC sample and added into 24-well plate inserts. The insert plates were incubated for 24 hours at 37°C, 5% CO_2. The inserts were removed and transferred to another plate containing calcein AM solution, and the plates were incubated for 90 minutes at 37°C, 5% CO_2. A fluorescence plate reader with bottom-reading capabilities at excitation/emission wavelengths of 494/517 nm was used to quantify fluorescence of the cells that successfully migrated. The fold migration was calculated by the fluorescence value of the treated cells over the untreated cells

3.6.8 Nitric Oxide Measurement

Production of nitric oxide was determined using HPLC measurement of nitrite in media after 24 hrs of cell conditioning. Following media collection, the cells were lysed with RIPA buffer containing protease inhibitors and the protein concentration for each cell type was measured using BCA assay to adjust nitrite levels for cell number.

3.6.9 RNA Extraction, Microarray, and qRT-PCR validation

All cells were washed with PBS and placed in Trizol (Invitrogen). Total RNA was collected using phenol/chloroform extraction with phase-lock tubes (5 Prime,

Gaithersburg, MD). The RNA was cleaned and DNAse digested on RNeasy columns (Qiagen, Valencia, CA). RNA was amplified, fragmented, and labeled using NuGEN Technologies Applause Plus kits and the manufacturer's instructions. Labeled samples were then hybridized to Affymetrix Human Gene 1.0 ST GeneChips. The GeneChips were then washed and stained on Affymetrix 450 Fluidics Stations and scanned on an Affymetrix 3000 Scanner according to standard protocols. Validation of a selected set of differentially expressed genes was performed by quantitative reverse transcriptase-PCR (qRT-PCR) using standard Taq-Man primer sets (Applied Biosystems) on an ABI-7900 HT.

3.6.10 Bioinformatics Analysis

Microarrays were normalized to control for array-specific effects with the Affymetrix Power Tools software using Robust Multi-Array normalization. For statistical analyses, all probe sets in which none of the groups had an average log2 intensity greater than 3.0 were removed. This is a standard cutoff, under which the expression levels are indistinguishable from background. All array data are available from Gene Expression Omnibus (accession number GSE37631). Linear models were fitted for each gene using the limma package (Smyth 2008) in R/Bioconductor. Moderated t-statistics and the associated P-values were calculated. P-values were adjusted for multiple testing by controlling for false-discovery rate (FDR, which is the expected percentage of falsely-declared differentially expressed genes among the set of all declared differentially expressed genes) using the Benjamini-Hochberg

method. Differential expression was defined using a threshold of 2–4-fold change as indicated and a P-value of < 0.05. Hierarchical cluster analysis was performed on normalized array values with Cluster 3.0 with Euclidean distance and single linkage for >10,000 genes and average linkage for smaller gene sets. Heatmaps were generated with Java TreeView. GO Analysis was completed using GO Elite with default settings.

3.6.11 Statistical Analysis

All experiments were performed at least three times unless otherwise stated. All statistical analysis was completed using GraphPad Prism software. Two-way analysis was completed with two-tailed unpaired t tests with a 95% confidence interval. Multiple comparison tests were performed by One-way ANOVA with Bonferroni post test with Alpha = 0.05 (95% confidence interval).

Chapter 4:

Summary, Future Directions, and Perspective

Uncovering the detailed role of NOTCH1 signaling in aortic valve disease is just beginning. Following the discovery by our lab of NOTCH1 mutations causing bicuspid aortic valves with a rapid onset of calcification in 2005, two mouse models with decreased NOTCH signaling further indicated the important role of NOTCH signaling in this disease. Unfortunately, the cell types responsible and a genome wide description of NOTCH1 targets involved in the pathologic aspects of this disease remain unclear. Our study provides a global overview of NOTCH1 signaling during static and laminar shear stress in endothelial cells. Shear stress seems to directly activate a gene program responsible for maintaining non-calcified regions of long bones called the epiphyseal plate in a NOTCH1 dependent manner. One of these genes, *MGP*, is the most potent inhibitor of vascular calcification described to date in a mouse model. We find NOTCH1 directly activates *MGP* through an upstream, CSL dependent endothelial enhancer. In an attempt to determine if similar gene programs are altered in our patients, we generated iPS cells from members of the families with NOTCH1 mutations. We also developed an efficient method to generate endothelial cells from human ES or iPS cells. ECs from both pluripotent cell types are arterial-like and have limited gene expression differences. While we have

made great progress in defining the molecular mechanisms of this disease, some important questions remain.

4.1 Which genes are responsible for the NOTCH1 calcification phenotype?

Our studies provide a global overview of genes affected by a 50% reduction in *NOTCH1,* including those potentially directly targeted. In addition, based on the gene expression changes induce by shear stress in a NOTCH1 dependent manner, we have identified 21 high priority genes that may play a role in valve calcification, but we have not tested their direct involvement in our NOTCH1 patients, or in the phenotypic outcome *in vivo*.

To test the role of these downstream genes in patients, we generated iPS cells and derived endothelial cells from 3 unaffected patients and 4 affected patients with NOTCH1 mutations. These cells were placed in either static, or shear stress conditions, and then we used RNA–seq to profile gene expression transcriptome-wide. Pending the results of this analysis, we will cross reference our primary cell data generated by RNA–seq and ChIP–seq to identify similar gene expression changes from both cells types. This analysis will allow us to further prioritize our targeted gene lists to those relevant to the affected patients.

To evaluate the impact of each target gene on the NOTCH disease phenotype in vivo, we would utilize mouse models. Simple expression profiling of endothelial cells from *NOTCH1* (+/-), or *CSL* (+/-) mice compared to control

endothelial cells could uncover conserved sets of NOTCH signaling dependent genes between human and mouse. Then, conserved genes could be overexpressed in endothelial cells to systematically test for rescue of the valve calcification phenotype. In addition, could test genetic interactions of two genes using epistatic experiments. To this end, we have tested wildtype, *NOTCH1* (+/-), or *NOTCH1* (+/-)/*MGP* (+/-) mice on a high fat/cholesterol diet. Unfortunately, even after 10 months, we failed to see an increase in valve calcification in any of the groups (data not shown). Going forward, one might try using a diet with higher levels of vitamin D to induce more rapid bone ectopic formation. The *CSL* heterozygous mouse on a high fat diet is the most viable candidate model with the most consistent valve calcification phenotype developing in a relatively short amount of time (4 months) (Nus et al., 2011). We would attempt to replicate this phenotype and then add back genes down–regulated by inhibition of NOTCH signaling. A CAG-flox–stop–flox–(gene of interest) transgenic mouse could be targeted to the rosa locus. Then, we could activate the gene of interest specifically in the endothelium by crossing to Cdh5(PAC) –CreERT2 transgenic mice. To address the cell type specific importance of NOTCH signaling in valve calcification, we could add back *CSL* just to the endothelium in the *CSL* global (+/-) mouse.

4.2 What cell type is responsible for the phenotype?

The original characterization of both the *NOTCH1* mutant families and the *CSL* (+/-) mice focused on valve interstitial cells to explain the molecular mechanisms of the

disease. Unfortunately, neither study characterized nor provided proof of the cell type most affected by *NOTCH1* mutations. In addition, recent evidence suggests atherosclerotic calcifications are driven by multi-potent vascular progenitor cells, not resident smooth muscle cells, challenging the dogma of the field (Tang et al., 2012). Therefore, careful lineage tracing analysis of cells involved in valve calcification will be vital to understanding and ultimately preventing or treating this disease. The removal of Jagged1 from mouse endothelial and interstitial cells results in valve calcification, thus potentially ruling out altered NOTCH signaling in immune cells playing a role in the disease process. Currently, there are no valve interstitial cell specific Cre recombinase mice. Endothelial cell specific removal of Jagged1 or *CSL* in adulthood using Cdh5(PAC)-CreERT2 could at least test if endothelial expression of this gene is necessary to prevent calcification. We have generated mice with the endothelial specific Cdh5(PAC)-CreERT2 and either *CSL* (fl/+) or *CSL* (fl/fl), and induced recombination of this allele after adulthood. These mice were placed on a high fat diet for 10 months and then echoed to determine blood flow rate across the aortic valve. We saw no significant increase in flow rate that would indicate valve stenosis, but more detailed histological analysis has yet to be completed. In addition, to determine what cell type differentiates into the ostoblast like cell that drives the calcification and thus the disease, we could perform cell lineage tracing using cell lineage specific expression of Cre recombinase and a Cre activated reporter in combination with staining for RUNX2. Some evidence suggests that this cell may originate from the endothelium through an EMT process.

4.3 Does altering NOTCH1 signaling change the rate of EMT in adults?

A recent study showed a subset of valve endothelial cells are progenitor cells capable of undergoing EMT and repopulating the pool of interstitial cells during homeostasis and in response to disease (Bischoff and Aikawa, 2011). This cell type acts in a similar fashion to the endocardial cushion endothelial cells that eventually populate the valve interstitium. TGFβ and NOTCH1 signaling promote endothelial cell EMT during valve development, though the role of NOTCH1 in adult EMT has yet to be determined. Lineage tracing of endothelial cells in the context of Wt or decreased levels of NOTCH signaling, could determine how this signaling pathway affects the pool of valve interstitial cells. Also, we could test *in vitro* cultures of human aortic for their rate of EMT and subsequent capacity for osteoblast cell differentiation in the context of normal or low amounts of NOTCH signaling. Finally, we could potentially test similar parameters using our NOTCH1 patient–derived endothelial cells.

4.4 How is NOTCH1 activated by shear stress?

One of the biggest outstanding questions resulting from this body of work is the molecular mechanism by which NOTCH1 signaling is activated by shear stress. NOTCH receptors and ligands are activated by shear stress within 30 minutes of shear stress onset (Masumura et al., 2009). Intriguingly, since NOTCH1 is

membrane bound, the receptor itself could act as a mechanosensor. Mapping the temporal kinetics of NICD translocation to the nucleus could help determine this possibility. The proposed endothelial cell mechanosensory complex includes PECAM–1, VE–Cadherin, and VEGFR2. Interestingly, longer term NOTCH1 activation via shear stress requires phosphorylation of VEGFR2 and activation of both the PKC–MAPKK–ERK and PI3K–Akt pathways. We are interested in determining whether NOTCH1 signaling is activated directly by shear stress or indirectly via other known flow regulated signaling pathways in a short temporal window. Finally, testing NOTCH1 activation ligand dependence and/or cell autonomy will help define the molecular mechanism.

4.5 Is NOTCH signaling playing a role in the neoangiogenesis of calcifying cells?

After lesion formation in aortic valve disease, neoangiogenesis can occur in the normally avascular valve. This increase in vascularity is thought to induce inflammation and potentially contribute to osteoblast migration and proliferation. NOTCH signaling plays an important role in stabilizing vessels and preventing cell proliferation. In addition, a new study shows MGP inhibition of BMP signaling also helps resolve and stabilized newly formed blood vessels (Sharma and Albig, 2012). Thus, decreased NOTCH1 receptor and subsequent decreases in MGP may lead to an increase in endothelial cell proliferation and neoangiogenesis in the valve during calcification. Quantification of blood vessel density in calcifying aortic valves in this

context may help determine if this is taking place. This also calls for the generation of a floxed allele of *MGP*, so this important protein's role can be dissected in different cell types.

4.6 Can we develop a better protocol to generate more in vivo like endothelial cells?

We believe that Matrix Gla Protein is one of the most important downstream targets of NOTCH1 in endothelial cells. MGP is also arterial specific and activated by shear stress in a NOTCH1 dependent manner. Unfortunately, MGP is not expressed in endothelial cells derived from pluripotent stem cells using our new differentiation method, though we have shown these cells to be arterial–like. In order to determine if mutations in NOTCH1 alter MGP expression in ECs from our patients, we must alter our differential protocol to obtain cells expressing this protein at similar levels to primary arterial cells from the aorta or aortic valve. One of the main differences between endothelial cells that differentiate *in vivo,* versus our *in vitro,* is the presence of shear stress. Placing freshly sorted KDR^{+} endothelial progenitor cells from mice in shear stress conditions activates expression of the arterial endothelial cell specific marker EphrinB2 via the VEGF and NOTCH signaling pathways (Masumura et al., 2009). Adding a similar step to our protocol may produce a cell with a similar phenotype. In addition, additional factors may be necessary for the initial activation of MGP including VEGF or NOTCH ligands to further "arterialize" the cells, or addition of retinoic acid, which we have shown activates MGP in endothelial cells.

We may find even with modifications, our protocol will never generate an endothelial cell expressing adequate levels of MGP to test our hypothesis. In this case, several other recently published protocols may provide alternate strategies to accomplish this goal. The direct conversion of mature amniotic cells to endothelial cells has been accomplished by forced expression of ETV2, FLI1 and ERG1 in combination with TGFβ inhibition. A similar method using iPS cells or adult human fibroblasts may also yield endothelial cells. In addition, a new protocol using modulators of Wnt signaling generates large numbers of cardiac myocytes from pluripotent stem cells. We could use this method to generate cardiac mesoderm and then potentially endothelial cells by adding VEGF and FGF and/or shear stress. Finally, we have preliminary evidence that addition of *ETV2* and *FOXC2* mRNA to human ES cells rapidly induces expression of CD31, a marker of endothelial cells. Further optimization and characterization of this method may provide an alternative method to generate MGP expressing endothelial cells. Hopefully, an alteration of existing methods, or adopting new differentiation methods will allow us to test if *NOTCH1* mutations in endothelial cells derived from our patients actually affect MGP expression levels.

4.7 Concluding Remarks

Our lab was the first to link a genetic mutation with the presence of a bicuspid aortic valve and subsequent early onset valve calcification. It is our hope that deeply understanding the molecular mechanisms of this extreme form of the disease may

provide insights applicable to the general process of valve calcification and potentially the similar process of atherosclerosis. We showed NOTCH1 signaling in human aortic valves controls a genetic program similar to that of the epiphyseal plate. Many questions remain unanswered and there are many experiments left to complete. By defining the compendium of genes directly and indirectly impacted by shear stress and NOTCH1, we hope to provide a global overview and basis to test additional hypotheses in order to more fully understand this disease. Finally, we hope this research may one day lead to discoveries that help slow or reverse the progression of aortic valve calcification and ultimately positively impact the quality of life for patients suffering from this terrible disease.

References

1. Akat K, Borggrefe M, Kaden JJ. Aortic valve calcification: basic science to clinical practice. Heart. 2008;95(8):616–623.

2. Ankeny RF, Thourani VH, Weiss D, et al. Preferential Activation of SMAD1/5/8 on the Fibrosa Endothelium in Calcified Human Aortic Valves - Association with Low BMP Antagonists and SMAD6. Cardona P-J, ed. PLoS ONE. 2011;6(6):e20969.

3. Bailey TL, Boden M, Buske FA, et al. MEME SUITE: tools for motif discovery and searching. Nucleic Acids Res. 2009;37(Web Server):W202–W208.

4. Bischoff J, Aikawa E. Progenitor Cells Confer Plasticity to Cardiac Valve Endothelium. J. of Cardiovasc. Trans. Res. 2011;4(6):710–719.

5. Bock C, Kiskinis E, Verstappen G, et al. Reference maps of human ES and iPS cell variation enable high-throughput characterization of pluripotent cell lines. Cell. 2011; 144:439-452

6. Bossé Y, Mathieu P, Pibarot P. Genomics: the next step to elucidate the etiology of calcific aortic valve stenosis. J Am Coll Cardiol. 2008;51(14):1327–1336.

7. Bouchard-Martel J, Roussel É, Drolet M-C, Arsenault M, Couet J. Interstitial cells from left-sided heart valves display more calcification potential than from right-sided valves: an in-vitro study of porcine valves. J Heart Valve Dis. 2009;18(4):421–428.

8. Bray SJ. Notch signalling: a simple pathway becomes complex. Nat Rev Mol Cell Biol. 2006;7(9):678–689.

9. Brütsch R, Liebler SS, Wüstehube J, et al. Integrin cytoplasmic domain-associated protein-1 attenuates sprouting angiogenesis. Circulation Research. 2010;107(5):592–601.

10. Buschmann I, Pries A, Styp-Rekowska B, et al. Pulsatile shear and Gja5 modulate arterial identity and remodeling events during flow-driven arteriogenesis. Development. 2010;137(13):2187–2196.

11. Butcher JT, Nerem RM. Valvular endothelial cells and the mechanoregulation of valvular pathology. Philos Trans R Soc Lond, B, Biol Sci. 2007;362(1484):1445–1457.

12. Byrne JA, Nguyen HN, Reijo Pera RA. Enhanced generation of induced pluripotent stem cells from a subpopulation of human fibroblasts. PLoS ONE 2009;4:7118.

13. Cancela ML, Price PA. Retinoic acid induces matrix Gla protein gene expression in human cells. Endocrinology. 1992;130(1):102–108.

14. Chadjichristos CE, Scheckenbach KEL, van Veen TAB, et al. Endothelial-Specific Deletion of Connexin40 Promotes Atherosclerosis by Increasing CD73-Dependent Leukocyte Adhesion. Circulation. 2010;121(1):123–131.

15. Chakraborty S, Cheek J, Sakthivel B, Aronow BJ, Yutzey KE. Shared gene expression profiles in developing heart valves and osteoblast progenitor cells. Physiological Genomics. 2008;35(1):75–85.

16. Chandra S, Rajamannan NM, Sucosky P. Computational assessment of bicuspid aortic valve wall-shear stress: implications for calcific aortic valve disease. Biomech Model Mechanobiol. 2012.

17. Chen J-H, Yip CYY, Sone ED, Simmons CA. Identification and Characterization of Aortic Valve Mesenchymal Progenitor Cells with Robust Osteogenic Calcification Potential. American Journal Of Pathology. 2009;174(3):1109–1119.

18. Chin MH, Mason MJ, Xie W, et al. Induced Pluripotent Stem Cells and Embryonic Stem Cells Are Distinguished by Gene Expression Signatures. Cell Stem Cell 2009;5:111–123.

19. Cho SW, Moon SH, Lee SH, et al. Improvement of Postnatal Neovascularization by Human Embryonic Stem Cell-Derived Endothelial-Like Cell Transplantation in a Mouse Model of Hindlimb Ischemia. Circulation 2007;116(21):2409–2419.

20. Cola C, Almeida M, Li D, Romeo F, Mehta JL. Regulatory role of endothelium in the expression of genes affecting arterial calcification. Biochem Biophys Res Commun. 2004;320(2):424–427.

21. Combs MD, Yutzey KE. Heart Valve Development: Regulatory Networks in Development and Disease. Circulation Research. 2009;105(5):408–421.

22. Cooke JP. Flow, NO, and atherogenesis. Proc Natl Acad Sci USA. 2003;100:768–770.

23. Cross MJ, Claesson-Welsh L. FGF and VEGF function in angiogenesis: signalling pathways, biological responses and therapeutic inhibition. Trends Pharmacol Sci 2001;22:201–207.

24. Danziger J. Vitamin K-dependent proteins, warfarin, and vascular calcification. Clin J Am Soc Nephrol. 2008;3(5):1504–1510.

25. Davies PF, Civelek M, Fang Y, Guerraty MA, Passerini AG. Endothelial heterogeneity associated with regional athero-susceptibility and adaptation to disturbed blood flow in vivo. Semin Thromb Hemost. 2010;36(3):265–275.

26. Descamps B, Emanueli C. Vascular differentiation from embryonic stem cells: Novel technologies and therapeutic promises. Vascular Pharmacology 2012;56(5-6):267–279.

27. Dodou E, Xu S-M, Black BL. mef2c is activated directly by myogenic basic helix-loop-helix proteins during skeletal muscle development in vivo. Mechanisms of Development. 2003;120(9):1021–1032.

28. Egan KP, Kim JH, Mohler ER, Pignolo RJ. Role for Circulating Osteogenic Precursor Cells in Aortic Valvular Disease. Arteriosclerosis, Thrombosis, and Vascular Biology. 2011;31(12):2965–2971.

29. Ernst J, Kheradpour P, Mikkelsen TS, et al. Mapping and analysis of chromatin state dynamics in nine human cell types. Nature. 2011;473(7345):43–49.

30. Fedak PWM. Clinical and Pathophysiological Implications of a Bicuspid Aortic Valve. Circulation. 2002;106(8):900–904.

31. Garg V, Muth AN, Ransom JF, et al. Mutations in NOTCH1 cause aortic valve disease. Nature. 2005;437(7056):270–274.

32. Ge G. Bone Morphogenetic Protein-1/Tolloid-related Metalloproteinases Process Osteoglycin and Enhance Its Ability to Regulate Collagen Fibrillogenesis. Journal of Biological Chemistry. 2004;279(40):41626–41633.

33. Geleijnse JM, Vermeer C, Grobbee DE, et al. Dietary intake of menaquinone is associated with a reduced risk of coronary heart disease: the Rotterdam Study. J. Nutr. 2004;134(11):3100–3105.

34. Geleijnse JM, Vermeer C, Grobbee DE, et al. Dietary intake of menaquinone is associated with a reduced risk of coronary heart disease: the Rotterdam Study. J. Nutr. 2004;134(11):3100–3105.

35. Ghaisas NK, Foley JB, O'Briain DS, Crean P, Kelleher D, Walsh M. Adhesion molecules in nonrheumatic aortic valve disease: endothelial expression, serum levels and effects of valve replacement. J Am Coll Cardiol. 2000;36(7):2257–2262.

36. Grant DS, Kleinman HK, Martin GR. The role of basement membranes in vascular development. Ann N. Y. Acad Sci 1990;588:61–72.

37. Gupta MK, Illich DJ, Gaarz A, et al. Global transcriptional profiles of beating clusters derived from human induced pluripotent stem cells and embryonic stem cells are highly similar. BMC Dev Biol 2010;10:98.

38. Ho M, Yang E, Matcuk G, et al. Identification of endothelial cell genes by combined database mining and microarray analysis. Physiol Genomics 2003;13:249–262.

39. Hofmann JJ, Briot A, Enciso J, et al. Endothelial deletion of murine Jag1 leads to valve calcification and congenital heart defects associated with Alagille syndrome. Development. 2012.

40. Holden RM, Sanfilippo AS, Hopman WM, Zimmerman D, Garland JS, Morton AR. Warfarin and aortic valve calcification in hemodialysis patients. J Nephrol. 2007;20(4):417–422.

41. Holliday CJ, Ankeny RF, Jo H, Nerem RM. Discovery of shear- and side-specific mRNAs and miRNAs in human aortic valvular endothelial cells. AJP: Heart and Circulatory Physiology. 2011;301(3):H856–H867.

42. Huang HP, Chen PH, Hwu WL, et al. Human Pompe disease-induced pluripotent stem cells for pathogenesis modeling, drug testing and disease marker identification. Human Molecular Genetics. 2011;20(24):4851–4864.

43. Hubbard T, Barker D, Birney E, et al. The Ensembl genome database project. Nucleic Acids Res. 2002;30(1):38–41.

44. Ishibashi S, Goldstein JL, Brown MS, Herz J, Burns DK. Massive xanthomatosis and atherosclerosis in cholesterol-fed low density lipoprotein receptor-negative mice. Journal of Clinical Investigation. 1994;93(5):1885.

45. James D, Nam H-S, Seandel M, et al. Expansion and maintenance of human embryonic stem cell-derived endothelial cells by TGFbeta inhibition is Id1 dependent. Nat Biotechnol 2010;28:161–166.

46. Johnson RC, Leopold JA, Loscalzo J. Vascular calcification: pathobiological mechanisms and clinical implications. Circulation Research. 2006;99(10):1044–1059.

47. Kane NM, Meloni M, Spencer HL, et al. Derivation of endothelial cells from human embryonic stem cells by directed differentiation: analysis of microRNA and angiogenesis in vitro and in vivo. Arterioscler Thromb Vasc Biol 2010;30:1389–1397.

48. Kane NM, Xiao Q, Baker AH, et al. Pluripotent stem cell differentiation into vascular cells: A novel technology with promises for vascular regeneration. Pharmacology and Therapeutics 2011;129:29–49.

49. Kattman SJ, Huber TL, Keller GM. Multipotent flk-1+ cardiovascular progenitor cells give rise to the cardiomyocyte, endothelial, and vascular smooth muscle lineages. Dev Cell 2006;11:723–732.

50. Kattman SJ, Witty AD, Gagliardi M, et al. Stage-specific optimization of activin/nodal and BMP signaling promotes cardiac differentiation of mouse and human pluripotent stem cell lines. Cell Stem Cell 2011;8:228–240.

51. Kharchenko PV, Tolstorukov MY, Park PJ. Design and analysis of ChIP-seq experiments for DNA-binding proteins. Nat. Biotechnol. 2008;26(12):1351–1359.

52. Kirfel J, Kelter M, Cancela LM, Price PA, Schüle R. Identification of a novel negative retinoic acid responsive element in the promoter of the human matrix Gla protein gene. Proc Natl Acad Sci USA. 1997;94(6):2227–2232.

53. Koos R, Mahnken AH, Mühlenbruch G, et al. Relation of Oral Anticoagulation to Cardiac Valvular and Coronary Calcium Assessed by Multislice Spiral Computed Tomography. Am. J. Cardiol. 2005;96(6):747–749.

54. Kronenberg HM. Developmental regulation of the growth plate. Nature. 2003;423(6937):332–336.

55. Langmead B, Trapnell C, Pop M, Salzberg SL. Ultrafast and memory-efficient alignment of short DNA sequences to the human genome. Genome Biol. 2009;10(3):R25.

56. Lanner F, Sohl M, Farnebo F. Functional arterial and venous fate is determined by graded VEGF signaling and notch status during embryonic stem cell differentiation. Arterioscler Thromb Vasc Biol 2007;27:487–493.

57. Leeper NJ, Hunter AL, Cooke JP. Stem Cell Therapy for Vascular Regeneration: Adult, Embryonic, and Induced Pluripotent Stem Cells. Circulation 2010;122:517–526.

58. Lewin MB. The Bicuspid Aortic Valve: Adverse Outcomes From Infancy to Old Age. Circulation. 2005;111(7):832–834.

59. Lewis NP, Henderson AH. Calcific aortic stenosis in twins: a clue to its pathogenesis? Eur Heart J. 1990;11(1):90–91.

60. Li Y-SJ, Haga JH, Chien S. Molecular basis of the effects of shear stress on vascular endothelial cells. J Biomech. 2005;38(10):1949–1971.

61. Li Z, Hu S, Ghosh Z, Han Z, Wu JC. Functional characterization and expression profiling of human induced pluripotent stem cell- and embryonic stem cell-derived endothelial cells. Stem Cells And Development. 2011;20:1701-1710.

62. Lincoln J, Lange AW, Yutzey KE. Hearts and bones: Shared regulatory mechanisms in heart valve, cartilage, tendon, and bone development. Developmental Biology. 2006;294(2):292–302.

63. Liu AC, Joag VR, Gotlieb AI. The emerging role of valve interstitial cell phenotypes in regulating heart valve pathobiology. Am J Pathol. 2007;171(5):1407–1418.

64. Luo G, Ducy P, McKee MD, et al. Spontaneous calcification of arteries and cartilage in mice lacking matrix GLA protein. Nature. 1997;386(6620):78–81.

65. Marchetto MCN, Yeo GW, Kainohana O, et al. Transcriptional Signature and Memory Retention of Human-Induced Pluripotent Stem Cells Reh TA, ed. PLoS ONE 2009;4:e7076.

66. Marino D, Dabouras V, Brändli AW, Detmar M. A role for all-trans-retinoic acid in the early steps of lymphatic vasculature development. J Vasc Res 2011;48:236–251.

67. Masumura T, Yamamoto K, Shimizu N, Obi S, Ando J. Shear Stress Increases Expression of the Arterial Endothelial Marker EphrinB2 in Murine

ES Cells via the VEGF-Notch Signaling Pathways. Arteriosclerosis, Thrombosis, and Vascular Biology. 2009;29(12):2125–2131.

68. Matys V. TRANSFAC(R) and its module TRANSCompel(R): transcriptional gene regulation in eukaryotes. Nucleic Acids Res. 2006;34(90001):D108–D110.

69. Meng X, Ao L, Song Y, et al. Expression of functional Toll-like receptors 2 and 4 in human aortic valve interstitial cells: potential roles in aortic valve inflammation and stenosis. Am J Physiol, Cell Physiol. 2008;294(1):C29–35.

70. Moretti A, Bellin M, Welling A, et al. Patient-Specific Induced Pluripotent Stem-Cell Models for Long-QT Syndrome. N Engl J Med. 2010;363(15):1397–1409.

71. Nakamura K, Salomonis N, Tomoda K, Yamanaka S, Conklin BR. G(i)-coupled GPCR signaling controls the formation and organization of human pluripotent colonies. PLoS ONE 2009; 4:7780.

72. Neph S, Kuehn MS, Reynolds AP, et al. BEDOPS: high-performance genomic feature operations. Bioinformatics. 2012;28(14):1919–1920.

73. Newburger DE, Bulyk ML. UniPROBE: an online database of protein binding microarray data on protein-DNA interactions. Nucleic Acids Res. 2009;37(Database):D77–D82.

74. Newburger DE, Bulyk ML. UniPROBE: an online database of protein binding microarray data on protein-DNA interactions. Nucleic Acids Res. 2009;37(Database):D77–D82.

75. Nigam V, Srivastava D. Notch1 represses osteogenic pathways in aortic valve cells. J Mol Cell Cardiol. 2009;47(6):828–834.

76. Nourse MB, Halpin DE, Scatena M, et al. VEGF induces differentiation of functional endothelium from human embryonic stem cells: implications for tissue engineering. Arterioscler Thromb Vasc Biol 2010;30:80–89.

77. Nus M, Macgrogan D, Martínez-Poveda B, et al. Diet-Induced Aortic Valve Disease in Mice Haploinsufficient for the Notch Pathway Effector RBPJK/CSL. Arteriosclerosis, Thrombosis, and Vascular Biology. 2011.

78. Oliver G, Srinivasan RS. Endothelial cell plasticity: how to become and remain a lymphatic endothelial cell. Development 2010;137:363–372.

79. Olsson A-K, Dimberg A, Kreuger J, Claesson-Welsh L. VEGF receptor signalling - in control of vascular function. Nat Rev Mol Cell Biol 2006;7:359–371.

80. Osman L, Yacoub MH, Latif N, Amrani M, Chester AH. Role of human valve interstitial cells in valve calcification and their response to atorvastatin. Circulation. 2006;114(1 Suppl):I547–52.

81. Perez-Pinera P, Berenson JR, Deuel TF. Pleiotrophin, a multifunctional angiogenic factor: mechanisms and pathways in normal and pathological angiogenesis. Curr. Opin. Hematol. 2008;15(3):210–214.

82. Perez-Pinera P, Berenson JR, Deuel TF. Pleiotrophin, a multifunctional angiogenic factor: mechanisms and pathways in normal and pathological angiogenesis. Curr. Opin. Hematol. 2008;15(3):210–214.

83. Price PA, Faus SA, Williamson MK. Warfarin causes rapid calcification of the elastic lamellae in rat arteries and heart valves. Arteriosclerosis, Thrombosis, and Vascular Biology. 1998;18(9):1400–1407.

84. Quarto N, Leonard B, Li S, et al. Skeletogenic phenotype of human Marfan embryonic stem cells faithfully phenocopied by patient-specific induced-pluripotent stem cells. Proceedings of the National Academy of Sciences. 2012;109(1):215–220.

85. Rattazzi M, Iop L, Faggin E, et al. Clones of Interstitial Cells From Bovine Aortic Valve Exhibit Different Calcifying Potential When Exposed to Endotoxin and Phosphate. Arteriosclerosis, Thrombosis, and Vascular Biology. 2008;28(12):2165–2172.

86. Resnick N, Yahav H, Shay-Salit A, et al. Fluid shear stress and the vascular endothelium: for better and for worse. Prog. Biophys. Mol. Biol. 2003;81(3):177–199.

87. Roberts A, Pimentel H, Trapnell C, Pachter L. Identification of novel transcripts in annotated genomes using RNA-Seq. Bioinformatics. 2011;27(17):2325–2329.

88. Roberts WC. The congenitally bicuspid aortic valve. A study of 85 autopsy cases. Am. J. Cardiol. 1970;26(1):72–83.

89. Roberts WC. Frequency by Decades of Unicuspid, Bicuspid, and Tricuspid Aortic Valves in Adults Having Isolated Aortic Valve Replacement for Aortic Stenosis, With or Without Associated Aortic Regurgitation. Circulation. 2005;111(7):920–925.

90. Robinton DA, Daley GQ. The promise of induced pluripotent stem cells in research and therapy. Nature 2012;481:295–305.

91. Rodés-Cabau J, Dumont E, Boone RH, et al. Cerebral Embolism Following Transcatheter Aortic Valve Implantation. J Am Coll Cardiol. 2011;57(1):18–28.

92. Rufaihah AJ, Huang NF, Jame S, et al. Endothelial Cells Derived From Human iPSCS Increase Capillary Density and Improve Perfusion in a Mouse Model of Peripheral Arterial Disease. Arterioscler Thromb Vasc Biol 2011;31(11):e72–e79.

93. Salomonis N, Hanspers K, Zambon AC, et al. GenMAPP 2: new features and resources for pathway analysis. BMC Bioinformatics. 2007;8(1):217.

94. Savage T, Clarke AL, Giles M, Tomson CR, Raine AE. Calcified plaque is common in the carotid and femoral arteries of dialysis patients without clinical vascular disease. Nephrol. Dial. Transplant. 1998;13(8):2004–2012.

95. Schoen FJ. Evolving Concepts of Cardiac Valve Dynamics: The Continuum of Development, Functional Structure, Pathobiology, and Tissue Engineering. Circulation. 2008;118(18):1864–1880.

96. Schoen FJ, Levy RJ. Calcification of Tissue Heart Valve Substitutes: Progress Toward Understanding and Prevention. Ann Thorac Surg. 2005;79(3):1072–1080.

97. Schurgers LJ, Aebert H, Vermeer C, Bültmann B, Janzen J. Oral anticoagulant treatment: friend or foe in cardiovascular disease? Blood. 2004;104(10):3231–3232.

98. Schurgers LJ, Spronk HMH, Skepper JN, et al. Post-translational modifications regulate matrix Gla protein function: importance for inhibition of vascular smooth muscle cell calcification. J. Thromb. Haemost. 2007;5(12):2503–2511.

99. Schurgers LJ, Spronk HMH, Soute BAM, Schiffers PM, DeMey JGR, Vermeer C. Regression of warfarin-induced medial elastocalcinosis by high intake of vitamin K in rats. Blood. 2007;109(7):2823–2831.

100. Sharma B, Albig AR. Matrix Gla protein reinforces angiogenic resolution. Microvascular Research. 2012:1–10.

101. Shea MK, Holden RM. Vitamin K Status and Vascular Calcification: Evidence from Observational and Clinical Studies. Advances in Nutrition: An International Review Journal. 2012;3(2):158–165.

102. Shin V, Zebboudj AF, Bostr ouml m K. Endothelial Cells Modulate Osteogenesis in Calcifying Vascular Cells. J. Vasc. Res. 2004;41(2):193–201..

103. Sider KL, Blaser MC, Simmons CA. Animal Models of Calcific Aortic Valve Disease. International Journal of Inflammation. 2011;2011:1–18.

104. Smits P, Li P, Mandel J, et al. The transcription factors L-Sox5 and Sox6 are essential for cartilage formation. Dev. Cell. 2001;1(2):277–290.

105. Speer MY, McKee MD, Guldberg RE, et al. Inactivation of the Osteopontin Gene Enhances Vascular Calcification of Matrix Gla Protein-deficient Mice: Evidence for Osteopontin as an Inducible Inhibitor of Vascular Calcification In Vivo. Journal of Experimental Medicine. 2002;196(8):1047–1055.

106. Stewart BF, Siscovick D, Lind BK, et al. Clinical factors associated with calcific aortic valve disease. Cardiovascular Health Study. J Am Coll Cardiol. 1997;29(3):630–634.

107. Suda N, Shibata S, Yamazaki K, et al. Parathyroid hormone-related protein regulates proliferation of condylar hypertrophic chondrocytes. J. Bone Miner. Res. 1999;14(11):1838–1847.

108. Sun C, Liu X, Qi L, et al. Modulation of vascular endothelial cell senescence by integrin β4. J Cell Physiol 2010;225:673–681.

109. Takahashi K, Tanabe K, Ohnuki M, et al. Induction of Pluripotent Stem Cells from Adult Human Fibroblasts by Defined Factors. Cell. 2007;131(5):861–872.

110. Tanaka K, Sata M, Fukuda D, et al. Age-associated aortic stenosis in apolipoprotein E-deficient mice. J Am Coll Cardiol. 2005;46(1):134–141.

111. Tanaka KI, Matsumoto E, Higashimaki Y, et al. Role of Osteoglycin in the Linkage between Muscle and Bone. Journal of Biological Chemistry. 2012;287(15):11616–11628.

112. Tang Z, Wang A, Yuan F, et al. Differentiation of multipotent vascular stem cells contributes to vascular diseases. Nature Communications. 2012;3:1–13.

113. Tao G, Kotick JD, Lincoln J. Heart valve development, maintenance, and disease: the role of endothelial cells. Curr. Top. Dev. Biol. 2012;100:203–232.

114. Tatsumi R, Suzuki Y, Sumi T, Sone M, Suemori H, Nakatsuji N. Simple and highly efficient method for production of endothelial cells from human embryonic stem cells. Cell Transplant. 2011;20(9):1423–1430.

115. Teichert-Kuliszewska K. Bone Morphogenetic Protein Receptor-2 Signaling Promotes Pulmonary Arterial Endothelial Cell Survival: Implications for Loss-of-Function Mutations in the Pathogenesis of Pulmonary Hypertension. Circulation Research. 2006;98(2):209–217.

116. Tkatchenko TV, Moreno-Rodriguez RA, Conway SJ, Molkentin JD, Markwald RR, Tkatchenko AV. Lack of periostin leads to suppression of Notch1 signaling and calcific aortic valve disease. Physiological Genomics. 2009;39(3):160–168.

117. Traub O, Berk BC. Laminar Shear Stress : Mechanisms by Which Endothelial Cells Transduce an Atheroprotective Force. Arteriosclerosis, Thrombosis, and Vascular Biology. 1998;18(5):677–685.

118. Tzima E, Irani-Tehrani M, Kiosses WB, et al. A mechanosensory complex that mediates the endothelial cell response to fluid shear stress. Nature. 2005;437(7057):426–431.

119. Wallin R, Wajih N, Greenwood GT, Sane DC. Arterial calcification: a review of mechanisms, animal models, and the prospects for therapy. Med Res Rev. 2001;21(4):274–301.

120. Wamstad JA, Alexander JM, Truty RM, et al. Dynamic and Coordinated Epigenetic Regulation of Developmental Transitions in the Cardiac Lineage. Cell. 2012;151(1):206–220.

121. Wamstad JA, Alexander JM, Truty RM, et al. Dynamic and Coordinated Epigenetic Regulation of Developmental Transitions in the Cardiac Lineage. Cell. 2012;151(1):206–220.

122. Wang H, Zou J, Zhao B, et al. Genome-wide analysis reveals conserved and divergent features of Notch1/RBPJ binding in human and murine T-lymphoblastic leukemia cells. Proc Natl Acad Sci USA. 2011;108(36):14908–14913.

123. Wang ZZ, Au P, Chen T, et al. Endothelial cells derived from human embryonic stem cells form durable blood vessels in vivo. Nat Biotechnol 2007;25(3):317–318.

124. Weinberg EJ, Mack PJ, Schoen FJ, García-Cardeña G, Kaazempur Mofrad MR. Hemodynamic Environments from Opposing Sides of Human Aortic Valve Leaflets Evoke Distinct Endothelial Phenotypes In Vitro. Cardiovasc Eng. 2010;10(1):5–11.

125. Yamamizu K, Matsunaga T, Uosaki H, et al. Convergence of Notch and -catenin signaling induces arterial fate in vascular progenitors. The Journal of Cell Biology 2010;189:325–338.

126. Yamashita J, Itoh H, Hirashima M, et al. Flk1-positive cells derived from embryonic stem cells serve as vascular progenitors. Nature 2000;408:92–96.

127. Yang L, Soonpaa MH, Adler ED, et al. Human cardiovascular progenitor cells develop from a KDR+ embryonic-stem-cell-derived population. Nature 2008;453:524–528.

128. Yang X, Meng X, Su X, et al. Bone morphogenic protein 2 induces Runx2 and osteopontin expression in human aortic valve interstitial cells: role of Smad1 and extracellular signal-regulated kinase 1/2. The Journal of Thoracic and Cardiovascular Surgery. 2009;138(4):1008–1015.

129. Yang X, Tare RS, Partridge KA, et al. Induction of human osteoprogenitor chemotaxis, proliferation, differentiation, and bone formation by osteoblast stimulating factor-1/pleiotrophin: osteoconductive biomimetic scaffolds for tissue engineering. J. Bone Miner. Res. 2003;18(1):47–57.

130. Yatim A, Benne C, Sobhian B, et al. NOTCH1 Nuclear Interactome Reveals Key Regulators of Its Transcriptional Activity and Oncogenic Function. Molecular Cell. 2012:1–14.

131. Yokoi H, Kasahara M, Mori K, et al. Pleiotrophin triggers inflammation and increased peritoneal permeability leading to peritoneal fibrosis. Kidney International. 2011;81(2):160–169.

132. Zambon AC, Gaj S, Ho I, et al. GO-Elite: a flexible solution for pathway and ontology over-representation. Bioinformatics. 2012;28(16):2209–2210.

133. Zhou HY, Ohnuma Y, Takita H, Fujisawa R, Mizuno M, Kuboki Y. Effects of a bone lysine-rich 18 kDa protein on osteoblast-like MC3T3-E1 cells. Biochem Biophys Res Commun. 1992;186(3):1288–1293.

Appendix

Supp. Table 2.1 Flow and NOTCH Dependent Genes with ChIP Peak

Gene Name	No Flow Control siRNA	No Flow N1 siRNA	Flow Control siRNA	Flow N1 siRNA	ChIP Score
CRHBP	0	-1.3	6.2	4.7	8
SEMA3G	0	-2.9	4.5	3.0	9
VWA1	0	-2.4	3.5	2.1	5
SOX6	0	-1.4	5.7	3.3	16
PLVAP	0	-1.6	4.0	2.7	11
HTRA3	0	-1.6	3.4	1.1	9
AL359832.2	0	-1.3	2.5	1.1	7
TMEM100	0	-1.6	2.9	1.7	9
CNNM2	0	-1.9	2.8	1.4	9
KCNC3	0	-1.5	2.2	1.1	8
GJA5	0	-1.9	5.1	2.8	21
AP001189.1	0	-2.0	2.9	0.9	13
SPSB1	0	-1.0	2.3	0.7	10
IMPG1	0	-1.0	2.0	0.7	8
AL162417.6	0	-1.2	2.6	0.7	14
LRRC32	0	-1.2	2.3	0.9	13
MARCH10	0	-1.8	1.3	-1.2	21
CALU	0	-1.7	1.1	-0.5	16
SLCO2A1	0	-1.8	2.1	-1.2	21
RILPL2	0	-1.3	2.1	0.0	23
PLAT	0	-1.1	1.8	0.2	30
F2R	0	-1.1	1.6	-0.1	24
AC002480.2	0	-1.0	1.3	0.1	18
KCTD12	0	-1.3	1.1	-0.2	18
RBKS	0	-1.3	1.1	-0.1	17
SERPINB1	0	-1.1	2.0	-0.3	18
RPL39P5	0	-2.4	2.4	0.7	24
ITGA1	0	-1.1	3.2	1.3	21
SAT1	0	-1.4	1.9	-0.4	14
CCDC11	0	-1.5	1.6	-0.2	11
AC021914.2	0	-1.4	1.5	-0.2	10

AC019201.2	0	-1.0	1.1	-0.1	8
GABRR2	0	-2.2	1.7	-0.1	14
GRIN2D	0	-1.6	1.1	-0.1	11
MGP	0	-1.5	2.3	0.2	16
EFNB2	0	-1.4	2.2	0.2	13
ARMCX2	0	-1.0	1.5	0.1	9
TIMP1	0	-1.0	1.2	0.0	10
DAB1	0	-1.2	1.1	0.0	10
RP11-27I1.1	0	-1.2	1.3	0.1	10
NPTXR	0	-1.0	1.1	0.0	8
ACTG2	0	-1.3	1.8	0.1	10
C4orf18	0	-1.5	2.4	0.4	15
DOM3Z	0	-1.4	2.2	0.4	14
RP1-5O6.1	0	-1.9	1.7	0.7	12
SEMA7A	0	-1.7	1.8	0.3	7
AL391421.6	0	-1.6	1.7	0.5	7
ABCD1	0	-1.3	2.8	0.3	8
VCAM1	0	-2.0	2.6	0.2	10
AL139397.1	0	-1.3	2.0	-0.1	7
TEDDM1	0	-1.3	2.1	0.1	9
SELE	0	-1.5	3.0	-0.4	12
C6orf165	0	-1.3	2.3	0.0	10
AL049636.1	0	-1.1	1.9	-0.9	9
TNFRSF8	0	-1.1	1.7	-0.4	9
MEIS3P1	0	-1.2	1.2	-0.5	8
P2RY6	0	-3.9	1.6	0.4	10
CTD-3105H18.1	0	-4.5	2.6	-0.7	13
IL18R1	0	-3.0	1.6	0.5	11
AC217773.2	0	-2.3	1.2	0.1	8
TREX2	0	-3.2	1.4	0.1	13
AC106864.5	0	-1.8	1.5	-0.4	8
AL161668.2	0	-3.0	1.1	-0.8	15
C10orf114	0	-2.4	1.0	-0.9	13
AC000032.1	0	-7.5	2.9	-1.0	10
AP001619.2	0	-3.7	3.7	-2.2	8
AL645811.2	0	-3.2	2.1	-2.5	7
SVOPL	0	-3.5	1.3	-1.7	9
AL671855.1	0	-2.3	1.2	-2.0	7
ZNF703	0	-1.8	1.9	-0.9	8
NPTX2	0	-1.5	1.3	-0.5	6
MORN3	0	-1.8	1.2	-1.0	7
AL357140.2	0	-1.3	2.0	-1.0	8
KCNJ10	0	-1.2	1.8	-1.9	9

C6orf50	0	-2.2	1.4	-2.1	11
GPR89B	0	-1.6	1.4	-1.6	10
ULBP3	0	-1.5	1.1	-1.2	8
AL356957.1	0	-1.5	1.1	-0.7	8
AC133473.1	0	-1.5	1.1	-0.5	7
AC134943.2	0	1.7	-2.8	2.6	7.5
RP11-165M8.1	0	1.6	-1.1	6.9	17
AL390797.1	0	3.0	-2.1	2.8	14
IGLV5-52	0	1.2	-1.0	1.8	6
AC005682.4	0	3.0	-1.2	0.8	10
CABP7	0	2.2	-1.3	0.9	7
SCN9A	0	1.6	-1.8	-0.6	19
OGN	0	1.1	-1.3	-0.2	12
AC010095.3	0	1.6	-1.3	0.4	23
AL049844.1	0	1.4	-1.1	0.3	15
AL121718.1	0	1.8	-1.6	1.6	23
LGI2	0	1.6	-1.2	1.1	20
SKAP1	0	1.2	-3.0	0.5	18
Y_RNA	0	1.4	-1.4	0.0	9
5S_rRNA	0	1.3	-1.3	0.4	11
AC106722.1	0	1.7	-1.5	0.1	13
AC095033.1	0	1.8	-1.4	0.3	12
7SK	0	2.5	-1.3	0.5	16
AC005250.1	0	1.8	-1.3	1.6	16
AL353895.1	0	1.4	-1.1	2.0	11
FGF12	0	1.1	-1.1	1.4	12
ZNF860	0	1.0	-1.5	1.2	11
C16orf74	0	1.8	-1.8	1.7	12
AC013461.1	0	1.8	-1.5	1.2	10
U6	0	1.3	-1.3	1.0	8
AL138999.1	0	1.5	-1.4	1.2	10
ANGPTL1	0	1.2	-1.2	0.8	8
AC097464.2	0	1.1	-1.3	0.8	9
Z95704.1	0	1.0	-2.2	0.6	11
SYNPO2	0	1.6	-1.7	0.7	9
AC011742.5	0	1.3	-1.3	0.4	7
PHEX	0	1.5	-2.1	1.0	10
POF1B	0	1.5	-2.1	0.9	8
C11orf70	0	2.3	-3.5	0.1	9
HSPA12B	0	1.1	-1.7	-0.5	9
AL160153.2	0	1.4	-1.7	-0.1	10
HCG27	0	1.5	-1.8	-0.2	10
AL450344.3	0	1.7	-1.8	-0.4	8

AC025918.1	0	2.1	-2.1	0.3	10
AL139294.2	0	1.2	-2.8	0.0	10
AC090516.2	0	1.4	-2.5	0.1	9
AP002812.1	0	1.1	-1.8	0.1	8
RP11-498B4.2	0	1.1	-2.0	0.1	8
AL139420.3	0	1.4	-1.8	0.1	8
MYH8	0	1.5	-2.1	-0.1	7
MYH15	0	1.9	-3.7	-0.5	13
PTN	0	1.4	-2.1	-0.4	8
AC068129.2	0	1.2	-1.7	-0.7	7
SULT1C2	0	1.2	-2.1	-0.6	7
PIK3CG	0	1.4	-3.8	-2.2	11
NEFM	0	1.3	-3.2	-1.3	9
KMO	0	1.7	-4.9	-1.1	11
AL589763.1	0	2.3	-5.8	-1.8	8
AL353354.1	0	1.1	-4.6	-2.0	6
AC004889.1	0	7.5	-6.4	-3.6	10
AP000347.3	0	3.9	-3.4	-0.2	6
RP11-460N11.1	0	1.8	-2.4	-0.2	5
ARL17P1	0	5.3	-1.0	0.4	8
OR2A20P	0	7.5	-5.9	6.7	10

Supp. Table 2.2 Flow and NOTCH Dependent Genes with ChIP Peak

Gene Name	No Flow Control siRNA	No Flow N1 siRNA	Flow Control siRNA	Flow N1 siRNA	ChIP Score
SOX6	0	-1.4	5.7	3.3	16
GJA5	0	-1.9	5.1	2.8	21
AL162417.6	0	-1.2	2.6	0.7	14
ITGA1	0	-1.1	3.2	1.3	21
DOM3Z	0	-1.4	2.2	0.4	14
C4orf18	0	-1.5	2.4	0.4	15
MGP	0	-1.5	2.3	0.2	16
RPL39P5	0	-2.4	2.4	0.7	24
SAT1	0	-1.4	1.9	-0.4	14
GABRR2	0	-2.2	1.7	-0.1	14
SERPINB1	0	-1.1	2.0	-0.3	18
RILPL2	0	-1.3	2.1	0.0	23

AC002480.2	0	-1.0	1.3	0.1	18
F2R	0	-1.1	1.6	-0.1	24
RBKS	0	-1.3	1.1	-0.1	17
KCTD12	0	-1.3	1.1	-0.2	18
PLAT	0	-1.1	1.8	0.2	30
CALU	0	-1.7	1.1	-0.5	16
MARCH10	0	-1.8	1.3	-1.2	21
SLCO2A1	0	-1.8	2.1	-1.2	21
AL161668.2	0	-3.0	1.1	-0.8	15

Supp. Table 3.1. Differential Expression Method A vs. Method B

	Gene Name	Affymetrix ID	Fold Change (Method A/Method B)
1	ZNF847P	7924821	2.94
2	ART4	7961507	2.39
3	HSP90AA6P	8103722	2.10
4	RASGEF1B	8101304	2.07
5	CXCL10	8101126	2.07
6	CGA	8128001	0.46
7	DNAH14	7910047	0.34

Supp. Table 3.2 Differential Expression iPS-EC vs. ES-EC 3 fold Change

	Gene Names	Affymetrix ID	Fold-Change (iPS-EC/ES-EC)	P-value
1	ECM1	7905220	9.01	0.0037
2	QPCT	8041508	8.77	0.0053
3	SYTL3	8123080	8.47	0.0034
4	TSPYL5	8151931	6.06	0.0000
5	TNIP3	8102594	4.63	0.0011
6	GFRAL	8120350	4.05	0.0003
7	PLA2G4C	8037970	3.72	0.0014
8	ACTA2	7934906	3.33	0.0001
9	TIMP1	8167185	3.25	0.0000
10	ZNF280D	7989159	3.24	0.0134
11	LGALS1	8072876	3.17	0.0000
12	AEBP1	8132557	3.14	0.0140
13	APOD	8092970	3.06	0.0062
14	CLEC2B	7961083	0.30	0.0000
15	NCAM2	8067985	0.23	0.0000
16	ALDH1A1	8161755	0.21	0.0011

17	MMP1	7951271	0.07	0.0101

Supp. Table 3. iPS vs.ES - 2 fold Change and P value < 0.05

	Gene Names	Affymetrix ID	Fold-Change (iPS-EC/ES-EC)	P-value
1	ECM1	7905220	9.01	0.0037
2	QPCT	8041508	8.77	0.0053
3	SYTL3	8123080	8.47	0.0034
4	TSPYL5	8151931	6.06	0.0000
5	TNIP3	8102594	4.63	0.0011
6	GFRAL	8120350	4.05	0.0003
7	PLA2G4C	8037970	3.72	0.0014
8	ACTA2	7934906	3.33	0.0001
9	TIMP1	8167185	3.25	0.0000
10	ZNF280D	7989159	3.24	0.0134
11	LGALS1	8072876	3.17	0.0000
12	AEBP1	8132557	3.14	0.0140
13	APOD	8092970	3.06	0.0062
14	TPP1	7946228	3.02	0.0000
15	GBP3	7917503	2.87	0.0070

16	POU5F1	8178470	2.82	0.0139
17	IL1B	8054722	2.76	0.0000
18	IL6	8131803	2.70	0.0084
19	DCLK1	7970954	2.70	0.0413
20	ITGA5	7963786	2.69	0.0000
21	ADAMTS9	8088560	2.62	0.0060
22	SRPX2	8168749	2.61	0.0026
23	SERPINE2	8059376	2.51	0.0270
24	DPP4	8056222	2.51	0.0178
25	MEG3	7981320	2.48	0.0008
26	NSMCE1	8000413	2.44	0.0000
27	TCTEX1D1	7902158	2.44	0.0019
28	CSRP1	7923378	2.43	0.0304
29	LAPTM5	7914270	2.43	0.0030
30	CREB5	8131996	2.42	0.0027
31	RORA	7989365	2.42	0.0018
32	ECH1	8036602	2.40	0.0000
33	IL8	8095680	2.40	0.0243
34	TGFBI	8108217	2.39	0.0064
35	PLOD1	7897803	2.36	0.0000
36	RTN1	7979455	2.36	0.0000

37	DOCK2	8109843	2.35	0.0043
38	SERPINB2	8021635	2.34	0.0442
39	TNC	8163637	2.31	0.0000
40	IAH1	8040163	2.30	0.0076
41	TRIM4	8141363	2.30	0.0000
42	ANO4	7957861	2.29	0.0003
43	NID1	7925320	2.29	0.0012
44	PAPPA	8157487	2.28	0.0019
45	NID2	7979133	2.28	0.0080
46	CDH6	8104663	2.27	0.0105
47	SLC16A9	7933750	2.27	0.0002
48	DPF2	7941243	2.26	0.0000
49	SERPINE1	8135069	2.26	0.0071
50	ADAM12	7936968	2.24	0.0001
51	VPS28	8153776	2.23	0.0000
52	MCAM	7952205	2.23	0.0021
53	FGF16	8168463	2.22	0.0181
54	SLC22A23	8123658	2.21	0.0042
55	S100A6	7920258	2.21	0.0005
56	GBP1	7917516	2.20	0.0420
57	PLTP	8066619	2.20	0.0018

58	PLXNA2	7923991	2.18	0.0003
59	HLA-B	8178498	2.17	0.0038
60	NCAM1	7943892	2.17	0.0012
61	NTNG1	7903461	2.16	0.0000
62	GRIA3	8169717	2.15	0.0015
63	ANPEP	7991335	2.15	0.0007
64	ICAM2	8017547	2.15	0.0002
65	TMEM63B	8119926	2.14	0.0000
66	SF3B5	8130003	2.14	0.0002
67	LIPH	8092541	2.12	0.0356
68	ABLIM3	8109093	2.11	0.0006
69	BMX	8166157	2.11	0.0254
70	PTPRM	8019988	2.11	0.0003
71	TBX15	7919028	2.10	0.0000
72	DLL4	7982854	2.09	0.0087
73	NEU1	8178676	2.09	0.0009
74	BHLHE40	8077441	2.08	0.0000
75	HLA-A	8177732	2.07	0.0023
76	TANC2	8009075	2.07	0.0020
77	SULF2	8066822	2.06	0.0018
78	PI3	8062927	2.05	0.0021

79	PODXL	8142981	2.05	0.0033
80	HLA-B	8124911	2.04	0.0067
81	GPR116	8161418	2.04	0.0342
82	PTHLH	7962000	2.03	0.0015
83	SEPW1	8029969	2.03	0.0001
84	ARRB1	7950473	2.03	0.0023
85	JAG1	8064978	2.03	0.0001
86	PGD	7897620	2.03	0.0016
87	CD44	7939341	2.01	0.0027
88	VCAN	8106743	2.01	0.0201
89	GPM6B	8171359	2.00	0.0125
90	GFPT2	8116418	2.00	0.0021
91	AADAC	8083415	0.50	0.0287
92	LIN9	7924712	0.50	0.0022
93	CENPI	8168794	0.50	0.0030
94	POLE2	7978846	0.50	0.0342
95	SGOL1	8085754	0.50	0.0223
96	CEP55	7929334	0.49	0.0398
97	MAD2L1	8102560	0.49	0.0440
98	FBXO5	8130374	0.49	0.0103
99	NUSAP1	7982889	0.49	0.0488

100	AF090895	8117161	0.49	0.0000
101	HELLS	7929438	0.49	0.0163
102	MTBP	8148124	0.49	0.0028
103	TRIM59	8091757	0.49	0.0000
104	KCNRG	7969166	0.48	0.0004
105	PTTG1	8109639	0.48	0.0365
106	RPL22L1	8092067	0.48	0.0060
107	SEPT14	7998117	0.48	0.0000
108	RNU5F	7915592	0.48	0.0105
109	CD69	7961075	0.47	0.0380
110	FBXO25	8049961	0.47	0.0378
111	GPR126	8122365	0.47	0.0483
112	KIF11	7929258	0.47	0.0388
113	SKA2	8017133	0.46	0.0030
114	CASC5	7982757	0.45	0.0451
115	HIST1H4C	8117368	0.45	0.0046
116	MOP-1	8101322	0.45	0.0149
117	PLK4	8097356	0.44	0.0076
118	RAD51AP1	7953218	0.44	0.0215
119	ARHGAP11A	7982358	0.44	0.0293
120	DEPDC1	7916898	0.44	0.0238

121	FSTL5	8103466	0.43	0.0036
122	DHFR	8043036	0.43	0.0017
123	KIF18A	7947248	0.43	0.0306
124	RALGPS2	7907657	0.43	0.0000
125	RNU5E	7897801	0.43	0.0002
126	PAR5	7981943	0.43	0.0306
127	DLEU2	7971653	0.42	0.0195
128	SCD	7935776	0.42	0.0000
129	EPCAM	8098439	0.41	0.0225
130	WDR76	7983306	0.41	0.0037
131	FAM111B	7940147	0.41	0.0177
132	CDC2	7927710	0.41	0.0236
133	ZNF596	8144230	0.41	0.0018
134	EMCN	8101957	0.40	0.0210
135	STAT4	8057771	0.40	0.0000
136	BRIP1	8017262	0.40	0.0136
137	SPC25	8056572	0.40	0.0174
138	TTK	8120838	0.39	0.0300
139	CENPK	8112376	0.38	0.0001
140	ALX1	7957452	0.38	0.0000
141	SLC40A1	8057677	0.35	0.0198

142	KIAA0101	7989647	0.34	0.0053
143	MGP	7961514	0.34	0.0342
144	CLEC2B	7961083	0.30	0.0000
145	NCAM2	8067985	0.23	0.0000
146	ALDH1A1	8161755	0.21	0.0011
147	MMP1	7951271	0.07	0.0101

Supp Table 3.4 iPS-EC Specific Gene Signatures Compared to Three Other Reports of iPS Specific Gene Signatures (Gupta et al., Chin et al., Marchetto et al.).

			Fold-Change (iPS-EC/ES-EC)	P-Value	FDR	Concordence to iPS Specific Gene Expression Reports
		>2 Fold Up in iPS ECs				
1	8109093	ABLIM3	2.11	0.00057	0.00570	
2	7934906	ACTA2	3.33	0.00006	0.00116	
3	7936968	ADAM12	2.24	0.00009	0.00159	
4	8088560	ADAMTS9	2.62	0.00601	0.03280	
5	8132557	AEBP1	3.14	0.01396	0.06110	
6	7957861	ANO4	2.29	0.00026	0.00327	
7	7991335	ANPEP	2.15	0.00074	0.00689	
8	8092970	APOD	3.06	0.00615	0.03330	
9	7950473	ARRB1	2.03	0.00232	0.01610	

10	8077441	BHLHE40	2.08	0.00001	0.00041	
11	8166157	BMX	2.11	0.02541	0.09490	
12	7968351	C13orf33	2.58	0.03793	0.12700	
13	7939341	CD44	2.01	0.00273	0.01810	Marchetto et al.
14	8104663	CDH6	2.27	0.01046	0.04930	Chin et al., Marchetto et al.
15	8131996	CREB5	2.42	0.00271	0.01810	
16	7923378	CSRP1	2.43	0.03043	0.10800	Marchetto et al.
17	7970954	DCLK1	2.70	0.04128	0.13500	
18	7982854	DLL4	2.09	0.00870	0.04290	
19	8109843	DOCK2	2.35	0.00425	0.02520	Marchetto et al.
20	7941243	DPF2	2.26	0.00004	0.00098	Marchetto et al.
21	8056222	DPP4	2.51	0.01777	0.07290	
22	8036602	ECH1	2.40	0.00001	0.00031	
23	7905220	ECM1	9.01	0.00369	0.02270	Chin et al.
24	8168463	FGF16	2.22	0.01814	0.07400	
25	7917516	GBP1	2.20	0.04202	0.13600	
26	7917503	GBP3	2.87	0.00698	0.03640	
27	8116418	GFPT2	2.00	0.00210	0.01490	Marchetto et al.
28	8120350	GFRAL	4.05	0.00032	0.00377	
29	8171359	GPM6B	2.00	0.01255	0.05640	Marchetto et al.
30	8161418	GPR116	2.04	0.03422	0.11800	
31	8169717	GRIA3	2.15	0.00149	0.01150	
32	8177732	HLA-A	2.07	0.00229	0.01590	
33	8178498	HLA-B	2.17	0.00375	0.02300	Gupta et al.
34	8040163	IAH1	2.30	0.00760	0.03870	
35	8017547	ICAM2	2.15	0.00018	0.00252	
36	8054722	IL1B	2.76	0.00003	0.00087	
37	8131803	IL6	2.70	0.00837	0.04170	Chin et al., Marchetto et al.
38	8095680	IL8	2.40	0.02425	0.09190	Marchetto et al.
39	7963786	ITGA5	2.69	0.00000	0.00025	
40	8064978	JAG1	2.03	0.00012	0.00191	
41	7914270	LAPTM5	2.43	0.00301	0.01950	
42	8072876	LGALS1	3.17	0.00000	0.00024	

43	8092541	LIPH	2.12	0.03564	0.12100	
44	7952205	MCAM	2.23	0.00208	0.01480	Marchetto et al.
45	7981320	MEG3	2.48	0.00082	0.00743	
46	7943892	NCAM1	2.17	0.00115	0.00950	Marchetto et al.
47	8178676	NEU1	2.09	0.00091	0.00801	
48	7925320	NID1	2.29	0.00124	0.01000	
49	7979133	NID2	2.28	0.00801	0.04030	Marchetto et al.
50	8000413	NSMCE1	2.44	0.00001	0.00052	
51	7903461	NTNG1	2.16	0.00001	0.00042	
52	8157487	PAPPA	2.28	0.00191	0.01380	
53	7897620	PGD	2.03	0.00162	0.01230	
54	8062927	PI3	2.05	0.00206	0.01470	
55	8037970	PLA2G4C	3.72	0.00135	0.01070	Marchetto et al.
56	7897803	PLOD1	2.36	0.00001	0.00036	
57	8066619	PLTP	2.20	0.00177	0.01310	Marchetto et al.
58	7923991	PLXNA2	2.18	0.00031	0.00369	Marchetto et al.
59	8142981	PODXL	2.05	0.00326	0.02070	
60	8178470	POU5F1	2.82	0.01387	0.06080	
61	7962000	PTHLH	2.03	0.00149	0.01150	
62	8019988	PTPRM	2.11	0.00033	0.00390	
63	8041508	QPCT	8.77	0.00528	0.02970	
64	7989365	RORA	2.42	0.00177	0.01310	
65	7979455	RTN1	2.36	0.00000	0.00014	Marchetto et al.
66	7920258	S100A6	2.21	0.00050	0.00516	Marchetto et al.
67	8029969	SEPW1	2.03	0.00014	0.00213	
68	8021635	SERPINB2	2.34	0.04424	0.14100	
69	8135069	SERPINE1	2.26	0.00707	0.03680	
70	8059376	SERPINE2	2.51	0.02703	0.09920	Marchetto et al.
71	8130003	SF3B5	2.14	0.00018	0.00257	
72	7933750	SLC16A9	2.27	0.00020	0.00267	
73	8123658	SLC22A23	2.21	0.00417	0.02480	
74	8168749	SRPX2	2.61	0.00265	0.01770	
75	8066822	SULF2	2.06	0.00179	0.01320	
76	8123080	SYTL3	8.47	0.00339	0.02130	

77	8009075	TANC2	2.07	0.00205	0.01460	
78	7919028	TBX15	2.10	0.00000	0.00015	
79	7902158	TCTEX1D1	2.44	0.00192	0.01390	
80	8108217	TGFBI	2.39	0.00645	0.03440	Marchetto et al.
81	8167185	TIMP1	3.25	0.00000	0.00009	
82	8119926	TMEM63B	2.14	0.00001	0.00052	
83	8163637	TNC	2.31	0.00001	0.00035	Marchetto et al.
84	8102594	TNIP3	4.63	0.00108	0.00910	
85	7946228	TPP1	3.02	0.00002	0.00064	
86	8141363	TRIM4	2.30	0.00002	0.00059	Gupta et al., Chin et al.
87	8151931	TSPYL5	6.06	0.00004	0.00099	Gupta et al., Chin et al.
88	8106743	VCAN	2.01	0.02008	0.07980	
89	8153776	VPS28	2.23	0.00001	0.00052	
90	7989159	ZNF280D	3.24	0.01338	0.05920	
		>2 Fold Down in iPS ECs				
91	8083415	AADAC	0.50	0.02868	0.10400	
92	8117161	AF090895	0.49	0.00002	0.00064	
93	8161755	ALDH1A1	0.21	0.00113	0.00940	
94	7957452	ALX1	0.38	0.00005	0.00107	
95	7982358	ARHGAP11A	0.44	0.02934	0.10500	
96	8017262	BRIP1	0.40	0.01364	0.06000	
97	7982757	CASC5	0.45	0.04506	0.14300	
98	7961075	CD69	0.47	0.03804	0.12700	
99	7927710	CDC2	0.41	0.02362	0.09010	
100	8168794	CENPI	0.50	0.00302	0.01960	
101	8112376	CENPK	0.38	0.00009	0.00157	
102	7929334	CEP55	0.49	0.03981	0.13100	
103	7961083	CLEC2B	0.30	0.00000	0.00006	
104	7916898	DEPDC1	0.44	0.02380	0.09060	Chin et al.

105	8043036	DHFR	0.43	0.00167	0.01250	Marchetto et al.
106	7971653	DLEU2	0.42	0.01954	0.07820	
107	8101957	EMCN	0.40	0.02100	0.08250	
108	8098439	EPCAM	0.41	0.02251	0.08690	
109	7940147	FAM111B	0.41	0.01771	0.07270	Chin et al.
110	7940147	FBXO25	0.41	0.01771	0.07270	Marchetto et al.
111	8130374	FBXO5	0.49	0.01035	0.04890	Chin et al. Marchetto et al.
112	8103466	FSTL5	0.43	0.00362	0.02240	
113	8122365	GPR126	0.47	0.04833	0.15000	
114	7929438	HELLS	0.49	0.01629	0.06830	Marchetto et al.
115	8117368	HIST1H4C	0.45	0.00464	0.02700	Chin et al.
116	8117368	KCNRG	0.45	0.00464	0.02700	
117	7969166	KIAA0101	0.48	0.00043	0.00469	
118	7929258	KIF11	0.47	0.03879	0.12900	Marchetto et al.
119	7947248	KIF18A	0.43	0.03056	0.10900	Chin et al. Marchetto et al.
120	7924712	LIN9	0.50	0.00219	0.01540	
121	8102560	MAD2L1	0.49	0.04403	0.14100	
122	7961514	MGP	0.34	0.03423	0.11800	
123	7951271	MMP1	0.07	0.01006	0.04790	
124	8101322	MOP-1	0.45	0.01490	0.06400	
125	8148124	MTBP	0.49	0.00283	0.01870	Marchetto et al.
126	8067985	NCAM2	0.23	0.00001	0.00032	
127	7982889	NUSAP1	0.49	0.04883	0.15200	
128	7982889	PAR5	0.49	0.04883	0.15200	
129	8097356	PLK4	0.44	0.00762	0.03880	
130	7978846	POLE2	0.50	0.03418	0.11800	
131	8109639	PTTG1	0.48	0.03646	0.12300	Marchetto et al.
132	7953218	RAD51AP1	0.44	0.02146	0.08390	
133	7907657	RALGPS2	0.43	0.00001	0.00044	
134	7897801	RNU5E	0.43	0.00024	0.00311	
135	7915592	RNU5F	0.48	0.01048	0.04940	
136	8092067	RPL22L1	0.48	0.00597	0.03250	
137	7935776	SCD	0.42	0.00003	0.00076	Marchetto et al.

138	7935776	SEPT14	0.42	0.00003	0.00076	
139	8085754	SGOL1	0.50	0.02233	0.08640	
140	8017133	SKA2	0.46	0.00302	0.01960	
141	8057677	SLC40A1	0.35	0.01977	0.07890	Marchetto et al.
142	8056572	SPC25	0.40	0.01741	0.07180	Marchetto et al.
143	8057771	STAT4	0.40	0.00000	0.00013	
144	8091757	TRIM59	0.49	0.00003	0.00072	
145	8120838	TTK	0.39	0.03000	0.10700	
146	7983306	WDR76	0.41	0.00368	0.02260	
147	8144230	ZNF596	0.41	0.00178	0.01310	

Comparison of Chin et al. done with late iPS vs ES cell data set. Green cells = iPS-EC Gene Expression Fold Change Matches Direction of Fold Change in Report Cited, Red cells= iPS-EC Gene Expression Fold Change is Opposite to Direction of Fold Change in Report Cited.

Publishing Agreement

It is the policy of the University to encourage the distribution of all theses, dissertations, and manuscripts. Copies of all UCSF theses, dissertations, and manuscripts will be routed to the library via the Graduate Division. The library will make all theses, dissertations, and manuscripts accessible to the public and will preserve these to the best of their abilities, in perpetuity.

I hereby grant permission to the Graduate Division of the University of California, San Francisco to release copies of my thesis, dissertation, or manuscript to the Campus Library to provide access and preservation, in whole or in part, in perpetuity.

Mark D White 12/20/12

Author Signature Date